Data Package C Item #4

PROGRAMMED OVERHEAD
JOB NO. 94444 (1983)
REPORT NO. SFPD-C/S-83-07
DIRECT GENERATION OF
PROBABILISTIC FLOOR RESPONSE
SPECTRA (DECEMBER 1983)

PROGRAMMED OVERHEAD

JOB NO. 94444 (1983)

REPORT NO. SFPD-C/S-83-07

DIRECT GENERATION OF PROBABILISTIC FLOOR RESPONSE SPECTRA

DECEMBER, 1983

	Signature	Date
Prepared by:	K. Lilhanand	3/26/84
Reviewed by:	W. S. Tseng	3/26/84
Approved by:	B. N. Pusheck	4/2/84

BECHTEL POWER CORPORATION
San Francisco, California

TABLE OF CONTENTS

1. INTRODUCTION

The floor response spectra (FRS) is of practical importance for seismic qualifications of equipment and piping systems supported on building floors and walls in nuclear power plants. Currently, it is a common practice to use the deterministic method to generate the FRS by performing a time history analysis. This method, however, does not take into account the randomness inherent in seismic ground motions. Furthermore, since seismic ground motions are usually prescribed in the form of the design response spectra (DRS) such as those given by the USNRC Regulatory Guide (R.G.) 1.60, which has been developed from statistical studies of the actual seismic records (Ref. 1), the deterministic method requires that seismic ground motion time histories be generated which are compatible with the DRS. There are many time histories which may be generated compatible with a given DRS. The effect on the floor response spectra due to variation of different time history inputs is generally not addressed by the deterministic method. Therefore, the deterministic method for generating the FRS is not methodologically rational, and generally is costly.

An alternative to the deterministic method is the probabilistic method, which uses the random vibration theory to determine the probabilistic floor responses to random seismic ground motions. This method can directly generate the FRS for a desired level of confidence from the DRS without having to perform the more costly time history analysis. However, because the probabilistic methods that are current available for generating the FRS (Refs. 2 through 6) have not been throughly tested to confirm its reliability and accuracy, additional validations are required before these methods can be implemented for applications.

The objective of this report is to present the evaluation of currently available probabilistic methods and the result of testing of the underlying theories against the simulation results obtained from 20 simulated time histories, in order to confirm the reliability and accuracy of the theories for application to the generation of probabilistic floor

response spectra of nuclear power plants subjected to seismic ground motion excitations.

An overview of the theoretical background and an evaluation of the probabilistic methods proposed by various researchers are presented in Section 2. Based on the result of the evaluation, the probabilistic method which explicitly uses the relationship between the power spectral density function (PSDF) and the response spectra (RS), i.e., the PSDF-RS relationship, is selected for a detailed evaluation using simulation results. The theoretical derivation of the PSDF-RS relationship is presented in Section 2.1. The peak factor which is one of the key parameter contained in the PSDF-RS relationship is presented in Section 2.2. In Section 3, the PSDF of random seismic ground motions compatible with the USNRC R.G. 1.60 spectra, which is a typical wide-band random process, is generated. This PSDF is used as the basis for simulation of both stationary and nonstationary seismic ground motions in Section 4.

Section 5 presents the structural transfer functions of a typical nuclear power plant structure. These transfer functions are used as the structural filters which transfer the wide-band seismic input motions to the narrow-band floor response output motions. Section 6 presents the simulation of floor responses, to both the stationary and nonstationary seismic ground motions. Comparisons of the analytical and the simulation results for the wide-band seismic ground motions and the narrow-band floor responses are made in Section 7 to validate the PSDF-RS relationship given in Section 2.1.

Based on the comparison results in Section 7, a procedure for direct generation of probabilistic floor response spectra is described in Section 8. Section 9 demonstrates applications of the proposed procedure described in Section 8. The summary and conclusions are given in Section 10.

2. OVERVIEW OF THEORIES

The probabilistic methods currently proposed in the literature for generating the FRS can be grouped according to the analytical procedure used, into two approaches: the implicit approach, and the explicit approach. Both approaches treat seismic ground motion as wide-band random processes, and the theories of random vibration are used to determine the probabilistic floor responses. It is noted that none of the proposed methods have been adequately tested for its reliability for actual applications.

In the implicit approach, typical of the method developed by Singh (Ref. 2) and Atalik (Ref. 3), the PSDF-RS relationship is implicitly used in deriving the FRS as a direct function of the prescribed seismic DRS. The approach is shown schematically in Fig. 2.1. The derivation of this approach assumes that the seismic ground motion and the floor response motion are stationary processes, that the structure possesses normal-mode properties, and that the peak factor used for raising the root-mean-square (rms) response to the maximum (spectral) response at a particular frequency is the same for the wide-band seismic ground motion and for the narrow-band floor response motion. This method also requires approximations to simplify the mathematical complexities involved in deriving the FRS. Furthermore, because of the assumption made on the peak factor, this method can only generate the FRS for one confidence level, i.e. non-exceedance probability, which is the same as that prescribed for the DRS.

The explicit approach, typical of the methods developed by Vanmarcke (Ref. 4), Grossmayer (Ref. 5), Romo-Organista (Ref. 6), Der Kiureghian (Ref. 7), among others, uses the PSDF-RS relationship explicitly in generating the FRS from the prescribed seismic DRS. This approach shown schematically in Fig. 2.2, generally assumes that seismic ground motion and structural response are stationary random processes. However, the floor spectral response at a particular frequency, which can be obtained from filtering the structural response motion through a single degree-of-freedom (SDOF) system, can be approximately treated as either

stationary or nonstationary process depending on the selected peak factor used in the PSDF-RS relationship. The explicit approach requires the following four major steps of computation:

1. Compute the PSDF of seismic ground motion from a prescribed DRS using the PSDF-RS relationship.

2. Compute the structural transmittancy functions which is the square of the transfer function amplitude.

3. Compute the structural response PSDF by multiplying the PSDF of seismic ground motion in Step 1 with the structural transmittancy functions in Step 2.

4. Compute the FRS for any desired confidence levels from the structural response PSDF in Step 3 using the reversed PSDF-RS relationship.

Comparing the two approaches outlined above, the explicit approach has the following advantages over the implicit approach:

1. The FRS can be generated from the prescribed DRS for any desired levels of confidence as opposed to only one level of confidence provided by the implicit approach.

2. The PSDF of seismic ground motion compatible with the prescribed DRS is readily available as a by-product which can be used for simulation of seismic ground motions, if needed

3. The nonstationary effects, which tend to reduce the ground and floor spectral responses, can approximately be included to reduce the overconservatism inherent in the implicit approach, especially for the lightly damped and soft (low frequency) systems.

4. The peak factors for the wide-band ground motion and the narrow-band structural response which are generally different, can be prescribed differently.

5. The linear structure does not require to possess normal-mode properties.

For actual seismic ground motions which are nonstationary random motions, the PSDF-RS relationship which is required in the explicit approach, generally cannot be analytically derived, thus is often obtained through empirical means. However, by approximately treating seismic ground motions as a random stationary process, which has been found to be applicable when the duration of seismic ground motion is longer than the fundamental period of structure (Ref. 8), the PSDF-RS Relationship can approximately be derived analytically as that developed by Vanmarcke (Ref. 4). This analytical relationship contains two critical parameters - the rms response and the peak factor. The theoretical derviation of the analytical PSDF-RS relationship is presented in Section 2.1. The stationary rms response can be approximated as a function of the PSDF of seismic ground motion as discussed in Section 2.1. The theoretical backgrounds of the peak factor and various widely known approximated peak factors are presented in Section 2.2.

2.1 The PSDF-RS Relationship

The equation of motion of a SDOF system subjected to a zero mean random seismic ground acceleration input, $\ddot{x}(t)$, can be written as

$$\ddot{y}(t) + 2\beta\omega_n\dot{y}(t) + \omega_n^2\, y(t) = -\ddot{x}(t) \qquad (2.1)$$

in which y(t) is the relative displacement, the dot above y(t) indicates the derivative with respect to time, ω_n is the circular frequency, and β is the critical damping ratio.

From Eq. (2.1), the transfer function relating the ground acceleration input to the relative displacement response output can be determined by letting

$$\left.\begin{aligned} \ddot{x}(t) &= e^{i\omega t} \\ \text{and} \\ y(t) &= H_y(\omega)\, e^{i\omega t} \end{aligned}\right\} \qquad (2.2)$$

in which $H_y(\omega)$ is the transfer function for y(t), and i is the imaginary number equal to $\sqrt{-1}$. Substituting Eq. (2.2) into Eq. (2.1), the transfer function can be obtained as follows:

$$H_y(\omega) = (\omega_n^2 - \omega^2 + 2\, i\beta\omega_n\omega)^{-1} \qquad (2.3)$$

For a stationary random process, it is well known from the stationary random vibration theory (see, e.g., Ref. 9) that the output PSDF of the relative displacement response of a linear system can be related to the input PSDF of the stationary ground motion by

$$S_y(\omega) = |\, H_y(\omega)^2 \,|^2\, S_{\ddot{x}}(\omega) \qquad (2.4)$$

in which $S_{\ddot{x}}(\omega)$ is the input PSDF, and $|\, H_y(\omega)|^2$ is the transmittancy function which is the square of the transfer function amplitude given by Eq. (2.3).

With $S_y(\omega)$ given by Eq. (2.4), the mean square (ms) relative displacement response, σ_y^2, can simply be obtained by integrating $S_y(\omega)$ over all frequencies as follows:

$$\sigma_y^2 = \int_0^\infty S_y(\omega)\, d\omega \qquad (2.5)$$

Since seismic ground motion is assumed to have a zero mean, the response of a linear system will also have a zero mean. Thus, the ms response in Eq. (2.5) is the same as the variance of the

response, and the root-mean-square (rms) response, σ_y, is the same as the standard deviation of the response (Ref. 10).

For a lightly damped system, i.e., when $\beta<<1$, the ms absolute acceleration, $\sigma^2_{\ddot{z}}$, can be estimated from σ^2_y by

$$\sigma^2_{\ddot{z}} \simeq \omega_n^4 \, \sigma_y^2 \tag{2.6}$$

where the subscript $\ddot{z}(t)$ = absolute acceleration = $\ddot{x}(t) + \ddot{y}(t)$. Substituting Eqs. (2.4) and (2.5) into Eq. (2.6) gives

$$\sigma^2_{\ddot{z}} = \omega_n^4 \int_0^\infty | H_y(\omega) |^2 \; S_{\ddot{x}}(\omega) \, d\omega \tag{2.7}$$

For the case of a lightly damped system subjected to a fairly wide-band ground motion whose PSDF is slowly varying around the vicinity of $\omega = \omega_n$ where the transmittancy function is sharply peaked, Eq. (2.7) can approximately be rewritten as

$$\sigma^2_{\ddot{z}} = \omega_n^4 \, S_x(\omega_n) \int_0^\infty | H_y(\omega) |^2 \, d\omega + \int_0^{\omega_n} [\, S_{\ddot{x}}(\omega) - S_{\ddot{x}}(\omega_n) \,] \, d\omega \tag{2.8}$$

The first term in Eq. (2.8) represents the contribution of $S_x(\omega)$ around $\omega = \omega_n$, the second term is the contribution of $S_{\ddot{x}}(\omega)$ over $S_{\ddot{x}}(\omega_n)$ in the frequency range up to ω_n. Since the first term in Eq. (2.8) is identical to the widely known stationary ms absolute acceleration response to white noise ground motion having a constant PSDF of $S_{\ddot{x}}(\omega_n)$, i.e., σ^2_s, it can readily be obtained from Refs. (4 and 9) as

$$\sigma^2_s = \omega_n^4 \, S_{\ddot{x}}(\omega_n) \int_0^\infty | H_y(\omega) |^2 \, d\omega = \frac{\pi \omega_n S_{\ddot{x}}(\omega_n)}{4\beta} \tag{2.9}$$

Substituting Eq. (2.9) into Eq.(2.8) yields

$$\sigma_z^2 = A\omega_n \, S_{\ddot{x}}(\omega_n) + \sigma_{\ddot{x}}^2 \, (\omega_n) \tag{2.10}$$

in which $A = (\pi-4\beta)/4\beta$, and $\sigma_{\ddot{x}}^2(\omega_n)$ is the "partial" ms absolute acceleration as given by

$$\sigma_{\ddot{x}}^2 \, (\omega_n) = \int_0^{\omega_n} S_{\ddot{x}}(\omega) \, d\omega \tag{2.11}$$

Note that Eq. (2.10) gives exact value of $\sigma_{\ddot{z}}^2$ when the ground motion is an ideal white noise. For this case, $\sigma_{\ddot{z}}^2$ in Eq. (2.10) reduced to σ_s^2 in Eq. (2.9).

With $\sigma_{\ddot{z}}$ obtained from Eq. (2.10), the maximum absolute acceleration response, i.e., the spectral acceleration at frequency ω_n, $R_{\ddot{z}}(\omega_n)$, can approximately be determined by multiplying $\sigma_{\ddot{z}}$ with the peak factor as follows

$$R_{\ddot{z}}(\omega_n) = r_p(\omega_n) \, \sigma_{\ddot{z}} \tag{2.12}$$

in which $r_p(\omega_n')$ is the peak factor at frequency ω_n with confidence level (non-exceedance probability) of p. The peak factor is to be presented in Section 2.2.

By substituting Eq. (2.10) into Eq. (2.12), the PSDF-RS relationship for seismic ground motions can be obtained as follows

$$R_{\ddot{z}}(\omega_n) = r_p(\omega_n) \left[A\omega_n \, S_{\ddot{x}}(\omega_n) + \sigma_{\ddot{x}}^2 \, (\omega_n) \right]^{\frac{1}{2}} \tag{2.13}$$

Rearranging the terms in Eq. (2.13), gives the following

$$S_{\ddot{x}}(\omega_n) = (A\omega_n)^{-1} \left[\frac{R_{\ddot{z}}^2(\omega_n)}{r_p^2(\omega_n)} - \sigma_{\ddot{x}}^2(\omega_n) \right] \tag{2.14}$$

The PSDF-RS relationship as given in Eq. (2.13) or (2.14) is essentially identical to that previously obtained by Vanmarcke in Ref. 4.

For application to the generation of FRS as previously outlined in Section 2.1, Eq. (2.14) can be used for computing the PSDF of seismic ground motions compatible with the prescribed DRS. The numerical computation of $S_{\ddot{x}}(\omega_n)$ can be initiated at the low frequency end where $\sigma_{\ddot{z}}^2(\omega_n)$ is negligible. Let $R_i(\omega_n)$ denotes the spectral acceleration of the ith floor at frequency ω_n, Eq. (2.13) can similarly be derived for the floor responses as follows

$$R_i(\omega_n) = r_p'(\omega_n) \left[A\omega_n S_i(\omega_n) + \sigma_i^2(\omega_n) \right]^{\frac{1}{2}} \tag{2.15}$$

in which $S_i(\omega_n)$ is the PSDF of structural response at floor i, and $r_p'(\omega_n)$ is the peak factor with confidence level of p for the structural response. Accordingly, Eq. (2.15) can be used for computing the FRS from the PSDF of structural response.

2.2 Peak Factor

The peak factor previously defined in Eq. (2.12) is a multiplier to raise the rms response to the maximum (spectral) response. The determination of the analytical peak factor requires the solution of the first-passage problem in the random vibration theory. To date, the exact solution of practical interests has not been found for the SDOF system considered herein. Consequently, approximations have to be made in deriving the analytical peak factor.

From the analytical and simulation studies of normal stationary random processes in Refs. (11 and 12), it has been found that the non-exceedance probability, p, which is the probability that the random process remains below the threshold level, say b, follows a decaying-exponential form, i.e.,

$$p = p_o \, e^{-\alpha T} \tag{2.16}$$

in which p_o is the probability starting below b, α is the decay rate, and T is the duration that the process remains below b. The parameters p_o and α in Eq. (2.16) are a function of the peak factor, among others.

Once p_o and α are determined, the peak factor corresponding to a specified value of p can be determined from numerically evaluating or inverting Eq. (2.16).

2.2.1 Stationary Response

In the following, some of the widely known peak factors for stationary response which have p in the form of Eq. (2.16) are presented.

a. The Davenport Peak Factor (Ref. 13). This peak factor has been derived on the assumption that the rate of threshold crossing occurs independently according to the Poisson process. As a result of the stated assumption, the parameters p_o and α in Eq. (2.16) can be written as

$$\left.\begin{aligned} p_o &= 1 \\ \alpha &= \nu_o \exp\left(-r_p^2/2\right) \end{aligned}\right\} \tag{2.17}$$

in which λ_o is the mean rate of zero level crossing as given by

$$\nu_o = \frac{1}{\pi} \sqrt{\frac{\lambda_2}{\lambda_o}} \tag{2.18}$$

and λ_i is the ith moment of the PSDF about the frequency origin which is given by

$$\lambda_i = \int_o^\infty \omega^i \, S(\omega) \, d\omega \qquad i = 0, 1, 2 \tag{2.19}$$

Detailed interpretations of the first three spectral moments in both time and frequency domain relating to reliability measures of a random motion can be found in Ref. 14. It suffices to note that λ_o and λ_2 are the stationary ms of the process and its first time derivative, respectively, and the center frequency, f_c, which is the dominant frequency of the process is given by

$$f_c = \frac{\nu_o}{2} = \frac{1}{2\pi} \sqrt{\frac{\lambda_2}{\lambda_o}} \tag{2.20}$$

One other important parameter which can be obtained from the spectral moments is the so-called dispersion parameter, δ, a dimensionless measure of the spectral bandwidth, as given by

$$\delta = \sqrt{1 - \frac{\lambda_1^2}{\lambda_o \, \lambda_2}} \tag{2.21}$$

From Schwarz' inequality, it can be shown that δ varies from 0 for a very wide-band process to 1 for a very narrow-band process.

For a lightly damped system, the parameter ν_o in Eq. (2.18) can be approximated by

$$\nu_o = \frac{\omega_n}{\pi} \tag{2.22}$$

in which ω_n is the circular frequency of the SDOF system. Substituting Eq. (2.22) into Eq. (2.20) gives

$$f_c = \frac{\omega_n}{2\pi} = f_n \tag{2.23}$$

in which f_n is the fundamental frequency in cps of the SDOF system.

With p_o and α given in Eq. (2.17), the mean (m) and standard deviation (σ) values of the Davenport peak factor, i.e., r_m and r_σ, can approximately be determined from Eq. (2.16) as follows:

$$r_m = \sqrt{2\ell n \nu_o T} + \frac{\gamma}{\sqrt{2\ell n \nu_o T}} \tag{2.24}$$

and

$$r_\sigma = \frac{\pi}{\sqrt{6}} \cdot \frac{1}{\sqrt{2\ell n \nu_o T}} \tag{2.25}$$

in which γ is the Euler constant (0.577), and ν_o is as given by Eq. (2.22).

b. <u>The Vanmarcke Peak Factor (Ref. 15)</u>. In the derivation of the parameters p_o and α in Eq. (2.16), Vanmarcke assumes that the successive time intervals spent below and above the threshold crossing follow the Markov process. Accordingly, these parameters can be written as

$$p_o = 1 - \exp\ (-r_p^2/2)$$

$$\alpha = \nu_o \frac{[\ 1 - \exp\ (-\delta_e r_p \sqrt{\pi/2})\ ]}{\exp\ (r_p^2/2) - 1} \qquad (2.26)$$

in which $\delta_e = \delta^{1+c}$, δ is defined in Eq. (2.21), and c is empirical constant equal to 0.2. It is of interest to note that, for high threshold level ($r >> 1$), Eq. (2.26) reduces to be essentially the same as Eq. (2.17). The so-called "Vanmarcke-Exact" peak factor will be referred to as the peak factor obtained from numerical evaluation of p in Eq. (2.16) with p_o and α given by Eq. (2.26).

Substituting p_o and α in Eq. (2.26) into Eq. (2.16), the peak factor can be determined approximately as

$$r_p = [\ 2\ell n\ \{n\ [\ 1-\exp\ (-\delta_e \sqrt{\pi\ \ell n\ n}\ )\ ]\ \}\ ]^{\frac{1}{2}} \qquad (2.27)$$

in which $n = \nu_o T/\ell np$. The approximate expression in Eq. (2.27) is referred to as the Vanmarcke peak factor.

For a lightly damped system, ν_o can be approximated as in Eq. (2.22), and δ_e can be approximated as

$$\delta_e = (4\beta/\pi)^{0.6} \qquad (2.28)$$

in which β is the critical damping ratio of the SDOF system.

c. The Der Kiureghian Peak Factor (Ref. 16). Der Kiureghian obtained r_m and r_σ by modifying the Davenport peak factors in Eqs. (2.24) and (2.25), respectively, to match the m and σ of the Vanmarcke-Exact peak factor. Accordingly, r_m and r_σ can be written as

$$r_m = \sqrt{2\ell n \nu_e T} + \frac{\gamma}{\sqrt{2\ell n \nu_e T}} \qquad (2.29)$$

$$r_\sigma = \begin{cases} \dfrac{1.2}{\sqrt{2\ell n \nu_e T}} - \dfrac{5.4}{13 + (2\ell n \nu_e T)^{3.2}} & , \ \nu_e T > 2.1 \\ 0.65 & , \ \nu_e T \leq 2.1 \end{cases} \qquad (2.30)$$

in which

$$\nu_o = \begin{cases} (1.65\sigma^{0.45} - 0.38)\ \nu_o & , \ 0.1 \leq \delta < 0.69 \\ \nu_o & , \ 0.69 \leq \delta \leq 1 \end{cases} \qquad (2.31\text{-a})$$

For a lightly damped system, ν_o is approximated as in Eq. (2.22), and δ is approximated as

$$\delta = (1.16\beta^{0.15} - 0.21)^{2.2} \ , \quad \beta > 0.01 \qquad (2.31\text{-b})$$

In this report, the limit imposed on β in Eq. (2.31-b) is extended to $\beta = .5\%$.

The m and $m \pm \sigma$ values of the peak factors given above by Davenport, Vanmarcke, and Der Kiureghian, are plotted against the parameter $f_n T$, which represents the equivalent number of response cycles, for damping values of 0.5%, 2% and 5% in Figs. 2.3 through 2.8. These peak

factors are computed using the approximate values of ν_o and δ given by Eqs. (2.22) and (2.28). In these figures, the p levels corresponding to the m and m+σ values for the Vanmarcke-Exact peak factor are selected to be 57% and 84%, respectively. These selected p levels can be compared with those obtained exactly from numerically evaluated p using Eq. (2.26) with p_o and α of Eq. (2.26) as shown in Table 2.1 for the 2% damping value. It can be seen from this table that the p level of 57% for the m value is slightly higher than the average p value given in this table which is about 54%, and that the p level of 84% for the m+σ value is about the same as the average p value given in this table. The slightly higher p level selected for the m value has little effect on the peak factor value. This can also be confirmed by the fact that, in Figs. 2.3 through 2.8, the Vanmarcke-Exact peak factor with p of 57% and 84% are compared closely with the m and m+σ values of the Der Kiureghian peak factor which were derived from matching with the m and m+σ values of the Vanmarcke-Exact peak factors. Therefore, the selected p levels of 57% and 84% are adequate for use in computing the m and m+σ values of the Vanmarcke-Exact peak factor.

2.2.2 Nonstationary Response

In the following, the peak factors by Vanmarcke and by Lutes for nonstationary response are presented. These peak factors have assumed p in the form similar to Eq. (2.16) except that the parameter α in this equation is replaced by a time-dependent function, i.e., $\alpha(t)$, so that Eq. (2.16) is rewritten as

$$p = p_o e^{-\int_o^T \alpha(t)\, dt} \qquad (2.32)$$

Although p_o in Eq. (2.32) for this situation should, by definition, be set at 1 since the response process builds up from rest, the simulation studies performed herein as well as by Lutes indicate otherwise. Therefore, p_o is treated herein as an empirical parameter for nonstationry response and should not be subjected to the same interpretation as given in Eq. (2.16).

a. <u>The Modified-Vanmarcke Peak Factor (Ref 4)</u>.

For a non-stationary response, Vanmarcke has suggested that p in Eq. (2.32) be approximated as in Eq. (2.16) except that p_o is equal to 1, and the damping β and the duration T be replaced by the effective damping β_s and effective duration T_s given by

$$\left.\begin{aligned} \beta_s &= \beta \;/\; [\, 1 - \exp\,(-2\beta\omega_n T)\,] \\ T_s &= T \exp\,(-2m) \end{aligned}\right\} \qquad (2.33)$$

in which $m = -1 + [1-\exp(-2\,\beta\omega_n T]\;/[1-\exp(-\beta\omega_n\, T)]$.

By empirically modified p_o to be the same as that in Eq. (2.26), the parameters p_o and α in Eq. (2.16) now become

$$\left.\begin{aligned} p_o &= 1 - \exp\,(-r_p^2/2) \\ \alpha &= \frac{\nu_o\,[\,1 - \exp\,(-\delta_e'\, r_p\sqrt{\pi/2})\,]}{\exp\,(r_p^2/2) - 1} \end{aligned}\right\} \qquad (2.34)$$

in which $\delta_e' = (4\beta_s/\pi)^{0.6}$, ν_o is as given by Eq. (2.22), and β_s is as given by Eq. (2.33).

Another modification made on this peak factor in order to include the nonstationary effect, is the modification on

the rms response. This nonstationary effect can be approximately obtained from comparing the stationary rms response with the nonstationary rms response to white noise ground motion. It is well known that the nonstationary rms response to white noise motion, σ_n, can be written as (Refs. 4 and 9).

$$\sigma_n = \sigma_s \left[1 - \exp\left(-2\beta\omega_n T\right) \right]^{\frac{1}{2}} \qquad (2.35)$$

in which σ_s is as given by Eq. (2.9). The term following σ_s in Eq. (2.35) is a reduction factor to account for the nonstationary effect on the rms response.

With the above modifications, the Modified-Vanmarcke peak factor for nonstationary processes can be computed as follows:

1. Compute the peak factor for stationary processes for a desired level of confidence p by numerically evaluated Eq. (2.16) with p_o and α from Eq. (2.34).

2. Multiply the peak factor computed from step 1 by the reduction factor, $(1-e^{2\beta\omega_n T})^{\frac{1}{2}}$.

b. <u>The Lutes Peak Factor (Ref. 17)</u>. Lutes derived the parameter p_o and α in Eq. (2.16) empirically based on simulation studies of the first-passage probability of the absolute value of the zero-start response of a SDOF system subjected to stationary white noise ground motion. These parameters can be written as follows:

$$\left.\begin{aligned} p_o &= \exp\left[\exp\left(-1.195-0.316 r_p^2\right)\right] \\ \alpha &= \nu_o \exp\left(-r_p^2/2\right)\left\{1-1.075\left[r_p \exp\left(-r_p/2\right)\right]^W\right\} \end{aligned}\right\} \qquad (2.36\text{-a})$$

in which ν_o is as given by Eq. (2.22), and

$$\left.\begin{aligned} w &= 0.2364 + 28.14\ \delta^2 \\ \delta &= (4\beta\ (1-1.1\beta)/\pi)^{\frac{1}{2}} \end{aligned}\right\} \quad (2.36\text{-b})$$

The δ given above is about the same value as that given by Eq. (2.28) when damping β is low. The Lutes peak factor can be determined for a desired level of confidence p by numerically evaluated Eq. (2.16) with p_o and α from Eq. (2.36).

In Figs. 2.9 and 2.10, the Modified-Vanmarcke and Lutes peak factors for nonstationary responses with p of 57% and 84% are plotted against f_nT for damping values of 5%, 2% and 5%. Table 2.2, provides the exact p values for the m and m+σ values of the Lutes peak factor. It is of interest to note that the p values of 57% and 84% selected for the Lutes peak factor are about the same order of accuracy as that previously found for the Vanmarcke-Exact peak factor for a stationary process. This implies that it is adequate to use the p values of 57% and 84% for computing the m and m+σ values for the Lutes peak factor.

2.3 Evaluation and Discussions

For a stationary process, the peak factors given in Section 2.2.1 are compared in Figs. 2.3 through 2.8. It can be seen from these figures that, due to the different assumptions used in obtaining the peak factors, the Davenport peak factor generally is higher than the other peak factors, especially when damping is low. This is because the Davenport peak factor assumes that the rate of threshold crossing occurs independently according to the Poisson process. This assumption has been shown by Cramer (Ref. 12) to be asymptotically exact as the threshold crossing approaches infinity. However, for the threshold crossing level of practical interests, this assumption

has been found to produce result erring on the unsafe side for a wide-band process and on the safe side for a narrow-band process. These errors occurred because the Poisson process does not allow the time actually spent above the threshold level for a wide-band process, and does not take into account the dependent occurrence of the threshold level for a narrow-band process. The peak factor by Vanmarcke, on the other hand, includes these effects on the threshold crossing by assuming that the successive time intervals spent below and above the threshold crossing follow the Markov process. Therefore, as noted before, the Davenport peak factor represents the upper bound of the peak factor by Vanmarcke.

For a nonstationary process, the peak factors given in Section 2.2.2 are compared in Figs. 2.9 and 2.10. It can be seen from these figures that the Modified-Vanmarcke peak factor is generally lower than the Lutes peak factor when $f_n T$ is less than about 10; otherwise, it is higher than the Lutes peak factor. These two peak factors, however, approach each other as damping increases from 0.5% to 5%.

The analytical peak factors discussed above, however, have not been adequately verified for their accuracies for actual applications. Since the accuracy of the PSDF-RS relationship required in the explicit approach depends on the accuracy of the peak factor and the rms response, it is necessary that the accuracy of these peak factors and the rms response be confirmed against simulation results.

The accuracy of the PSDF-RS relationship for both the wide-band seismic ground motion and the narrow-band floor response are systematically evaluated in Sections 3 through 7 using simulation results. In Section 3, the PSDF compatible with the 2% damping response spectrum from the USNRC R.G. 1.60 is generated from the PSDF-RS relationship with the use of the Der Kiureghian peak factor. Using this PSDF, twenty acceleration time histories are simulated for the wide-band stationary and nonstationary ground motions in Section 4. Also presented in Section 4 are the simulated results for

evaluating the accuracy of the PSDF-RS relationship for the wide-band ground motions in Section 7. The simulated narrow-band floor responses of a typical nuclear power plant containment structure are obtained in Section 6 by filtering the simulated wide-band ground motions in Section 4 with the structural response transfer functions presented in Section 5. Using the simulated results obtained from Sections 4 and 6, the accuracy of the analytical PSDF-RS relationship is then evaluated for the wide-band seismic ground motions and the narrow-band floor responses in Section 7.

3. PSDF FOR WIDE-BAND SEISMIC GROUND MOTIONS

For the purpose of generating the PSDF for the wide-band seismic ground motion, the design response spectra (DRS) from the USNRC R.G. 1.60 for the horizontal seismic ground motion with 1.0g maximum acceleration is used. The generated PSDF compatible with the 2% damping DRS will be used later in Section 4 for simulation of seismic ground motions.

The response spectra from the USNRC R.G. 1.60 are shown in Fig. 3.1 for 0.5%, 2%, and 5% damping values. These spectra were developed from statistical evaluations of a number of recorded seismic ground motions for the $m+\sigma$ confidence level, which was based on the 84.1% non-exceedance probability assuming a normal distribution for the spectral values (Ref. 1). In order to examine the PSDF of these recorded motions, forty-five of them as listed in Table 3.1 are selected. The raw data on the response spectral values and the Fourier amplitudes of these selected recorded motions for the 91 frequencies listed in Table 3.2 are obtained from the ground motion data tape supplied by the California Institute of Technology (Cal Tech). Using these raw data normalized to 1.0g maximum acceleration, the $m + \sigma$ level response spectra are computed and plotted as shown in Figs. 3.2 through 3.4 for 0%, 2% and 5% damping, respectively. The response spectra shown in these figures are consistent with those used as the basis in Ref. 1 for developing the USNRC R.G. 1.60 DRS shown in Fig. 3.1. Therefore, the forty-five recorded motions selected constitutes an adequate sample size for the computation of the PSDF compatible with the USNRC R.G. 1.60 spectra. It should be noted that, in Ref. 1, the normalization factors with respect to velocity and displacement are also used in minimizing the statistical variations of the response spectra. In order to show the statistical variations of the response spectra computed in Figs. 3.2 through 3.4, the coefficient of variation (COV) which is a dimensionless measure of the dispersion relative to the mean is computed as follows:

$$COV = \sigma/m \qquad (3.1)$$

The COV's corresponding to the the response spectra in Figs. 3.2 through 3.4 are computed using Eq. (3.1) for 0%, 2%, and 5% damping values and are shown in Fig. 3.5. It can be seen from this figure that COV gradually decreases as frequency increases. This trend of variation was also found in Ref. (1) when the maximum acceleration was used as the normalization factor. Note that COV at .1 cps is about 1 and decreases to as low as .08 for the 5% damping curve.

In order to approximately compute the PSDF of these recorded motions, these recorded motions are assumed to be a stationary process with duration T. Accordingly, the one-sided PSDF of these recorded motions can be approximated as follows:

$$S_{\ddot{x}}(\omega) = \frac{2}{N} \sum_{i=1}^{N} \left| \frac{\ddot{x}_i(\omega)}{T} \right|^2 \qquad (4.1)$$

where N is the total number of recorded motions equal to 45, T is the equivalent stationary duration, and $| \ddot{x}_i(\omega) |$ is the Fourier amplitude of the ith recorded motion obtained from Cal Tech. The duration T used in Eq. (4.1) is selected to be 15 seconds which is a typical duration of strong phase motion for high-intensity seismic motions. However, by visual examination of these recorded motions in Ref. 18, their strong phase durations are found to be varying from about 3 to 20 seconds. Thus, the duration of 15 seconds selected for T in Eq. (4.1) is merely an approximation of the duration of an ensemble of these recorded motions, treated as a stationary process. In Fig. 3.6, the PSDF of these recorded motions computed from Eq.(4.1) is plotted against frequency in cps. It can be seen from this figure that this PSDF is fairly wide-banded covering frequency ranging from about .25 cps to 2.5 cps.

In order to generate the analytical PSDF compatible with the USNRC R.G. 1.60 response spectra, the PSDF-RS relationship in Eq. (2.14) with the peak factor corresponding to the $m+\sigma$ level as prescribed for the spectra is used. The PSDF generated using Der Kiureghian peak factor in Eq. (2.14) is shown in Fig. 3.7, and the PSDF generated using the

Modified-Vanmarcke peak factor is shown in Fig. 3.8. Three response spectral curves corresponding to the .5%, 2% and 5% damping are shown in each figure. It is apparent from these figures that the PSDF's corresponding to the different damping response spectra are different. This implies that the USNRC R.G. 1.60 response spectra for different damping values can not be associated with a single random process. Furthermore, it can be seen by comparing Fig. 3.7 with Fig. 3.8 that the PSDF in Fig. 3.8 are higher than those in Fig. 3.7 especially for low damping values and in the low frequency range up to about 2.5 cps. This is because the peak factor used for generating the PSDF in Fig. 3.8 includes the nonstationary effect which reduces the stationary ms response for a lightly damped and soft system. Thus, in order to achieve the same response spectral value in Eq. (2.14), the PSDF in Fig. 3.8 obtained from using the nonstationary peak factor must be higher than that in Fig. 3.7 obtained from using the stationary peak factor. Comparing the analytical PSDF shown in Figs. 3.7 and 3.8 with the empirical PSDF shown in Fig. 3.6, it can be seen that the empirical PSDF is generally higher than the analytical PSDF in the low frequency range up to about 4 cps, but is lower in the higher frequency range. This difference can be attributed to the approximation used in computing the empirical PSDF according to Eq. (3.2).

4. SIMULATION OF WIDE-BAND SEISMIC GROUND MOTIONS

Using the PSDF for the wide-band seismic ground motions generated in the previous section, twenty acceleration time histories are simulated in Section 4.1 for the stationary seismic ground motion, and in Section 4.2 for the nonstationary seismic ground motion. The m and m+σ levels of response spectra of these simulated ground motions are then presented. In Section 4.1, the spectral moments of the absolute acceleration response to stationary ground motions and the simulated peak factors are also presented.

4.1 Stationary Ground Motion

The stationary ground motion, $\ddot{x}_s(t)$ is simulated using the Fast Fourier Transform (FFT) algorithm as follows:

$$\ddot{x}_s(t) = \frac{1}{2\pi} \mathrm{Re} \left\{ \sum_{k=1}^{N} \left[2 \sqrt{S_{\ddot{x}}(\omega_k)} \; e^{i\phi_k} \right] e^{i\omega_k t} \, \Delta\omega \right\} \qquad (4.1)$$

in which $S_{\ddot{x}}(\omega_k)$ is the PSDF corresponding to the 2% damping value in Fig. 3.7, ϕ_k is the phase angle with a uniform distribution in the range from 0 to 2π, $\omega_k = k\Delta\omega$, $\Delta\omega = 0.42$ radian per second, and the total number of sample points, N, is 1024. Therefore, the duration of the simulated stationary ground motion is 15 seconds digitized at a time increment of 0.0146 seconds. The maximum accelerations of the 20 simulated stationary ground motions are tabulated in Table 4.1. As shown in this table, the maximum ground acceleration varies from 0.77g to 1.23g with the m value of 0.95g and the m+σ value of 1.06g, which is close to 1.0g maximum ground acceleration specified for the DRS.

A typical stationary ground motion simulated using Eq. (4.1) and its response spectra for .5%, 2%, and 5% damping are plotted as shown in Figs. 4.1 and 4.2, respectively. The response spectra are computed for the 47 frequencies listed in Table 4.1. The m and m+σ response spectra are plotted as shown in Figs. 4.3 through 4.5 for .5%, 2%,

and 5% damping, respectively. It can be seen from comparing Fig. 4.2 with Fig. 4.3 through Fig. 4.5 that the m and m+σ response spectra are smoother than the response spectra generated from a single ground motion. The statistical variations of the response spectral values measured by the COV of Eq. (3.1) are shown in Fig. 4.6. It can be seen that the COV of spectral value of stationary ground motions is, on the average, fairly constant at about 0.15, and is less than the COV in Fig. 3.5 obtained for the ensemble of 45 recorded ground motions which varies from 1 to .1.

The properties of the PSDF of absolute acceleration response to stationary ground motions, which are closely related to the peak factor as shown in Section 2, are presented in Figs. 4.7 through 4.9. In Fig. 4.7, the square root of the three spectral moments, $\sqrt{\lambda_o}$, $\sqrt{\lambda_1}$, and $\sqrt{\lambda_2}$ are plotted against frequency in cps for 2% damping system. The spectral moments λ_s' in this figure are computed numerically from Eq. (2.19) in which $S(\omega)$ is obtained from multiplying Eq. (2.4) with the factor $(\omega_n^4 + 4\beta^2\omega_n^2\omega^2)$. Note that, since $\sqrt{\lambda_o}$ is the rms absolute acceleration response, the rms ground acceleration can be approximately obtained from Fig. 4.1 as the $\sqrt{\lambda_o}$ value at f ≈ 25 cps which is about 120 in/sec^2 or 0.3g. The spectral moments in Fig. 4.1 are used for computing the center frequency, f_c, in Eq. (2.20), and the spectral dispersion parameter in Eq. (2.21). In Fig. 4.8, the simulated f_c computed from Eq. (2.20) is plotted as the solid line, and the analytical f_c estimated by Eq. (2.23) as the dotted line. Similarly, the simulated δ computed from Eq. (2.21) is plotted as the solid line in Fig. 4.9 and the analytical δ estimated from Eq. (2.28) plotted as the dotted line. It can be seen from these figures that the analytical f_c and δ estimated from Eq. (2.23) and Eq. (2.28) compared on the average, quite well with the corresponding simulation results in the frequency range of less than 10 cps. When frequency exceeds 10 cps, the analytical f_c is higher but the analytical δ is lower than the corresponding simulated value. This difference, however, would produce small changes in the peak factor in Eq. (2.27).

Consequently, the estimated values of the analytical f_c and δ as given by Eq. (2.23) and Eq. (2.28), respectively, can be used with sufficient accuracy for computing the analytical peak factors, which also compare well with the simulated peak factors as will be shown in Section 7.1.1.

The simulated m and m+σ peak factors for 2% damping can be computed from Eq. (2.12) by dividing the m and m+σ response spectral values in Fig. 4.4 with $\sqrt{\lambda_o}$ in Fig. 4.7. Similar computations of the peak factor are also performed for .5% and 5% damping values. The simulated m and m+σ peak factors are plotted against frequency in cps in Figs. 4.10 through 4.12 for the three damping values respectively.

In Section 7.1.1, the simulation results presented in this subsection for the m and m+σ response spectra, $\sqrt{\lambda_o}$, and the peak factor will be used for the validation of the PSDF-RS relationship for stationary wide-band ground motions.

4.2 Nonstationary Ground Motion

The nonstationary ground motion, $\ddot{x}_N(t)$ is simulated as follows:

$$\ddot{x}_N(t) = E(t)\,\ddot{x}_S(t) \qquad (4.2)$$

in which $\ddot{x}_S(t)$ is the stationary ground motion as given by Eq. (4.1), and E(t) is the envelope function. The envelope functions used are the so-called Types B and C envelope functions proposed by Housner, Jenning and Tsai (Ref. 19). These envelope functions are shown in Fig. 4-13. For brevity, the nonstationary ground motion using Types B and C envelope functions will be referred to as the Type B ground motion and the Type C ground motion.

For the Type B ground motion, the duration used for simulation is 30 seconds digitized at a time increment of 0.0146 seconds. A typical of this ground motion and its response spectra for .5%, 2% and 5%

damping are shown in Figs. 4.14 and 4.15, respectively. The m and m±σ response spectra for these three damping values are shown in Figs. 4.16 through 4.18. The COV of spectral values for Type B ground motion spectra is plotted in Fig. 4.19. By comparing Fig. 4.19 with Fig. 4.6, it can be seen that the COV for the Type B ground motion is slightly larger than the COV for stationary ground motion.

For the Type C ground motion, the duration used for simulation is 12 seconds digitized at .0117 seconds. A typical of this ground motion and its response spectra for .5%, 2% and 5% damping are shown in Figs. 4.20 and 4.21, respectively. The m and m±σ response spectra for these three damping values are shown in Figs. 4.22 through 4.24. The COV of spectral values for Type C ground motion are plotted in Fig. 4.25. By comparing Fig. 4.25 with Fig. 4.19, it can be seen that the COV for the Type C ground motion has slightly more variation than the Type B ground motion.

It is apparent from the above comparisons of the COV of spectral values for stationary ground motions with that for Type B or Type C ground motions that the longer is the strong phase (stationary) duration, the smaller is the amount of relative dispersion.

The m and m±σ response spectra obtained from simulation for Types B and C ground motions as shown in Figs. 4.16 through 4.18, and Figs. 4.21 through 4.24, respectively, will be used for validation of the PSDF-RS relationship in Section 7.1.2 for nonstationary wide-band ground motion.

5. STRUCTURAL TRANSFER FUNCTIONS

In order to study the structural response due to seismic ground motions, the transfer functions of the containment and its internal structure of a pressurized water reactor (PWR) nuclear power plant are used as a typical example in this study. These structural transfer functions serves as filters to transfer the simulated wide-band seismic ground motions in Section 4 to the output of narrow-band floor responses to be described in Section 6.

The PWR containment and its internal structures supported on a flexible soil foundation are shown in Fig. 5.1. The mathematical model of the soil-structure system is also shown in Fig. 5.1 as a lumped-mass stick model consisting of 19 nodes and 16 beam elements, with the soil stiffness and damping represented by springs and viscous dampers attached to the base of structures at node 19. The properties of the structures, and the soil foundation are provided in Table 5.1, and Fig. 5.1, respectively. This soil-structure system has one translational dynamic degree-of-freedom (DDOF) per node and one rotational DDOF at node 19.

Using the Bechtel in-house computer program CE933 (FASS), the transfer functions relating the ground acceleration input to the absolute acceleration responses are computed for node 11 (top of the containment structure), and node 18 (top of the internal structure). Since this computer program requires that the fixed-base structures be characterized by their modal properties, the modal properties of the fixed-base structures are computed using the Bechtel in-house computer program CE917. The four lowest modal properties obtained from this computer run as shown in Table 5.2 are then used as the input to the computer program CE933 to compute the structural transfer functions for nodes 11 and 18 shown in Fig. 5.2.

It can be seen from Fig. 5.2 that the structural transfer functions for nodes 11 and 18 exhibit typical narrow-band filtering characteristics with two dominant peaks. The frequencies corresponding to these two dominant peaks are 3.4 cps and 17 cps for node 11, and 3.4 cps and 11 cps for node 18. These frequencies correspond to the system frequencies of the soil-structure interaction system.

6. SIMULATION OF NARROW-BAND FLOOR RESPONSES

The narrow-band floor responses for nodes 11 and 18 of the soil-structure system shown in Fig. 5.1 are simulated by filtering the wide-band seismic ground motions in Section 4 through the respective structural transfer functions in Section 5. The floor responses to stationary ground motions and to nonstationary ground motions are separately presented in Sections 6.1 and 6.2, respectively.

6.1 Responses to Stationary Ground Motion

The absolute acceleration response time histories for nodes 11 and 18 of the soil-structure system shown in Fig. 5.1 subjected to the 20 stationary ground motions generated in Section 4.1 are computed using the computer program CE933 (FASS). This computer program has the capability to perform the seismic soil-structure interaction analysis using the impedance approach and frequency domain analysis method via the Fast Fourier Transform (FFT) algorithm. The typical time history responses to one simulated ground motion time history input for nodes 11 and 18 are plotted in Figs. 6.1 and 6.2, respectively. The maximum accelerations for the 20 simulated stationary response motions for nodes 11 and 18 are tabulated in Table 6.1. As shown in this table, the maximum response acceleration varies from 3.3g to 4.7g with the m and $m+\sigma$ values of 3.8g and 4.1g for node 11, and from 2.5g to 3.9g with the m and $m+\sigma$ values of 2.9g and 3.2g for node 18. The response spectra of the response motions shown in Figs. 6.1 and 6.2 for .5%, 2%, and 5% damping are shown in Figs. 6.3 and 6.4, respectively. The m and $m+\sigma$ floor response spectra for nodes 11 and 18 for all 20 time history inputs are plotted for the same three damping values in Figs. 6.5 through 6.7, and Figs. 6.8 through 6.10, respectively. The statistical variations of these floor response spectral values measured by the COV computed from Eq. (3.1) are shown in Fig. 6.11 for node 11, and in Fig. 6.12 for node 18. By comparing Figs. 6.11 and 6.12 with Fig. 4.6, it can be seen that the COV of spectral value of the floor response motions are about the same order

of variation as that of the stationary ground motions in Fig. 4.6.

The PSDF's of the absolute acceleration floor response for nodes 11 and 18 are plotted against frequency in cps as shown in Fig. 6.13. These PSDF's are obtained from multiplying the absolute acceleration structural response transmittancy functions, which are the square of the transfer function amplitudes in Fig. 5.2, with the PSDF of the stationary ground motion in Fig. 3.7. In order to obtain the PSDF of the absolute acceleration floor spectral response, the PSDF of the absolute acceleration floor response in Fig. 6.13 is multiplied by the absolute acceleration transmittancy of a SDOF system having frequency f_n and damping β. The spectral properties of the PSDF of the absolute acceleration floor spectral response are plotted against frequency f_n in cps for damping β of 2% in Figs. 6.14 through 6.16 for node 11, and Figs. 6.17 through 6.19 for node 18. The square root of the three spectral moments, $\sqrt{\lambda_o}$, $\sqrt{\lambda_1}$ and $\sqrt{\lambda_2}$ shown in Figs. 6.14 and 6.17 for nodes 11 and 18, respectively, are computed according to Eq. (2.19). It can be seen that $\sqrt{\lambda_o}$ at 25 cps for nodes 11 and 18, which approximately are the rms absolute acceleration floor responses, are about 500 and 370 in/sec^2, or 1.3 and 0.96g, respectively. Using the three spectral moments in these figures, the center frequency, f_c, and the spectral dispersion parameter δ can accordingly be computed from Eqs. (2.20) and (2.21), respectively. The computed f_c and δ are plotted in Figs. 6.15 and 6.16 respectively for node 11, and Figs. 6.18 and 6.19 respectively for node 18. In these figures, the analytical f_c and δ computed from Eq. (2.23) and Eq. (2.28) are also plotted as dotted lines. It can be seen that the analytical f_c compares well with the simulated f_c when frequency is less than 10 cps, and is higher than the simulated f_c when frequency is greater than 10 cps. This difference between the analytical and the simulated f_c is very similar to that previously observed for the wide-band ground motion response in Section 4. On the other hand, the comparison of the analytical δ with the simulated δ for the narrow-band floor response in Figs. 6.16 and 6.19 does not show as good a comparison with that for the

wide-band ground motion in Fig. 4.9. The analytical δ is generally lower than the simulated δ except around the system frequencies at 3.4 and 11 cps where the analytical δ is higher than the simulated δ. This difference implies that the analytical peak factor in Eq. (2.27) with the analytical δ tends to overestimate the analytical peak factor with the simulated δ around the system frequencies and underestimate the analytical peak factor with the simulated elsewhere. As will be shown in Section 7.2.1, the estimated f_c and δ can be used with reasonable accuracy for computing the analytical peak factors for the narrow-band floor response, which generally compare well with the simulated peak factors, except near the system frequencies where slight overestimates result.

Using the m and m+δ floor response spectral values derived from the simulation and the rms response which is equal to $\sqrt{\lambda_o}$, the simulated m and m+σ peak factors for 2% damping can be computed for nodes 11 and 18, by respectively dividing the m and m+σ floor response spectral values in Figs. 6.6 and 6.9 with the $\sqrt{\lambda_o}$ values in Figs. 6.14 and 6.17. The simulated m and m+σ peak factors for 0.5% and 5% damping can be computed similarly. The resulting peak factors are shown in Figs. 6.20 through 6.22 for Node 11 and Figs. 6.23 through 6.25 for Node 18. As will be described in Section 7.2.1, these simulated peak factors will be used for validating the analytical PSDF-RS relationship presented in Section 2 for narrow-band floor response to stationary ground motion input.

6.2 Responses to Nonstationary Ground Motion

The absolute acceleration response motions for nodes 11 and 18 of the soil-structure system shown in Fig. 5.1 subjected to 20 simulated Type B nonstationary ground motion time histories are computed using the computer program CE933, and representative resulting time history responses are plotted in Figs. 6.26 and 6.27, respectively for Nodes 11 and 18. Their respective response spectra for .5%, 2% and 5%

damping are plotted in Figs. 6.28 and 6.29. The m and m+σ floor response spectra for three damping values computed from all 20 Type B time history inputs are plotted in Figs. 6.30 through 6.32 for node 11, and Fig. 6.33 through 6.35 for node 18.

The m and m+σ floor response spectra presented in this section will be used later in Section 7.2.2 for the validation of the analytical PSDF-RS relationship for the narrow-band floor responses to Type B nonstationary ground motion input.

The simulation of the narrow-band floor response to Type C ground motion inputs has not been performed since, as will be explained in Section 7.1.2, the analytical PSDF-RS relationship with the use of Modified-Vanmarcke peak factor and the equivalent stationary duration is found to be too conservative for the Type C ground motion response.

7. VALIDATION OF THE PSDF-RS RELATIONSHIP

The simulation results presented in Section 4 for the wide-band seismic ground motions and Section 6 for the narrow-band floor responses are used in this section to validate analytical the PSDF-RS relationship presented in Section 2.1.

7.1 Wide-Band Seismic Ground Motions

The validity and accuracy of the analytical PSDF-RS relationship is evaluated in Section 7.1.1 for the stationary ground motion, and Section 7.1.2 for the nonstationary ground motion. In Section 7.1.1, the accuracies of the analytical rms response and peak factor contained in the PSDF-RS relationship are also explicitly evaluated for the stationary ground motion. In Section 7.1.2, the validity of the PSDF-RS relationship for the nonstationary ground motion is evaluated using the equivalent stationary duration to represent the stationary portion of Types B and C ground motions.

7.1.1 Stationary Ground Motion

In order to evaluate the accuracy of the analytical rms responses given in Eq. (2.10), these analytical rms responses are compared with the simulated rms responses obtained in Section 4, as shown in Fig. 7.1 for .5%, 2% and 5% damping. The PSDF compatible with the 2% damping DRS is used in Eq. (2.10) for $S_{\ddot{x}}(\omega)$ in computing the analytical rms response. It can be seen from these comparisons that the analytical rms response generally compares well with the simulated rms response. Thus, the accuracy resulting from using the analytical rms response given in Eq. (2.10) to predict the rms response to the stationary wide-band ground motion is confirmed.

In order to evaluate the accuracy of the analytical peak factors shown in Figs. 2.3 through 2.10, these analytical

peak factors with duration T of 15 seconds are compared with the simulated m and m+σ peak factors shown in Figs. 4.10 through 4.12 for .5%, 2% and 5% damping, respectively. Based on these comparisons, the analytical peak factor that compares best with the simulated peak factor, is the Modified-Vanmarcke peak factor. The comparisons of the Modified-Vanmarcke peak factor with the simulated peak factor at the m and m+σ levels can also be seen in Figs. 7.2 through 7.4 for .5%, 2% and 5% damping, respectively. It is apparent from these figures that the Modified-Vanmarcke peak factor compares closely with the simulated peak factors.

The comparisons of the analytical peak factors in Figs. 2.3 through 2.8 with the simulated peak factors in Figs. 4.10 through 4.12 show that the Davenport and Der Kiureghian peak factors overestimate the simulated m and m+σ peak factors especially when the frequency and damping are low. As mentioned in Section 2.3, this overestimation can be attributed to the inaccuracy of the independent threshold crossings assumption made for the Davenport peak factor, and the neglect of the nonstationarity of the response by these two peak factors eventhough the input ground motion is stationary.

By comparing Figs. 2.9 and 2.10 with Figs. 4.10 through 4.12, it can be seen that the Lutes peak factor slightly underestimates the simulated m and m+σ peak factors when frequency exceeds 1 cps, and slightly overestimates the simulated m and m+σ peak factors when frequency is less than 1 cps. This difference may be due to the use of ideal white noise instead of the more realistic wide-band seismic ground motion for the derivation of the Lutes empirical peak factor. In summary, among the analytical peak factors surveyed in Section 2.2, the Modified-Vanmarcke peak factor gives the most accurate prediction as compared to the simulated peak

factor for the case of stationary wide-band ground motion input.

In order to evaluate the validity and accuracy of the PSDF-RS relationship for the stationary wide-band ground motion, the m and m+σ response spectra generated from the analytical PSDF-RS relationship are compared with the simulated m and m+σ response spectra in Figs. 7.5 through 7.7 respectively for .5%, 2% and 5% damping. The analytical m and m+σ response spectra, shown as dotted lines in these figures, are computed from Eq. (2.13) using the analytical rms response and the Modified-Vanmarcke peak factor. The simulated m and m+σ response spectra, shown as solid lines in these figures, are obtained from Section 4.1, Figs. 4.3 through 4.5. As can be seen in Figs. 7.5 through 7.7, the analytical m and m+σ response spectra compare closely with the simulated m and m+σ response spectra. Thus, the validity and accuracy of the PSDF-RS relationship in Eq. (2.13) with the use of the analytical rms response and the Modified-Vanmarcke peak factor, is confirmed for the stationary wide-band ground motion input.

7.1.2 Nonstationary Ground Motion

Since the PSDF-RS relationship derived in Section 2.1 is based on the assumption of stationary ground motion input, it is necessary that, for this relationship to be applicable to Types B and C nonstationary ground motion inputs, the ground motion duration T be characterized by an equivalent stationary motion duration, T_e. Various methods of determining T_e for nonstationary ground motions have been proposed in the literatures (e.g., Refs. 20 and 21). The method selected here for determining T_e is similar to that proposed by Trifunac and Brady in Ref. 20. The equivalent stationary duration, T_e, is defined as follows:

$$T_e = T_{.90} - T_{.05} \qquad (7.1)$$

where $T_{.90}$ and $T_{.05}$ are the times respectively corresponding to 90% and 5% of the total energy of the ground motion represented by the integral I(t) as follows:

$$I(t) = \int_0^t \ddot{x}_N^2(t)\, dt \qquad , 0 \leq t \leq T \qquad (7.2)$$

Note that the limits on input energy used by Trifunac and Brady in Ref. 22 are 5% and 95%. These limits have been modified to 5% and 90% because it has been found that T_e without modification would produce too conservative predictions on the response spectra. Using Eq. (7.1), the average values of T_e are determined to be 14 and 5 seconds, from the total durations of 30 and 12 seconds used for the Types B and C ground motion simulation, respectively.

For Type B ground motions, the validity and accuracy of the PSDF-RS relationship is evaluated by comparing the analytical m and m+σ response spectra with the simulated m and m+σ response spectra, as shown in Figs. 7.8 through 7.10 for .5%, 2% and 5%, respectively. The analytical m and m+σ response spectra plotted as dotted lines in these figures are computed from using T_e = 14 seconds, the analytical rms response, and the Modified-Vanmarcke peak factor in Eq. (2.13). The simulated m and m+σ response spectra plotted as solid lines in these figures are obtained from Section 4.2, Figs. 4.16 through 4.18. As can be seen from Figs. 7.8 through 7.10, the analytical m and m+σ response spectra compare closely with the simulated m and m+σ response spectra, respectively. Thus, the validity and accuracy of the PSDF-RS relationship in Eq. (2.13) with the use of T_e, the analytical rms response, and the Modified-Vanmarcke peak factor, is confirmed for Type B nonstationary ground motions.

For Type C ground motions, the validity and accuracy of the PSDF-RS relationship is evaluated by comparing the analytical m and m+σ response spectra with the simulated m and m+σ response spectra, as shown in Figs. 7.11 through 7.13 respectively for .5%, 2%, and 5% damping. The analytical m and m+σ response spectra, plotted in these figures as dotted lines, are computed from using T_e = 5 seconds, the analytical rms response, and the Modified-Vanmarcke peak factor in Eq. (2.13). The simulated m and m+σ response spectra plotted as solid lines in these figures are obtained from Section 4.2, Figs. 4.22 through 4.24. As can be seen from Figs. 7.11 through 7.13, the analytical m and m+σ response spectra generally overestimate the corresponding simulated m and m+σ response spectra, especially in the low to medium frequency range.

This is because the Type C ground motion has relatively short strong intensity portion to allow response to reach stationary. Thus, the PSDF-RS relationship in Eq.(2.13) with the use of T_e, the analytical rms response, and the Modified-Vanmarcke peak factor result in conservative estimates on the response spectra of Type C ground motion.

Based on the above findings, it can be concluded that the PSDF-RS relationship in Eq. (2.13) can be applied with sufficient accuracy for the nonstationary wide-band ground motion whose transient characteristics are similar to the Type B ground motion with an equivalent stationary duration as defined by Eq. (7.1) to be about 14 seconds.

7.2 Narrow-Band Floor Response

The validity and accuracy of the analytical PSDF-RS relationship is evaluated in Section 7.2.1 for the narrow-band floor responses to stationary ground motion, and in Section 7.2.2 for the narrow-band

floor responses to nonstationary ground motion. The accuracies of the analytical rms response and the peak factor contained in this relationship are also explicitly evaluated in Section 7.2.1. Using the same equivalent stationary duration determined in Section 7.1.2 for the Type B ground motion, the validity and accuracy of the PSDF-RS relationship is evaluated for narrow-band floor responses to Type B nonstationary ground motion. The validity and accuracy of the analytical PSDF-RS relation for narrow-band floor responses to the Type C ground motion will not be evaluated, since it has been found in Section 7.1.2 that it results in too conservative response estimates for the Type C ground motion response.

7.2.1 Responses to Stationary Motion

In order to evaluate the accuracy of the analytical rms response given in Eq. (2.10) for this case, the analytical rms floor spectral responses for .5%, 2%, and 5% damping are compared with the corresponding simulated rms floor spectral responses, as shown in Figs. 7.14.a through 7.14.c for node 11, and Figs. 7.15.a through 7.15.c for node 18. The analytical rms floor spectral responses for nodes 11 and 18 are computed from using Eq. (2.10) with $S_{\ddot{X}}(\omega)$ equal to their respective PSDF shown in Fig. 6.13. The simulated rms floor spectral responses for nodes 11 and 18 are obtained from Section 6, e.g., the simulated rms floor spectral responses for 2% damping are shown as $\sqrt{\lambda_0}$ in Figs. 6.14 and 6.17 for nodes 11 and 18, respectively. As can be seen from the comparisons in Figs. 7.14 and 7.15, the analytical rms floor spectral response overestimates the peaks and underestimates the valleys of the simulated rms floor spectral response. Thus, the analytical rms response given in Eq. (2.13) cannot be accurately used for predicting the narrow-band rms floor spectral response to stationary ground motions. Therefore, the simulated rms floor spectral response should be used instead of the analytical rms response for a more accurate prediction of the floor response spectra.

In order to evaluate the accuracy of the analytical peak factors shown in Figs. 2.3 through 2.10, these analytical peak factors are compared with their respective simulated peak factors in Figs. 6.20 through 6.22 for node 11, and Figs. 6.23 through 6.25 for node 18. The results from these comparisons are that the Modified-Vanmarcke peak factor can be used with reasonable accuracy for predicting the narrow-band floor response to stationary ground motion input, except near the system frequencies where slight overestimates occur.

Due to the inaccuracy of the analytical rms response, the analytical PSDF-RS relation in Eq. (2.15) cannot be expected to be accurate for predicting the narrow-band floor response spectra. To improve the accuracy, Eq. (2.12) with the simulated rms response in Figs. 7.14 and 7.15 and the Modified-Vanmarcke peak factor, can be used for generating the floor response spectra. The analytical m and $m \pm \sigma$ floor response spectra as generated are compared respectively with the simulated m and $m \pm \sigma$ floor response spectra in Figs. 7.22 through 7.24 for node 11, and Figs. 7.25 through 7.27 for node 18. The analytical and simulated m and $m \pm \sigma$ floor response spectra are plotted in these figures as dotted and solid lines, respectively. As can be seen from Figs. 7.22 through 7.27, the analytical m and $m \pm \sigma$ floor response spectra generally compare reasonably well with the simulated m and $m \pm \sigma$ floor response spectra. Thus, these comparison results confirm that the analytical floor response spectra of the narrow-band floor response motion to the stationary wide-band ground motion input, can be computed with reasonable accuracy from Eq. (2.12) with the use of the simulated rms floor spectral response, i.e. the rms floor spectral response given by $\sqrt{\lambda_o}$ and the Modified-Vanmarcke peak factor, except near the system frequencies where slight overestimates occur.

7.2.2 Response to Nonstationary Ground Motion

The equivalent stationary duration of 14 seconds as previously determined in Section 7.1.2 is used in generating the analytical m and m+σ floor response spectra of the narrow-band floor responses to the Type B ground motion. As in Section 7.2.1, the analytical m and m+σ floor response spectra are computed from using Eq. (2.12) with the simulated rms response and the Modified-Vanmarcke peak factor. These computed analytical m and m+σ floor response spectra are compared with the simulated m and m+σ floor response spectra in Figs. 7.28 through 7.30 for node 11, and Figs. 7.31 through 7.33 for node 18. The simulated and analytical response spectra are plotted in these figures as solid and dotted lines, respectivley. The simulated m and m+σ floor response spectra shown in these figures are obtained from Section 6.2, Figs. 6.30 through 6.32 for node 11, and Figs. 6.33 through 6.35 for node 18. As can be seen from Figs. 7.28 through 7.33, the analytical m and m+σ floor response spectra generally compare reasonably well with the simulated m and m+σ floor response spectra. Thus, these comparison results confirm that the analytical floor response spectra of the narrow-band floor response motion to the Type B ground motion input, can be computed with reasonable accuracy from Eq. (2.12) with the use of the simulated rms floor spectral response given by $\sqrt{\lambda_o}$ and the Modified-Vanmarcke peak factor, except near the system frequencies where slight overestimates occur.

8. DIRECT GENERATION OF PROBABILISTIC FLOOR RESPONSE SPECTRA

Based on the evaluation results in Section 7, the probabilistic floor response spectra (FRS) with any desired confidence levels can be generated directly with reasonable accuracy from the prescribed design ground response spectrum (DRS) as follows, see Fig. 8.1:

1. Compute the ground motion PSDF from the prescribed DRS using the PSDF-RS relationship in Eq. (2.14) with the Modified-Vanmarcke peak factor given in Section 2.2.1-b. The approximate values of δ in Eq. (2.28) and ν_o in Eq. (2.22) are used for computing the Modified-Vanmarcke peak factor.

2. Compute the structural response transmittancy function which is the square of the amplitude of the structural response transfer function.

3. Compute the structural response PSDF by multiplying the ground PSDF in Step 1 with the structural response transmittancy function in Step 2.

4. Compute the floor spectral response PSDF by multiplying the structural response PSDF in Step 3 with the transmittancy function of a SDOF system with specified spectral frequency and the desired spectral damping ratio.

5. Compute the rms floor spectral response by taking the square root of the area under the floor spectral response PSDF in Step 4.

6. Compute the floor spectral response value by multiplying the rms floor spectral response in Step 5 with the Modified-Vanmarcke peak factor in Step 1.

7. Generate the floor response spectrum for the desired spectral damping ratio by repeating the computations from Step 4 to Step 6 using different spectral frequencies for the SDOF system in Step 4.

The probabilistic FRS generated from the above procedure generally compare reasonably well with those obtained from simulations as shown in Section 7, although the floor spectral values at the peaks corresponding to the system frequencies are found to be slightly overestimated relative to the simulated results. These slight overestimates on the floor spectral response values at the peaks can be attributed to the slight overestimates on the Modified-Vanmarcke peak factor values at the system frequencies resulting from using the approximate value of δ in the above Step 6. As shown in Section 6.2, the approximate value of δ for the narrow-band floor response tends to overestimate the simulated (exact) value of δ near the system frequencies, and underestimate the exact value of δ elsewhere. As a result, the Modified-Vanmarcke peak factor computed from using the approximate value of δ for the narrow-band floor response tends to be higher than that computed from using the exact value of δ near the system frequencies, and lower than that computed from using the exact value of elsewhere. Therefore, in order to improve the accuracy of the probabilistic FRS at the system frequencies relative to the simulated results, the exact value of δ in Eq. (2.21) may be used, instead of the approximate value of δ in Eq. (2.28), for computing the Modified-Vanmarcke peak factor for the narrow-band floor response in the above Step 6. This, in effect, would lower the floor response spectral values near the peaks and raise the floor response spectral values, elsewhere, producing more accurate estimates near the peaks and slight overestimates elsewhere. The slight overestimates on the floor response spectral values in the high frequency range, however, can be reduced to improve the accuracy relative to the simulated results, by using the exact value of ν_o in Eq. (2.18) instead of the approximate value of ν_o in Eq. (2.22) for computing the Modified-Vanmarcke peak factor for the narrow-band floor response in the above Step 6. As shown in Section 6.1, the simulated center frequency computed from using the exact value of ν_o generally compares closely with the analytical center frequency computed from using the approximate value of ν_o, except in the high frequency region where the simulated frequency is smaller than the analytical center frequency. In fact, as frequency increases, the simulated center frequency approaches the center frequency of the floor response motion,

whereas the analytical center frequency approaches a large value. As a result, the Modified-Vanmarcke peak factor computed from using the exact value of ν_o is always smaller than that computed from using the approximate value of ν_o in the high frequency range.

In summary, the accuracies of the probabilistic FRS at the system frequencies as well as in the high frequency region relative to the simulated results may be improved by the use of the exact values of δ and ν_o for determining the Modified-Vanmarcke peak factor for the narrow-band floor response in the above Step 6. In the following section, the application of the proposed procedure of generating the probabilistic FRS discussed above is demonstrated for a typical nuclear power plant subjected to seismic ground motions. The effects on the probabilistic FRS due to the use of the exact values of δ and ν_o will also be discussed.

The spectra generated with the procedure proposed herein carry the following implied assumptions:

1. The structural system is linear.

2. The prescribed DRS for the seismic ground motion is for a low damping value and a known confidence level.

3. The seismic ground motion is a normal wide-band random process, and its nonstationarity can be characterized by an equivalent stationary process.

4. Similarly, the structural response to the seismic ground motion can be characterized by an equivalent stationary random process.

For practical applications, assumptions 1 and 2 can generally be met by the design requirements. However, in order to satisfy assumptions 3 and 4, the seismic ground motion, which is a nonstationary process, should have a sufficiently long equivalent stationary duration T_e as defined in Eq. 7.1, as compared to the lowest period T_1 of the structural system.

The results in Section 7 indicate that, when the ratio of T_e/T_1 is greater than about 40, the probabilistic response spectra can be generated from the above procedure with reasonable accuracy. However, when T_e/T_1 is less than about 40, the probabilistic response spectra as generated from the above procedure can be expected to be conservative.

9. APPLICATIONS

Applications of the proposed procedure for generating the probabilistic FRS directly from the prescribed DRS in Section 8 are demonstrated in this section. The probabilistic FRS of a typical nuclear power plant structure subjected seismic ground motions prescribed in the form of DRS are generated using the proposed procedure, and presented in details. Also, presented are the comparisons between the probabilistic FRS and the deterministic FRS generated from using a single time history compatible with the prescribed DRS, in order to provide some insights into the relative merits of the proposed procedure and the deterministic method currently used in practice. The analysis model used for generating the FRS is essentially the same as the soil-structure model of a typical nuclear power plant shown in Fig. 5.1, except that the structures are now fixed at the base. The material and sectional properties of the fixed-base structures are provided in Table 5.1. A constant damping value of 2% is assigned for the five lowest modes used in the analyses.

The 2% damping response spectrum from the USNRC R.G. 1.60 shown as a dashed line in Fig. 9.1 is used to prescribe the DRS at m+σ level (i.e., p = 84%) for seismic ground motions. Also shown as a solid line in this figure is the 2% damping response spectrum of the synthetic time history shown in Fig. 9.2. This synthetic time history is used as input for generating the deterministic FRS. The equivalent duration, T_e, of this synthetic time history used as input for generating the probabilistic FRS is determined from Eq. (7.1) to be about 12 seconds.

Using the proposed procedure in Section 8, the 2% damping FRS at m+σ level for nodes 11 and 18 are generated. The results obtained from various steps in the proposed procedure are plotted as shown in Fig. 9.3 through Fig. 9.16. Fig. 9.3 shows the Modified-Vanmarcke peak factor for seismic ground motions, computed from using the approximate values of δ and ν_o. The PSDF of ground motions computed according to Step 1 of the proposed procedure is shown in Fig. 9.4. The structural response transfer functions for nodes 11 and 18 required in Step 2 of the proposed procedure

are shown in Figs. 9.5 and 9.6, respectively. The PSDF's of the floor response motions at nodes 11 and 18 computed according to Step 3 of the proposed procedure are shown in Figs. 9.7 and 9.8, respectively. The spectral dispersion parameter δ for the PSDF's of the floor response motions at nodes 11 and 18 are plotted in Figs. 9.9 and 9.10, respectively. In each of these figures, the approximate value of δ computed from Eq. (2.21) and the exact value of δ computed numerically from Eq. (2.28) are plotted as dashed and solid lines, respectively. Similarly, the approximate and exact values of center frequency f_c computed from Eqs. (2.20) and (2.23), respectively, which equal to $\nu_o/2$, are plotted in Fig. 9.11 for node 11, and Fig. 9.12 for node 18. The Modified-Vanmarcke peak factor for floor spectral response computed from using the approximate and exact values of δ and ν_o are plotted respectively as dashed and solid lines in Fig. 9.13 for node 11, and Fig. 9.14 for node 18. Following Steps 4 through 6 of the proposed procedure, the probabilistic FRS at $m+\sigma$ level computed from using the approximate values and the exact values of δ and ν_o are generated and shown as dotted lines in Figs. 9.15 and 9.17 for node 11, and Figs. 9.16 and 9.18 for node 18, respectively.

The deterministic FRS generated from performing a time history analysis of the fixed-base structures subjected to the synthetic time history shown in Fig. 9.2 are also shown as solid lines in Figs. 9.15 and 9.17 for node 11, and Figs.9.16 and 9.18 for node 18.

It can be seen from Figs. 9.15 and 9.16 that the probabilistic FRS computed from using the approximate values of δ and ν_o compare reasonably well with the deterministic FRS, except at the spectral peaks and in the high frequency region where the probabilistic FRS are higher than the deterministic FRS.

As discussed in Section 8, the accuracy of the floor response spectral values at the peaks and in the high frequency region can be improved by using the exact values of δ and ν_o for computing the Modified-Vanmarcke peak factors in Step 6 of the proposed procedure. The effects of using

the exact values rather than the approximate values of δ and ν_o on the Modified-Vanmarcke peak factor can be seen in Figs. 9.13 and 9.14 for nodes 11 and 18, respectively. The comparisons in these figures clearly show that the Modified-Vanmarcke peak factor using the exact values of δ and ν_o is generally lower near the system frequencies and in the high frequency region, but is slightly higher elsewhere than that using the approximate values of δ and ν_o. This same trend applies to the FRS as can be seen from comparing Figs. 9.15 and 9.16 with Figs. 9.17 and 9.18, respectively.

The comparison of the probabilistic FRS generated from using the exact values of δ and ν_o with the deterministic FRS as shown in Figs. 9.17 and 9.18, shows that the probabilistic FRS remain slightly higher near the system frequencies and in the high frequency region than those of the deterministic FRS. These differences can be attributed to the fact that the probabilistic FRS are generated based on treating an ensemble of seismic ground motions as an equivalent normal stationary random process, whereas the deterministic FRS are generated from using a single time history analysis. Furthermore, these differences could also be contributed by the fact that the nonstationarity of seismic ground motions is treated approximately as an equivalent stationary process in the generation of the probabilistic FRS.

Since the comparisons in Figs. 9.17 and 9.18 show that the probabilistic FRS at $m+\sigma$ level generated from the prescribed DRS at the same confidence level generally are consistently slightly more conservative than the deterministic FRS currently used in practice, and since the cost of generating the probabilistic FRS is much less than that by the deterministic method, the proposed approach in Section 8 can effectively be used to generate the FRS for use in a preliminary or generic seismic qualification of equipment and piping in a nuclear power plant.

10. SUMMARY AND CONCLUSIONS

The procedure for a direct generation of the probabilistic FRS from the prescribed DRS for seismic ground motions has been developed and presented in Section 8. This procedure, which can be used to generate the FRS for any desired level of confidence, makes explicit use of the PSDF-RS relationship in Section 2.1, which contains two key parameters - the rms response and the peak factor. This relationship has been systematically evaluated using simulation results for the wide-band ground motions and for the narrow-band floor response motions. Various widely-known peak factors were also included in the evaluation.

Twenty time histories were simulated in Section 4 for each of the three types of the wide-band ground motions, namely, the stationary, Types B and C nonstationary ground motions, considered in the evaluations. These simulated time histories were generated from the PSDF compatible with the 2% damping response spectrum from the USNRC R.G. 1.60. The PSDF's corresponding to the different damping of the USNRC R. G. 1.60 response spectra were found to be different; therefore, they cannot be associated with a single random process. The narrow-band floor response motions considered in the evaluation were simulated in Section 6 for a typical nuclear power plant structure subjected to both the wide-band stationary and Type B nonstationary ground motions.

Based on the evaluation results of the PSDF-RS relationship in Section 7, the major findings can be summarized as follows:

1. For the wide-band stationary ground motion, the response spectra at m and m+σ levels generated from the PSDF-RS relationship, with the use of the Modified-Vanmarcke peak factor computed from using the approximate values of δ and ν_0, are sufficiently accurate as compared with those obtained from simulations.

2. For the wide-band Type B nonstationary ground motion, the findings on the validity and accuracy of PSDF-RS relationship were similar to those found for the wide-band stationary ground motion. An equivalent

stationary duration of this type of ground motions computed from Eq. (7.1) and used in the PSDF-RS relationship, was about 14 seconds.

3. For the wide-band, Type C nonstationary ground motion, the m and $m+\sigma$ response spectra generated from the PSDF-RS relationship were found to be too conservative, especially when damping is low, as compared with the simulation results. An equivalent stationary duration of this ground motion computed from Eq. (7.1) and used in the PSDF-RS relationship, was about 5 seconds.

4. For the narrow-band floor response motions to the wide-band stationary ground motion input, the PSDF-RS relationship as used for the wide-band motions can not be used with sufficient accuracy as compared with the simulation results, due to the inaccuracy of the rms response contained in the PSDF-RS relationship. It was, however, found that the accuracy can be improved with the use of the rms floor spectral response computed numerically from the floor spectral response PSDF. With this improvement, the generated floor response spectra at the m and $m+\sigma$ levels were found to be reasonably accurate, with slight overestimates at the spectral peaks, as compared to the simulation results.

5. For the narrow-band floor response motions to the wide-band Type B nonstationary ground motion input, the findings on the validity and accuracy of the PSDF-RS relationship are similar to those found for the narrow-band floor response motions to the wide-band stationary ground motion input.

Based on the above findings, it can be concluded that the procedure presented in Section 8 can be used for generating the probabilistic FRS directly from the prescribed DRS with reasonable accuracy as compared to the simulation results, except for the values near the floor response spectral peaks where slight overestimates result. The accuracy of the floor response spectral values at the peaks and in the high frequency region can, however, be improved by using the exact values of δ and ν_o computed numerically from the floor spectral response PSDF instead of

using the approximate values of δ and ν_o for computing the Modified-Vanmarcke peak factor for the floor spectral response. This was demonstrated in the application in Section 9. Thus it may be concluded that, in order to improve the accuracy of the floor response spectral values at the peaks and in the high frequency region generated from the procedure in Section 8, different peak factors should be used for the wide-band ground motions and for the narrow-band floor response motions.

The comparisons between the probabilistic FRS and the deterministic FRS generated from using the conventional time history analysis demonstrated in Section 9, show that the probabilistic FRS generally are slightly more conservative than the deterministic FRS, and that the use of the exact values of δ and ν_o gives spectral values at the peaks and in the high frequency region closer to those of the deterministic FRS than those generated from using the approximate values of δ and ν_o.

The generation of probabilistic FRS using the proposed procedure is found to be very cost-effective as compared with the use of the deterministic method. For the example demonstrated in Section 9, the cost of probabilistic FRS is about one fourth of the cost of the deterministic FRS. The cost effectiveness is expected to be even larger for system with many more degrees-of-freedom. Because of its cost effectivenesss, this procedure can effectively be used for generating FRS for a preliminary or generic design and qualification purposes. Further refinements of the proposed procedure for generating the probabilistic FRS may be possible. However, such refinements must be based upon further studies on the floor responses to actual seismic ground motions which are inherently nonstationary.

11. REFERENCES

1. Newmark, N. M., Blume, J. A., and K.K. Kanpur, "Seismic Design Spectra for Nuclear Power Plants," ASCE Structural Engineering Meeting, San Francisco, April, 1973.

2. Singh, M. P., "Seismic Design Input for Secondary Systems," ASCE, ST2, February, 1980.

3. Atalik, T.S., "Instructure Spectra from Ground Spectra," Journal of Earthquake Engineering and Structural Dynamics, to be published in 1984.

4. Vanmarcke, E. H., "Structural Response to Earthquakes" in Seismic Risk and Engineering Decisions, Lomnitz, C. and E. Rosenblueth, Editors, Elsevier Publishing Co., Amsterdam, 1976.

5. Grossmayer, R., "A Response-Spectrum Based Probabilistic Design Method," the Sixth European Conference on Earthquake Engineering, Yugoslavia, September, 1978.

6. Romo-Organista, M. P., "Soil-Structure Interaction in a Random Seismic Environment," Ph.D. Dissertation, U.C., Berkeley, January, 1977.

7. Der Kiureghian, A., Sackman, J. L., and B. Nour-Omid, "Dynamic Analysis of Light Equipment in Structures: Response to Stochastic Input," ASCE, EM1, February, 1983.

8. Newmark, N. M., and Rosenblueth, E., Fundamentals of Earthquake Engineering, Prentice Hall, Inc., N. J., 1971.

9. Lin, Y. K., Probabilistic Theory of Structural Dynamics, McGraw-Hill Book Co., N. Y., 1967.

10. Feller, W., An Introduction to Probability Theory and Its Applications, Vol. I, John Wiley & Sons, Inc., N. Y., 1968.

11. Crandall, S. H., "First-Crossing Probabilities of the Linear Oscillator," Journal of Sound and Vibration, London, Vol. 12, No. 3, 1970.

12. Cramer, H., "On the Intersections Between the Trajectories of a Normal Stationary Stochastic Process and a High Level," Arkiv. Mat., Vol. 6, 1966.

13. Davenport, A. G., "Note on the Distribution of the Largest Value of a Random Function with Application to Gust Loading," Proc. Inst. Civ. Eng., Vol. 28, 1964.

14. Vanmarcke, E. H., "Properties of Spectral Moments with Applications to Random Vibration," ASCE, EM2, Vo. 98, April, 1972.

15. Vanmarcke, E. H., "On the Distribution of the First-Passage Time for Normal Stationary Random Processes," Jour. Appl. Mech., Vol. 42, March, 1975.

16. Der Kiureghian, A., "Structural Response to Stationary Excitation," ASCE, EM6, December, 1980.

17. Lutes, L.D., Chen, Y.-T. T., and Tzuang, S.H., "First-Passage Approximations for Simple Oscillators," ASCE, EM, December, 1980.

18. "Strong-Motion Earthquake Accelerograms Digitized and Plotted Data," Vol. II - Corrected Accelerograms and Integrated Ground Velocity and Displacement Curves, Cal Tech Reports, EERL 71-50, 72-50, 72-51, 72-52, 74-50, 74-53.

19. Jennings, P. C., Housner, G. W., and Tsai, N. C, "Simulated Earthquake Motions," Earthquake Engineering Research Laboratory, Cal Tech, April, 1968.

20. Trifunac, M. D., and Brady, A. G., "A Study on the Duration of Strong Earthquake Ground Motion," Bulletin of the Seismological Society of America, June, 1975.

21. Vanmarcke, E. H., and Lai, S.-S. P., "Strong-Motion Duration of Earthquakes," MIT Publication No. R77-16, Dept. of Civil Engineering, July, 1977.

TABLE 2.1 THE VANMARCKE-EXACT PEAK FACTOR AT m AND m + σ LEVELS FOR 2% DAMPING

f_nT	r_m	r_σ	$r_{m+\sigma}$	p for r_m	p for $r_{m+\sigma}$
3.000	.1727+01	.6312+00	.2358+01	.5346+00	.8397+00
4.500	.1864+01	.6170+00	.2481+01	.5319+00	.8406+00
6.000	.1971+01	.6035+00	.2575+01	.5304+00	.8413+00
7.500	.2059+01	.5912+00	.2650+01	.5295+00	.8419+00
9.000	.2133+01	.5802+00	.2713+01	.5291+00	.8424+00
10.500	.2196+01	.5703+00	.2766+01	.5290+00	.8429+00
12.000	.2251+01	.5613+00	.2813+01	.5291+00	.8432+00
13.500	.2300+01	.5532+00	.2854+01	.5292+00	.8435+00
15.000	.2344+01	.5459+00	.2890+01	.5295+00	.8438+00
16.500	.2384+01	.5392+00	.2923+01	.5298+00	.8440+00
18.000	.2420+01	.5331+00	.2953+01	.5301+00	.8442+00
19.500	.2453+01	.5275+00	.2980+01	.5304+00	.8444+00
21.000	.2483+01	.5223+00	.3006+01	.5307+00	.8446+00
22.500	.2512+01	.5175+00	.3029+01	.5310+00	.8447+00
24.000	.2539+01	.5130+00	.3051+01	.5313+00	.8449+00
27.000	.2586+01	.5049+00	.3091+01	.5320+00	.8451+00
30.000	.2628+01	.4977+00	.3126+01	.5326+00	.8453+00
33.000	.2666+01	.4914+00	.3158+01	.5331+00	.8455+00
36.000	.2701+01	.4856+00	.3186+01	.5336+00	.8456+00
39.000	.2732+01	.4805+00	.3213+01	.5341+00	.8458+00
42.000	.2761+01	.4758+00	.3237+01	.5346+00	.8459+00
45.000	.2788+01	.4715+00	.3259+01	.5350+00	.8460+00
49.500	.2824+01	.4656+00	.3290+01	.5356+00	.8462+00
54.000	.2857+01	.4604+00	.3318+01	.5362+00	.8463+00
60.000	.2897+01	.4543+00	.3351+01	.5369+00	.8464+00
66.000	.2932+01	.4489+00	.3381+01	.5375+00	.8466+00
70.500	.2956+01	.4452+00	.3401+01	.5379+00	.8467+00
75.000	.2978+01	.4419+00	.3421+01	.5383+00	.8468+00
82.500	.3013+01	.4367+00	.3450+01	.5389+00	.8469+00
90.000	.3044+01	.4322+00	.3477+01	.5394+00	.8470+00
97.500	.3073+01	.4281+00	.3501+01	.5399+00	.8471+00
105.000	.3099+01	.4245+00	.3523+01	.5403+00	.8472+00
112.500	.3123+01	.4211+00	.3544+01	.5407+00	.8473+00
120.000	.3145+01	.4180+00	.3563+01	.5411+00	.8474+00
127.500	.3166+01	.4152+00	.3581+01	.5415+00	.8475+00
135.000	.3186+01	.4126+00	.3598+01	.5418+00	.8475+00
150.000	.3221+01	.4079+00	.3629+01	.5424+00	.8477+00
165.000	.3253+01	.4037+00	.3657+01	.5429+00	.8478+00
180.000	.3282+01	.4000+00	.3682+01	.5433+00	.8479+00
195.000	.3309+01	.3967+00	.3705+01	.5437+00	.8480+00
210.000	.3332+01	.3937+00	.3725+01	.5441+00	.8481+00
225.000	.3355+01	.3910+00	.3746+01	.5445+00	.8481+00
247.500	.3385+01	.3873+00	.3772+01	.5449+00	.8482+00
270.000	.3413+01	.3840+00	.3797+01	.5453+00	.8483+00
300.000	.3446+01	.3801+00	.3826+01	.5458+00	.8484+00
330.000	.3476+01	.3767+00	.3852+01	.5462+00	.8485+00
375.000	.3515+01	.3723+00	.3887+01	.5468+00	.8487+00

TABLE 2.2 THE LUTES PEAK FACTOR AT m AND m + σ LEVELS FOR 2% DAMPING

f_nT	r_m	r_σ	$r_{m+\sigma}$	p for r_m	p for $r_{m+\sigma}$
3.000	.1184+01	.4913+00	.1675+01	.5334+00	.8391+00
4.500	.1425+01	.5233+00	.1949+01	.5522+00	.8450+00
6.000	.1589+01	.5383+00	.2127+01	.5589+00	.8441+00
7.500	.1712+01	.5461+00	.2259+01	.5608+00	.8425+00
9.000	.1811+01	.5502+00	.2362+01	.5604+00	.8411+00
10.500	.1894+01	.5520+00	.2446+01	.5592+00	.8401+00
12.000	.1964+01	.5526+00	.2517+01	.5575+00	.8395+00
13.500	.2026+01	.5522+00	.2578+01	.5557+00	.8390+00
15.000	.2080+01	.5513+00	.2631+01	.5539+00	.8388+00
16.500	.2129+01	.5499+00	.2679+01	.5522+00	.8387+00
18.000	.2173+01	.5483+00	.2721+01	.5506+00	.8386+00
19.500	.2213+01	.5465+00	.2760+01	.5491+00	.8387+00
21.000	.2250+01	.5446+00	.2795+01	.5478+00	.8387+00
22.500	.2285+01	.5426+00	.2827+01	.5466+00	.8389+00
24.000	.2317+01	.5405+00	.2857+01	.5454+00	.8390+00
27.000	.2374+01	.5363+00	.2910+01	.5435+00	.8393+00
30.000	.2425+01	.5322+00	.2957+01	.5419+00	.8396+00
33.000	.2470+01	.5281+00	.2998+01	.5406+00	.8400+00
36.000	.2511+01	.5241+00	.3036+01	.5396+00	.8403+00
39.000	.2549+01	.5203+00	.3069+01	.5387+00	.8407+00
42.000	.2583+01	.5166+00	.3100+01	.5380+00	.8410+00
45.000	.2615+01	.5131+00	.3128+01	.5374+00	.8412+00
49.500	.2658+01	.5081+00	.3166+01	.5367+00	.8416+00
54.000	.2697+01	.5034+00	.3200+01	.5362+00	.8420+00
60.000	.2744+01	.4975+00	.3241+01	.5357+00	.8424+00
66.000	.2785+01	.4922+00	.3277+01	.5354+00	.8428+00
70.500	.2814+01	.4884+00	.3302+01	.5353+00	.8431+00
75.000	.2840+01	.4849+00	.3325+01	.5352+00	.8433+00
82.500	.2880+01	.4794+00	.3360+01	.5352+00	.8436+00
90.000	.2917+01	.4744+00	.3391+01	.5353+00	.8439+00
97.500	.2950+01	.4698+00	.3419+01	.5354+00	.8442+00
105.000	.2980+01	.4655+00	.3445+01	.5356+00	.8444+00
112.500	.3008+01	.4616+00	.3469+01	.5357+00	.8446+00
120.000	.3033+01	.4580+00	.3491+01	.5359+00	.8448+00
127.500	.3057+01	.4546+00	.3512+01	.5361+00	.8450+00
135.000	.3080+01	.4514+00	.3531+01	.5364+00	.8451+00
150.000	.3121+01	.4456+00	.3566+01	.5368+00	.8454+00
165.000	.3157+01	.4404+00	.3597+01	.5372+00	.8456+00
180.000	.3190+01	.4358+00	.3626+01	.5376+00	.8458+00
195.000	.3219+01	.4317+00	.3651+01	.5380+00	.8460+00
210.000	.3247+01	.4279+00	.3675+01	.5384+00	.8462+00
225.000	.3270+01	.4244+00	.3696+01	.5388+00	.8463+00
247.500	.3306+01	.4197+00	.3726+01	.5393+00	.8465+00
270.000	.3337+01	.4155+00	.3753+01	.5398+00	.8466+00
300.000	.3374+01	.4105+00	.3785+01	.5403+00	.8468+00
330.000	.3407+01	.4062+00	.3813+01	.5408+00	.8470+00
375.000	.3451+01	.4005+00	.3851+01	.5415+00	.8472+00

TABLE 3.1 EARTHQUAKE ACCELEROGRAMS CONSIDERED

Earthquake	Year	Recording Station	Component	Peak Ground Acceleration, in g Units
El Centro (Imperial Valley)	1940	El Centro	S00E S90W	.35 .21
Ferndale (NW California)	1951	Ferndale	S44W N46W	.104 .112
Kern Co.	1952	Taft	N21E S69E	.16 .18
Kern Co.	1952	Hollywood Storage Basement	S00W N90W	.055 .044
Kern Co.	1952	Hollywood Storage PE Lot	S00W N90E	.059 .042
Eureka	1954	Eureka	N11W N79E	.17 .26
Eureka (Ferndale)	1954	Ferndale	N44E N46W	.159 .201
El Centro (El Alamo)	1956	El Centro	S00W S90W	.033 .051
San Francisco	1957	Golden Gate Park	N10E S80E	.08 .10
Hollister	1961	Hollister	S01W N89W	.065 .179
El Centro (Borrego Mtn)	1968	El Centro	S00W S90W	.130 .057
El Centro (Lower California)	1934	El Centro	S00W S90W	.16 .18
Helena	1935	Helena	S00W S90W	.15 .15
Olympia (W. Washington)	1949	Olympia	N04W N86E	.16 .28
Olympia (Puget Sound)	1965	Olympia	S04E S86W	.14 .20
Parkfield	1966	Cholame-Shandon No. 2	N6SE	.49

TABLE 3.1 EARTHQUAKE ACCELEROGRAM CONSIDERED (CONT'D)

Earthquake	Year	Recording Station	Component	Peak Ground Acceleration, in g Units
Parkfield	1966	Cholame-Shandon No. 5	N05W N85E	.35 .43
Parkfield	1966	Temblor #2	N65W S25W	.27 .35
San Fernando	1971	Pacoima Dam	S16E S74W	1.171 1.076
San Fernando	1971	V. N. Holiday Inn (8244 Orion)	N00W S90W	.25 .13
San Fernando	1971	Castaic ORR	N21E N69W	.32 .27
San Fernando	1971	Bank of California (15250 Ventura Bl) basement	N11E N79W	.22 .15
San Fernando	1971	Universal-Sheraton (3838 Lankershim) basement	N00E S90W	.17 .15

TABLE 3.2 LIST OF 91 FREQUENCIES IN CPS

.06670	.07140	.07690	.08330	.09090	.10000	.10500	.11100
.11800	.12500	.13300	.14300	.15400	.16700	.18200	.20000
.20800	.21700	.22700	.23800	.25000	.26300	.27800	.29400
.31300	.33300	.35700	.38500	.41700	.45500	.50000	.52600
.55600	.58800	.62500	.66700	.71400	.76900	.83300	.90900
1.00000	1.05000	1.11000	1.18000	1.25000	1.33000	1.43000	1.54000
1.67000	1.82000	2.00000	2.08000	2.17000	2.27000	2.38000	2.50000
2.63000	2.78000	2.94000	3.12000	3.33000	3.57000	3.85000	4.17000
4.55000	5.00000	5.26000	5.56000	5.88000	6.25000	6.67000	7.14000
7.69000	8.33000	9.09000	10.00000	10.50000	11.10000	11.80000	12.50000
13.30000	14.30000	15.40000	16.70000	18.20000	20.00000	20.80000	21.70000
22.70000	23.80000	25.00000					

TABLE 3.3 MAXIMUM ACCELERATION OF SIMULATED STATIONARY GROUND MOTIONS

Ground Motion No.	Maximum Acceleration, in g Unit
1	1.09
2	0.83
3	0.86
4	1.13
5	0.77
6	1.04
7	0.84
8	1.06
9	0.86
10	0.91
11	0.83
12	0.83
13	0.86
14	0.89
15	0.92
16	0.92
17	0.98
18	1.23
19	0.92
20	0.88

TABLE 4.1 LIST OF 47 FREQUENCIES IN CPS

.200+00	.300+00	.400+00	.500+00	.600+00	.700+00	.800+00	.900+00
.100+01	.110+01	.120+01	.130+01	.140+01	.150+01	.160+01	.180+01
.200+01	.220+01	.240+01	.260+01	.280+01	.300+01	.330+01	.360+01
.400+01	.440+01	.470+01	.500+01	.550+01	.600+01	.650+01	.700+01
.750+01	.800+01	.850+01	.900+01	.100+02	.110+02	.120+02	.130+02
.140+02	.150+02	.165+02	.180+02	.200+02	.220+02	.250+02	

TABLE 5.1

PROPERTIES OF THE STRUCTURAL MODELS OF THE CONTAINMENT BUILDING AND INTERNALS

(*Concrete Modulus E = 6.9 x 10^5ksf, G=2.7 x 10^5ksf)

Joint Properties				Member Properties			
Mass No.	m_i (kips)	$I_i x 10^{-6}$ (kip-ft^2)		Location between Joint No.	Area (ft^2)	Shear Area (ft^2)	Moment of Inertia x 10^{-6} (ft^4)
19	20000	21.1					
1	4600	9.4		19 to 1	1400	700	2.8
2	4200	8.5		1 to 2			
3				2 to 3			
4				3 to 4			
5				4 to 5			
6			CONTAINMENT	5 to 6			
7	4610	9.4		6 to 7			
8	3020	5.9		7 to 8	990	500	1.9
9	2470	3.7		8 to 9			1.5
10	2120	1.7		9 to 10			0.8
11	190	0.1		10 to 11			0.2
12	2800	2.4		19 to 12	2000	1320	1.1
13	2510	1.9		12 to 13	2560	1560	1.2
14	6290	5.0		13 to 14	2210	1460	1.2
15	3760	6.6		14 to 15	1960	730	1.3
16	8540	12.6	INTERNALS	15 to 16	1740	600	0.9
17	1220	0.8		16 to 17	780	360	0.2
18	820	0.1		17 to 18	190	70	0.004

TABLE 5.2 FIXED-BASE MODAL PROPERTIES OF THE CONTAINMENT BUILDING AND INTERNALS

Mode No.	Frequency (CPS)	Participating Factor	Damping (%)
1	5.26*	30.1	2
2	11.95#	13.5	2
3	16.24#	-13.4	2
4	17.48#	-20.4	2

Notes: * - Frequencies of the fixed-base containment structure

- Frequencies of the fixed-base internal system

TABLE 6.1 MAXIMUM RESPONSE ACCELERATIONS TO STATIONARY GROUND MOTIONS

Response Motion No.	Maximum Acceleration in g	
	Node No. 11	Node No. 18
1	3.93	2.92
2	3.68	2.51
3	3.33	2.81
4	3.79	2.69
5	3.60	3.24
6	3.89	2.93
7	3.68	2.97
8	3.92	2.79
9	4.02	3.47
10	4.25	3.18
11	4.06	2.73
12	3.52	2.76
13	3.96	2.76
14	3.41	3.25
15	4.05	2.62
16	3.67	3.94
17	3.56	2.93
18	3.63	2.69
19	3.97	2.61
20	4.68	2.72

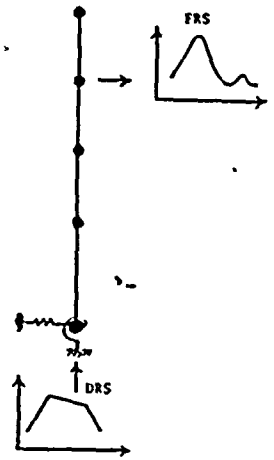

Fig. 2.1 Schematic Diagram of Implicit Approach

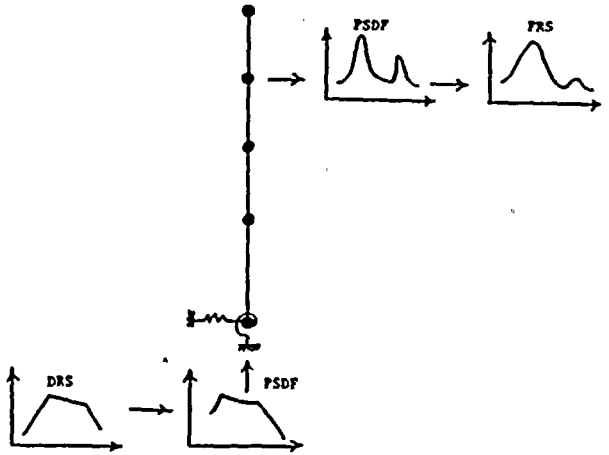

Fig. 2.2 Schematic Diagram of Explicit Approach

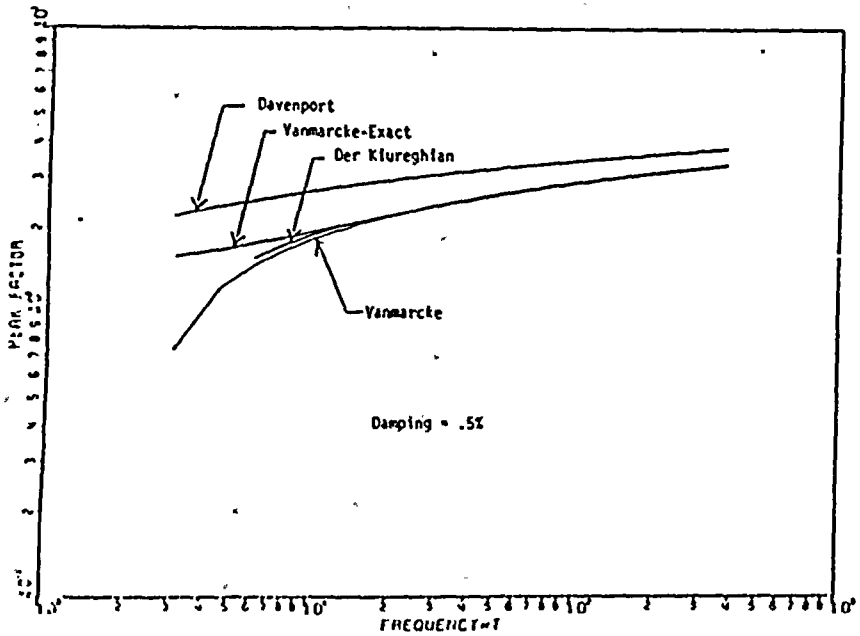

Fig. 2.3 Analytical Peak Factors with Non-Exceedance Probability of 5%

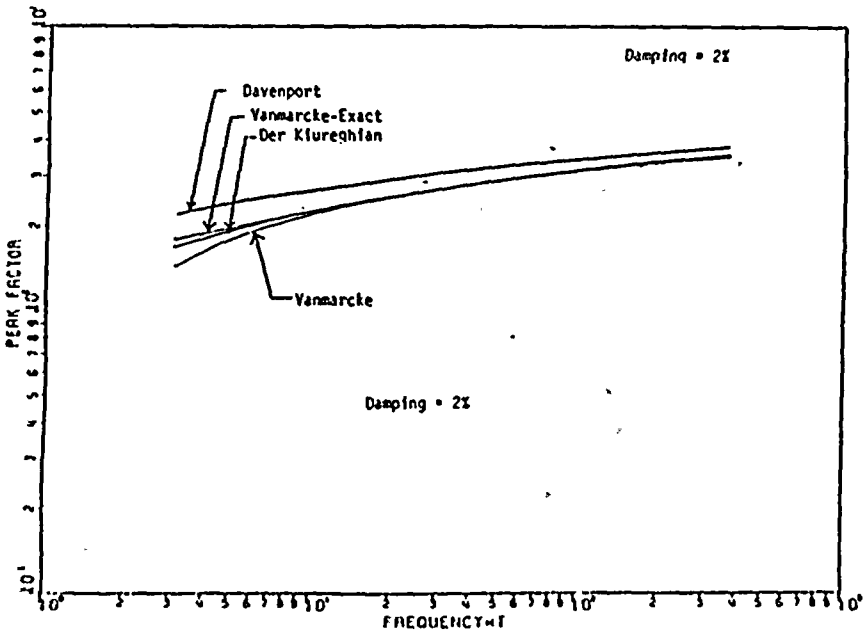

Fig. 2.4 Analytical Peak Factors with Non-Exceedance Probability of 57%

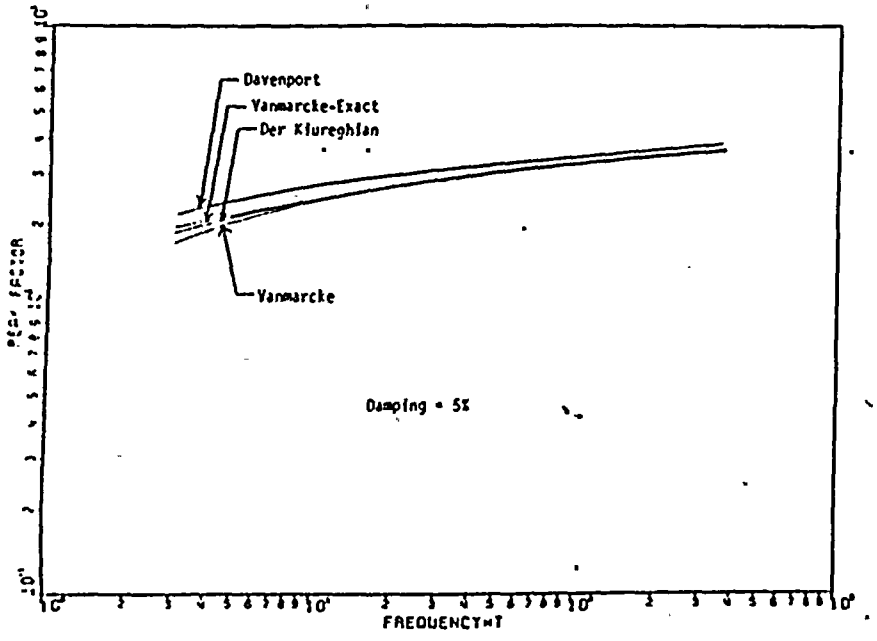

Fig. 2.5 Analytical Peak Factors with Non-Exceedance Probability of 57%

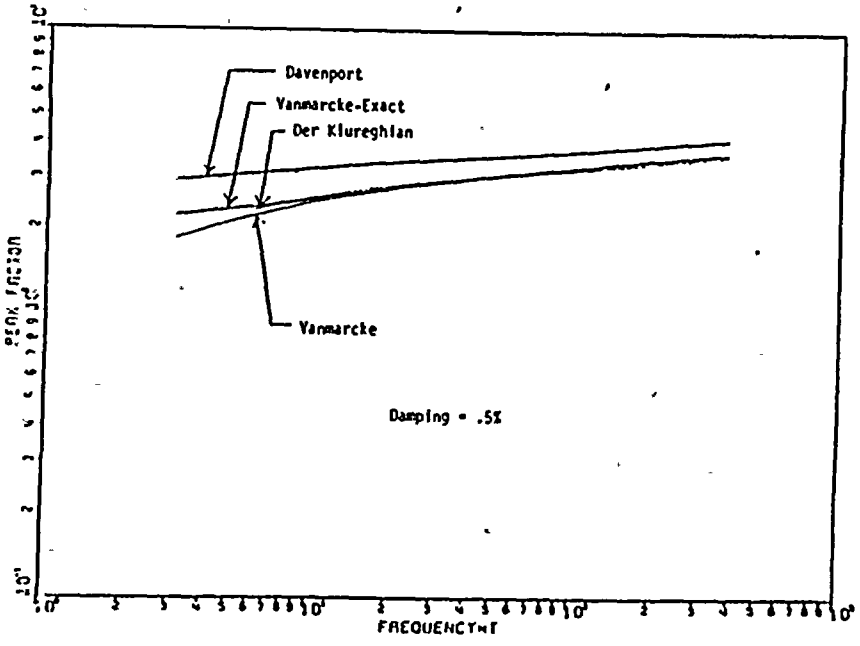

Fig. 2.6 Analytical Peak Factors with Non-Exceedance Probability of 84%

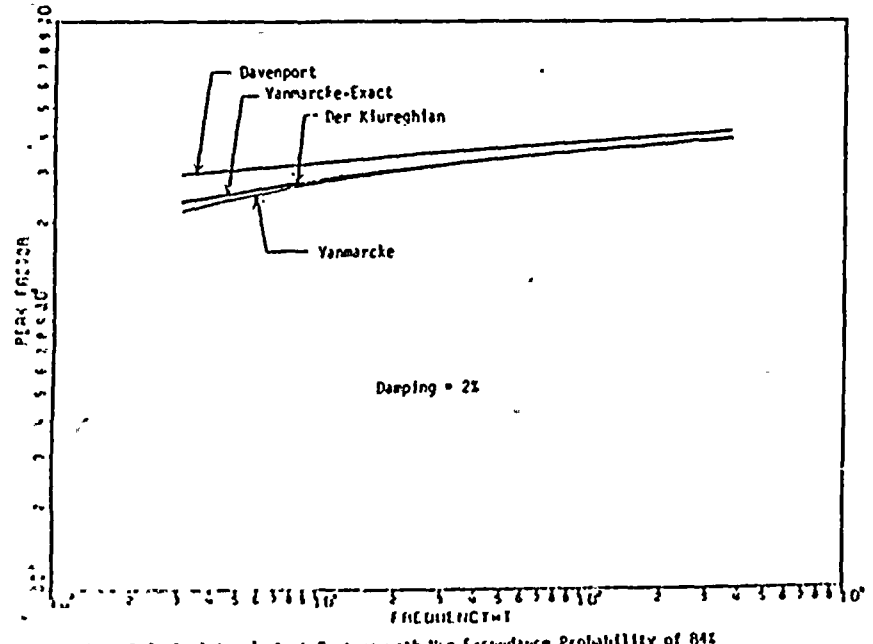

Fig. 2.7 Analytical Peak Factors with Non-Exceedance Probability of 84%

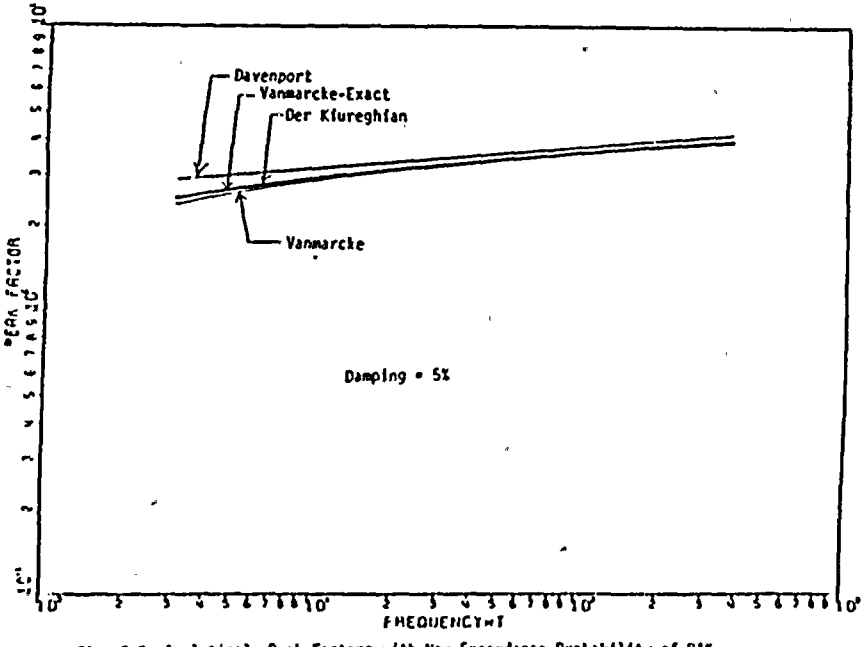

Fig. 2.8 Analytical Peak Factors with Non-Exceedance Probability of 81%

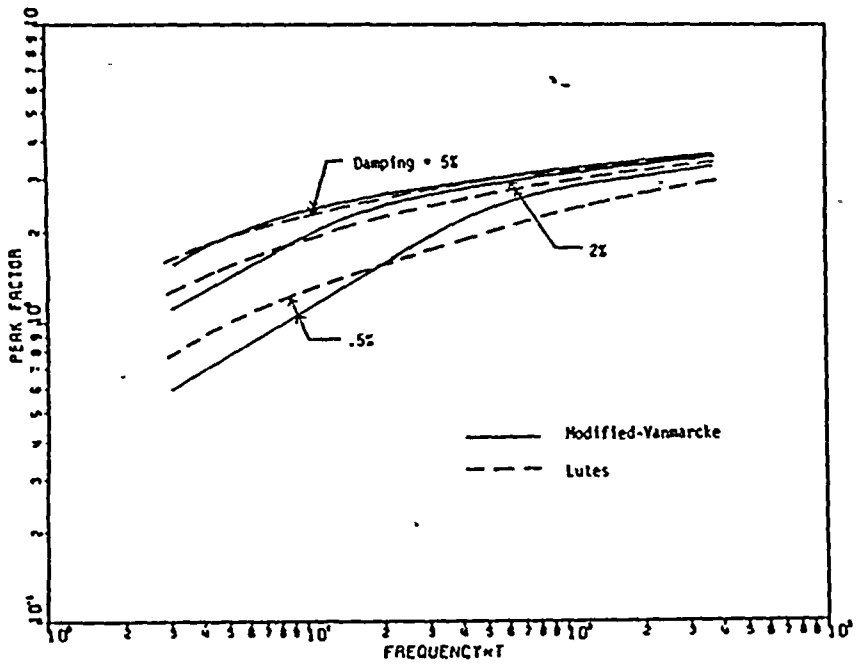

Fig. 2.9 Analytical Peak Factors with Non-Exceedance Probability of 57%

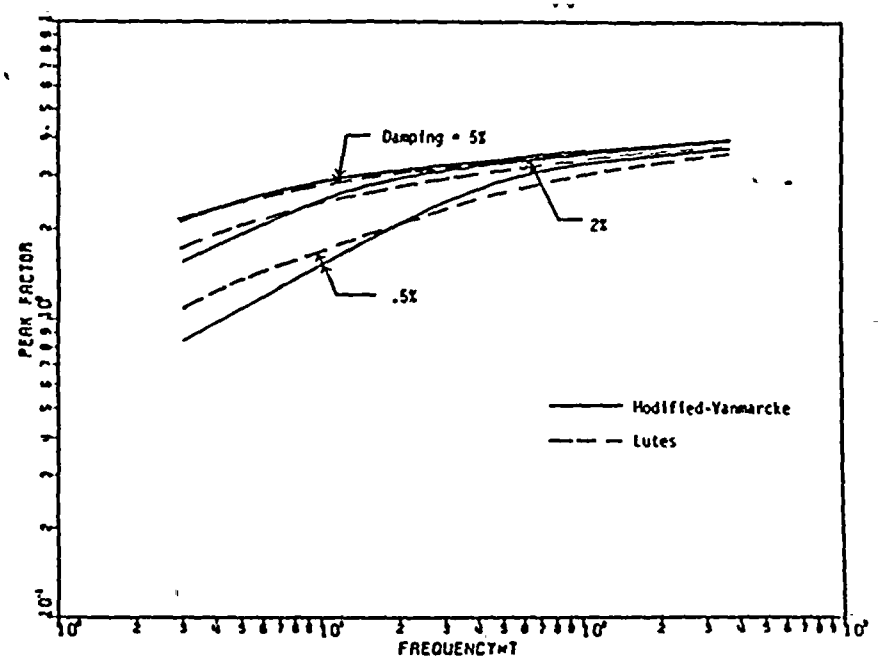

Fig. 2.10 Analytical Peak Factors with Non-Exceedance Probability of 84%

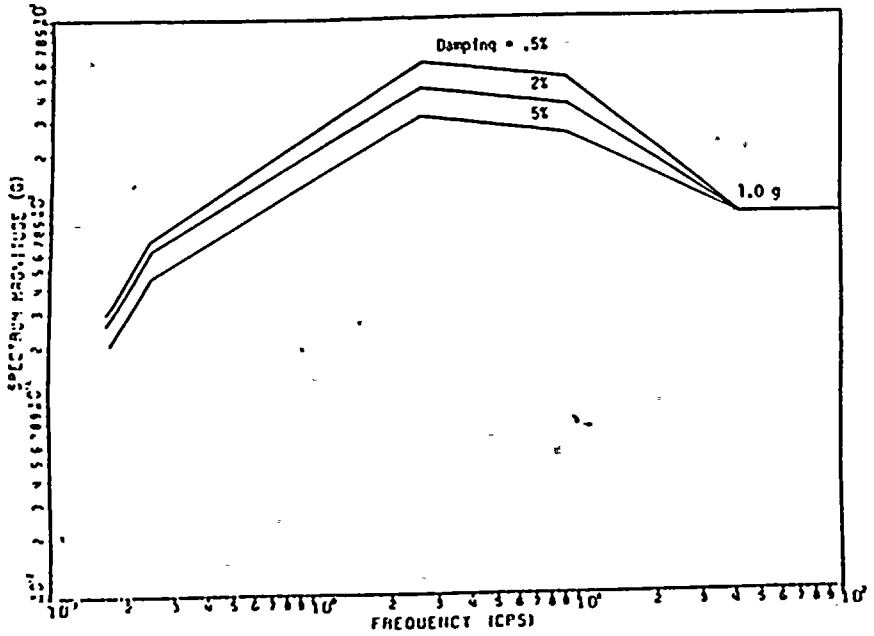

Fig. 3.1 The USNRC R.G. 1.60 Response Spectra

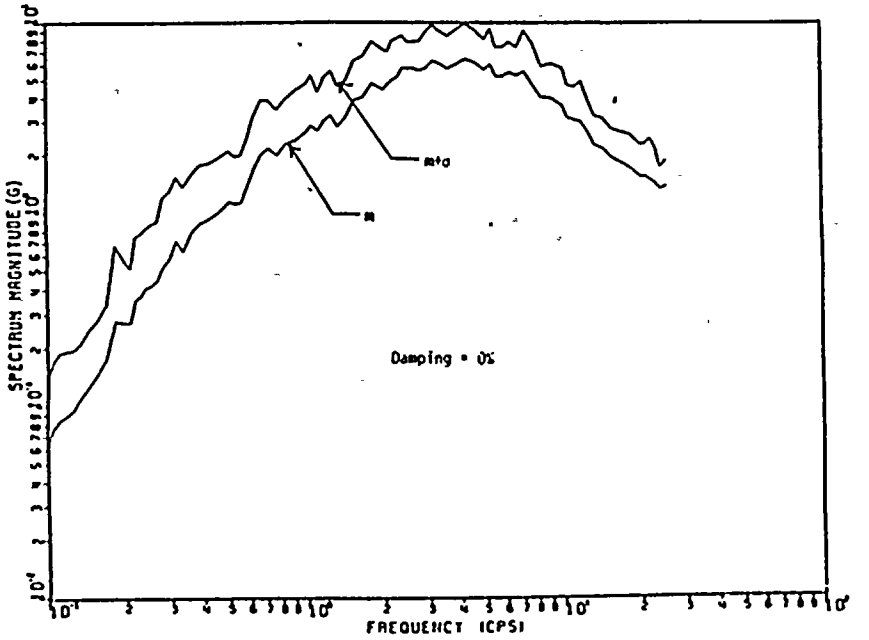

Fig. 3.2 The m and m+σ Response Spectra of 45 Recorded Seismic Ground Motions

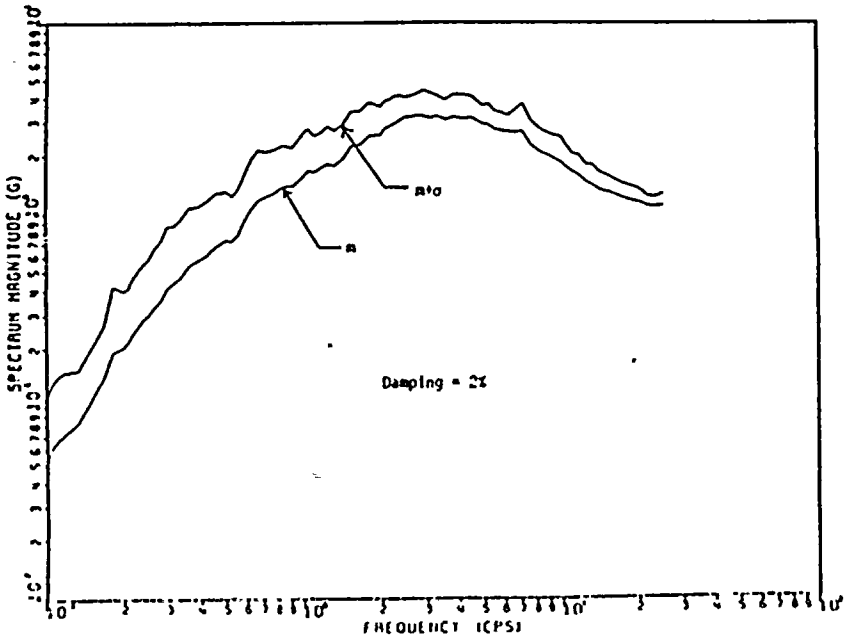

Fig. 3.3 The m and m+σ Response Spectra of 45 Recorded Seismic Ground Motions

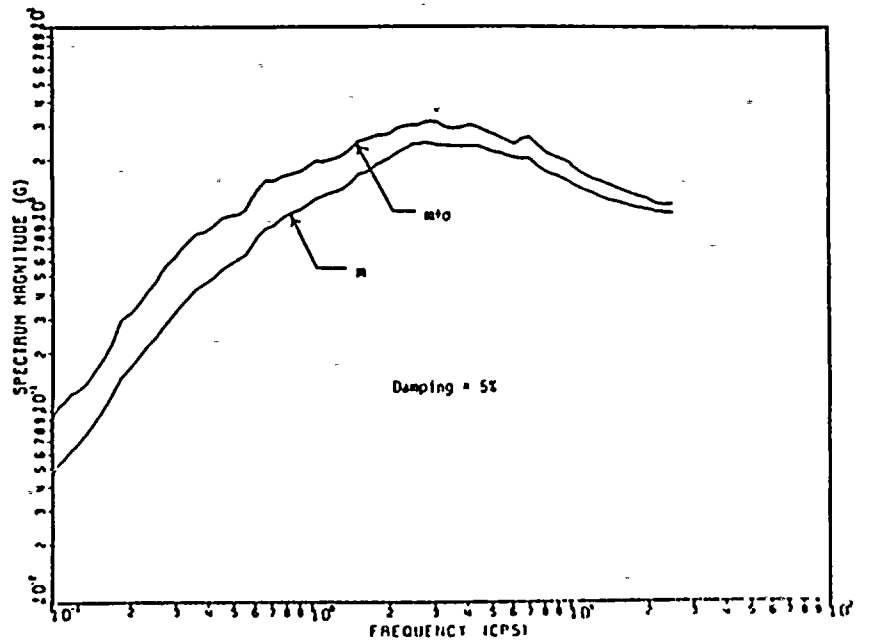

Fig. 3.4 The m and m+σ Response Spectra of 45 Recorded Seismic Ground Motions

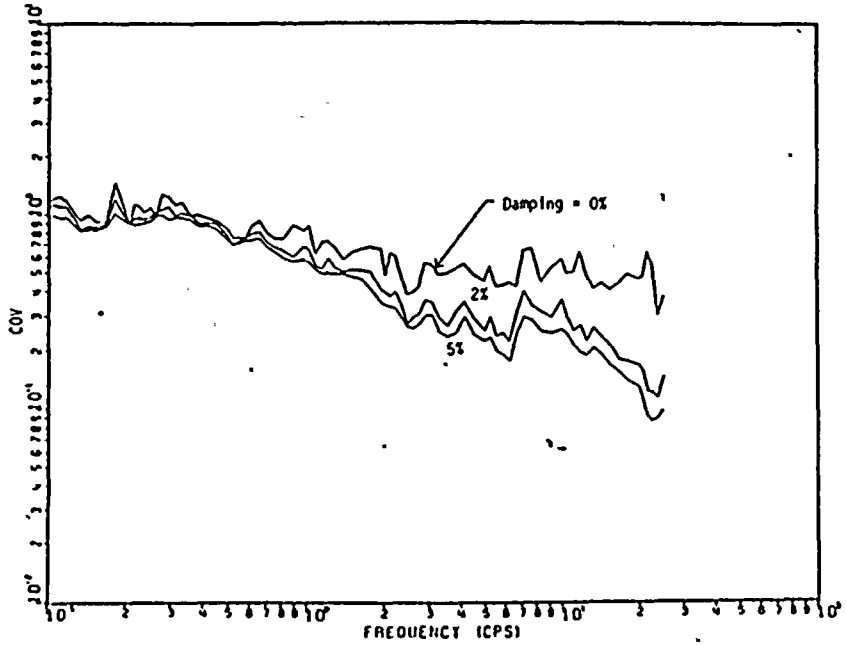

Fig. 3.5 COV of Response Spectra of 45 Recorded Seismic Ground Motions

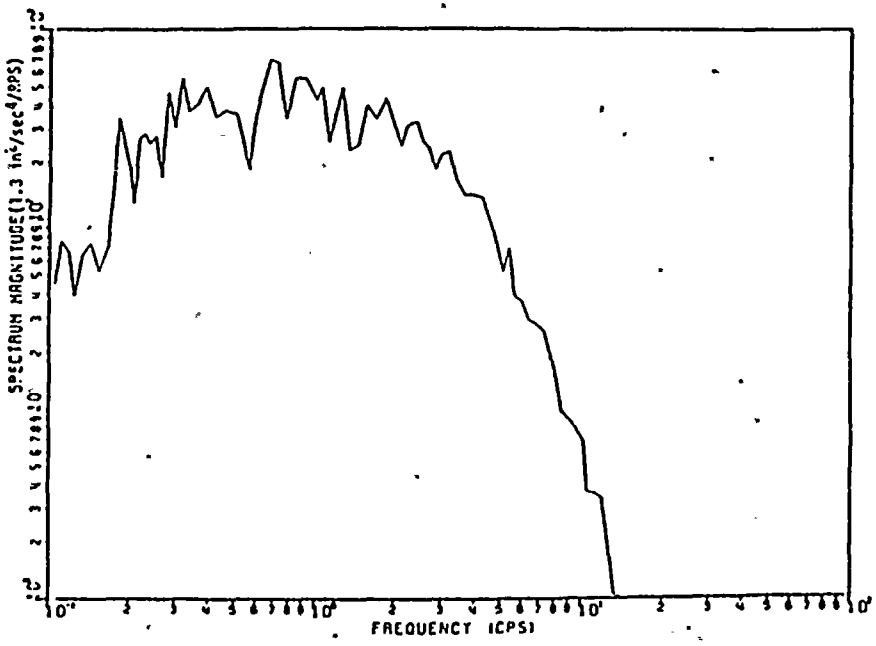

Fig. 3.6 PSDF of 45 Recorded Seismic Ground Motions

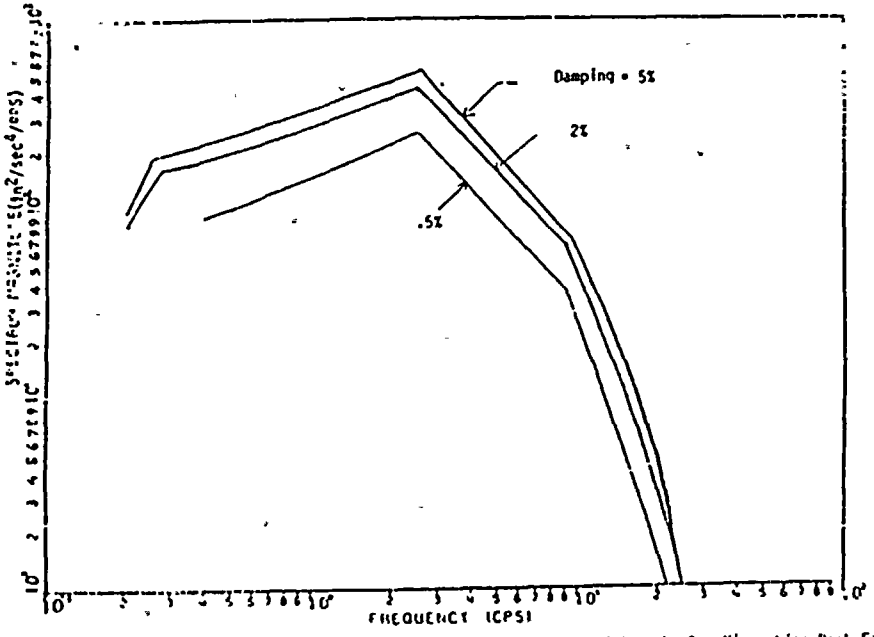

Fig. 3.7 PSDF Generated from the USNRC R.G. 1.60 Response Spectra Using the Der Kiureghian Peak Factor

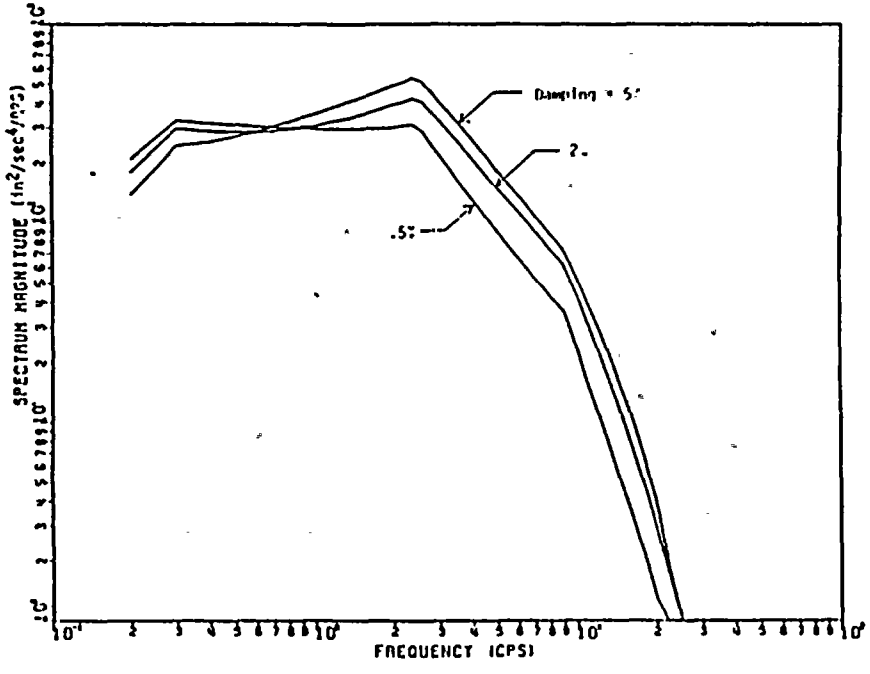

Fig. 3.8 PSDF Generated from the USNRC R.G. 1.60 Response Spectra Using the Modified-Vanmarcke Peak Factor

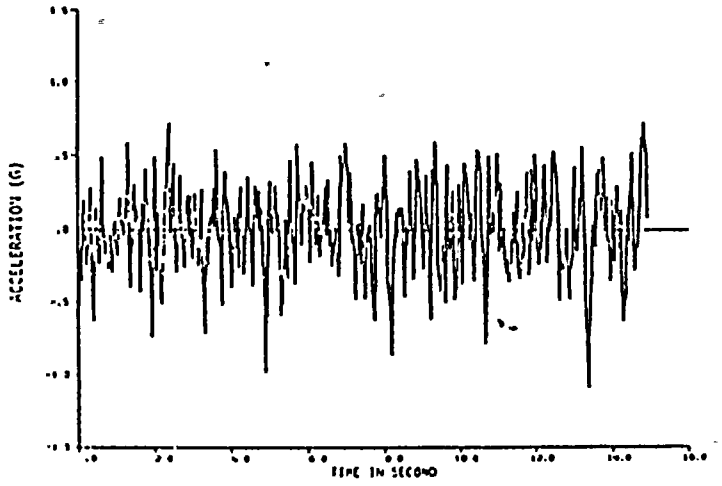

Fig. 4.1 A Typical Stationary Ground Motion

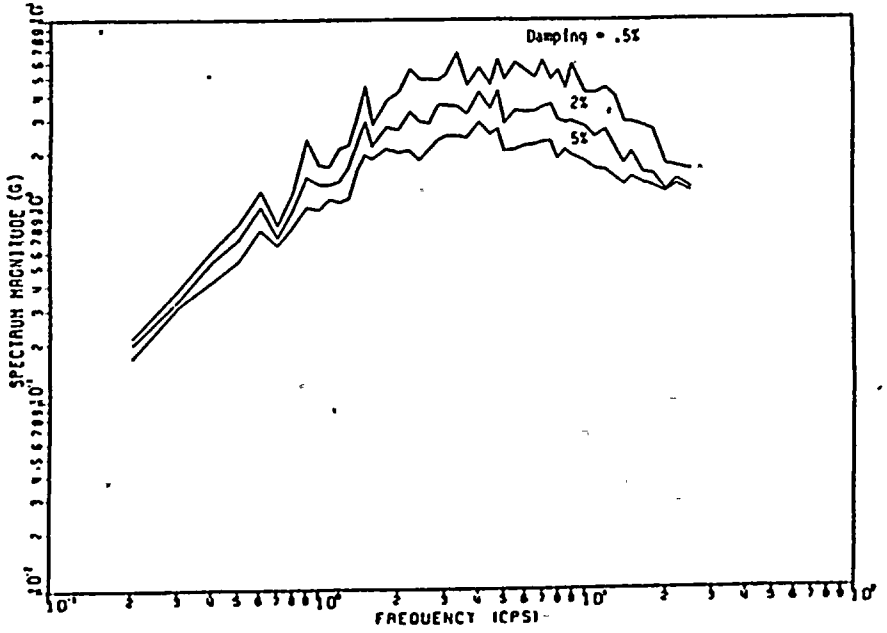

Fig. 4.2 Response Spectra of the Stationary Ground Motion in Fig. 4.1

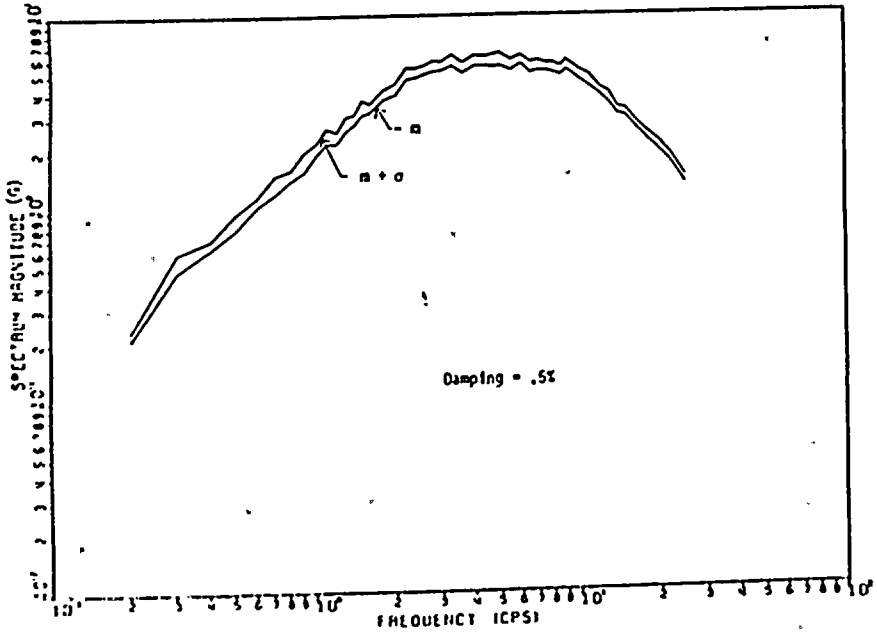

Fig. 4.3 Simulated Response Spectra of Stationary Ground Motions

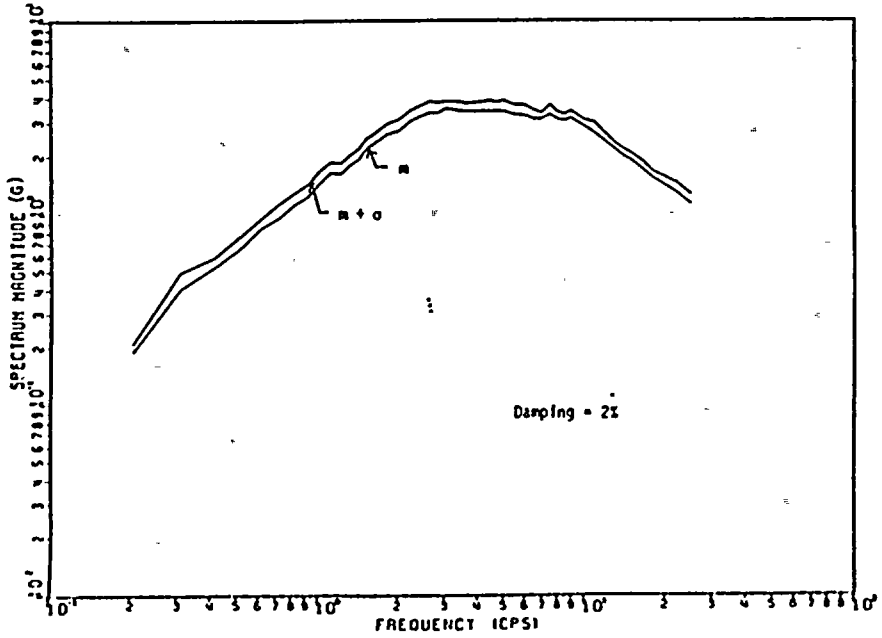

Fig. 4.4 Simulated Response Spectra of Stationary Ground Motions

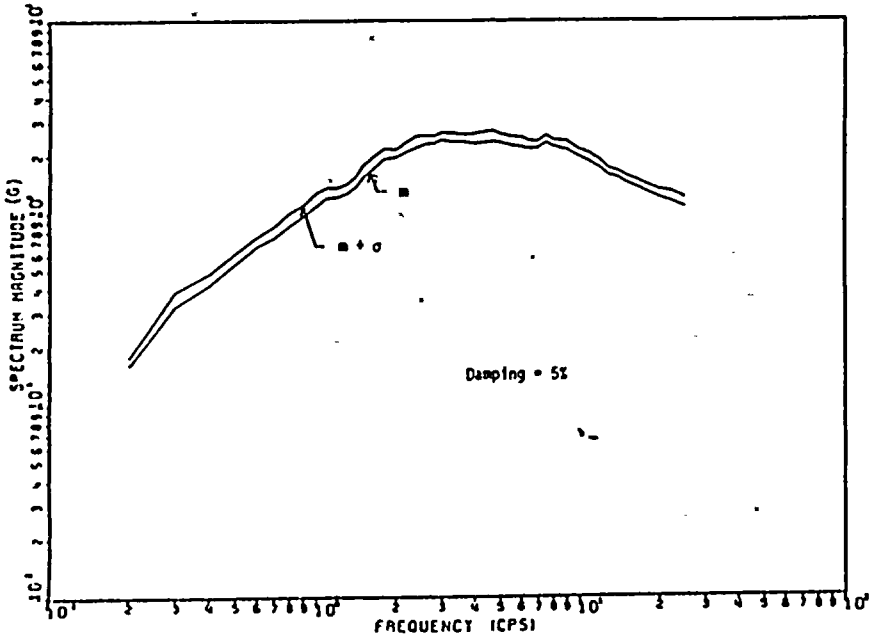

Fig. 4.5 Simulated Response Spectra of Stationary Ground Motions

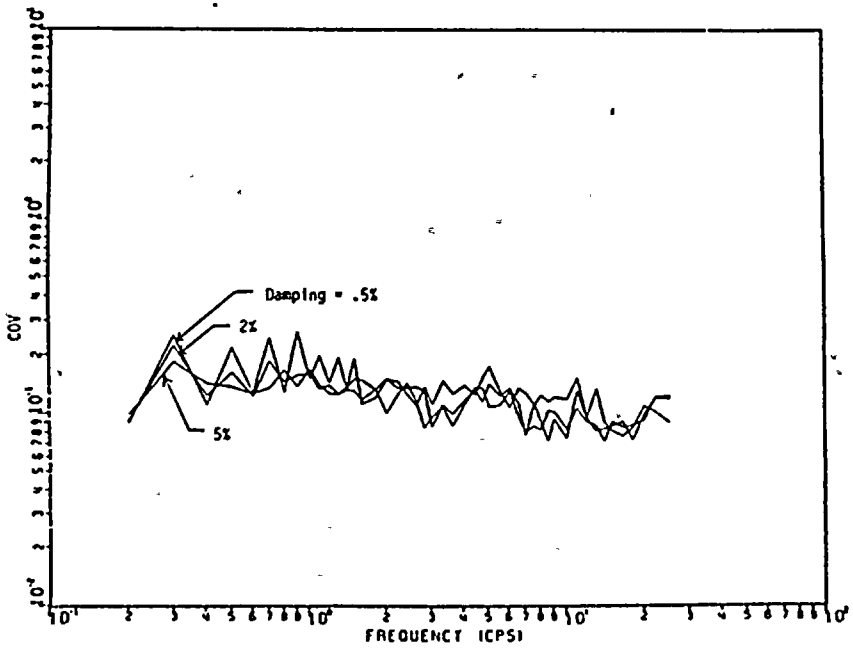

Fig. 4.6 COV of Simulated Response Spectra of Stationary Ground Motions

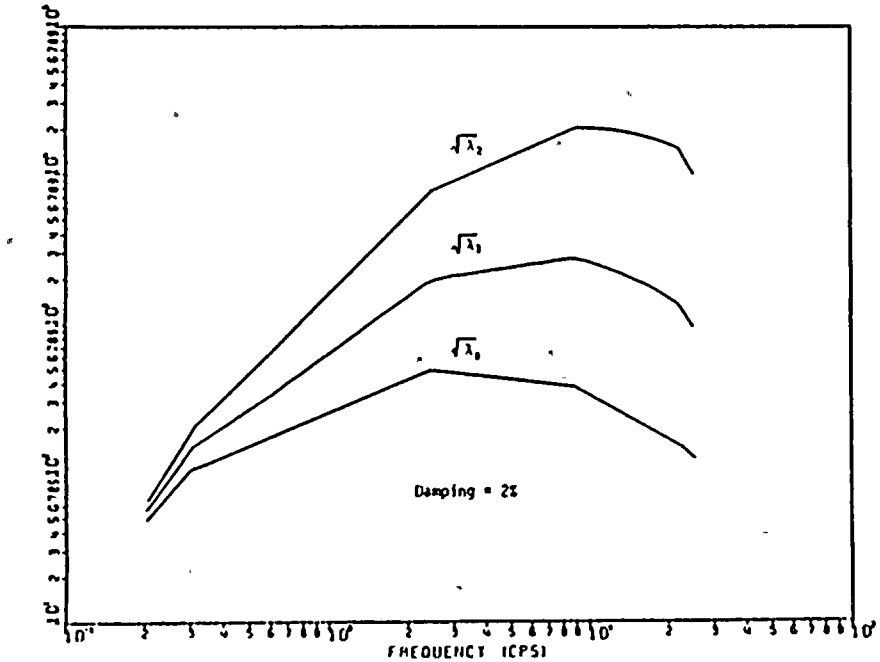

Fig. 4.7 Spectral Moments of Response Motions to Stationary Ground Motions

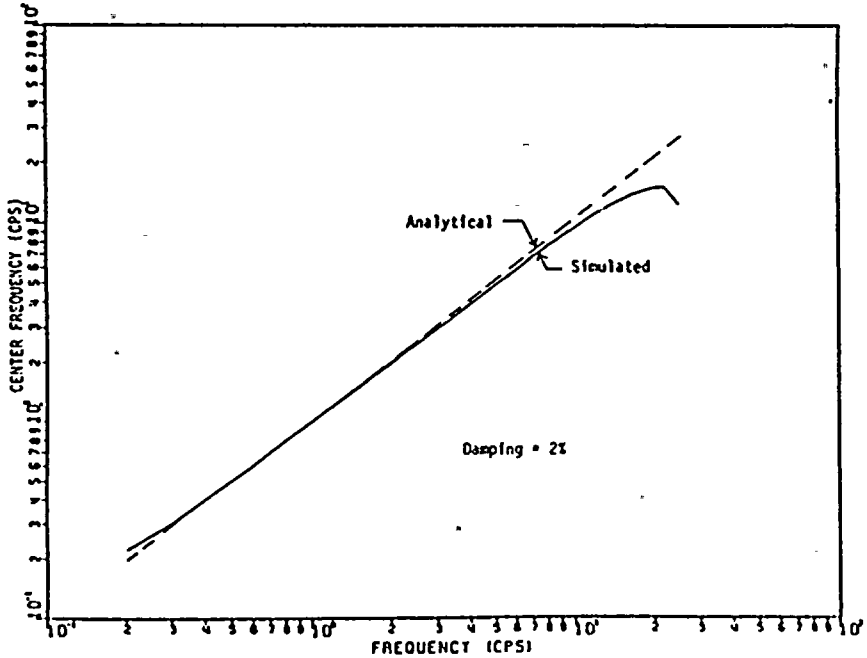

Fig. 4.8 Spectral Center Frequencies of Response Motions to Stationary Ground Motions

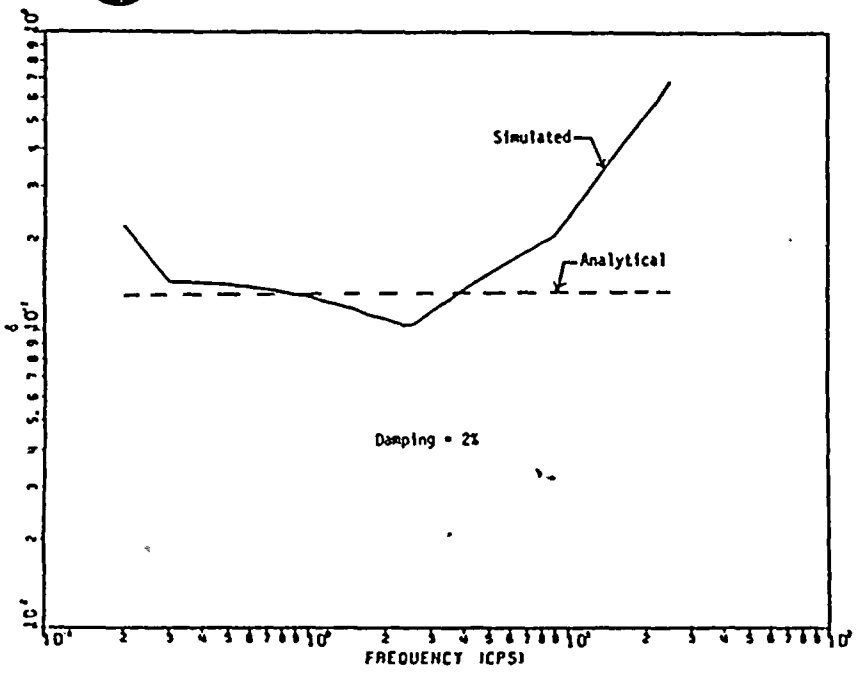

Fig. 4.9 Spectral Dispersion Parameter δ of Response Motions to Stationary Ground Motions

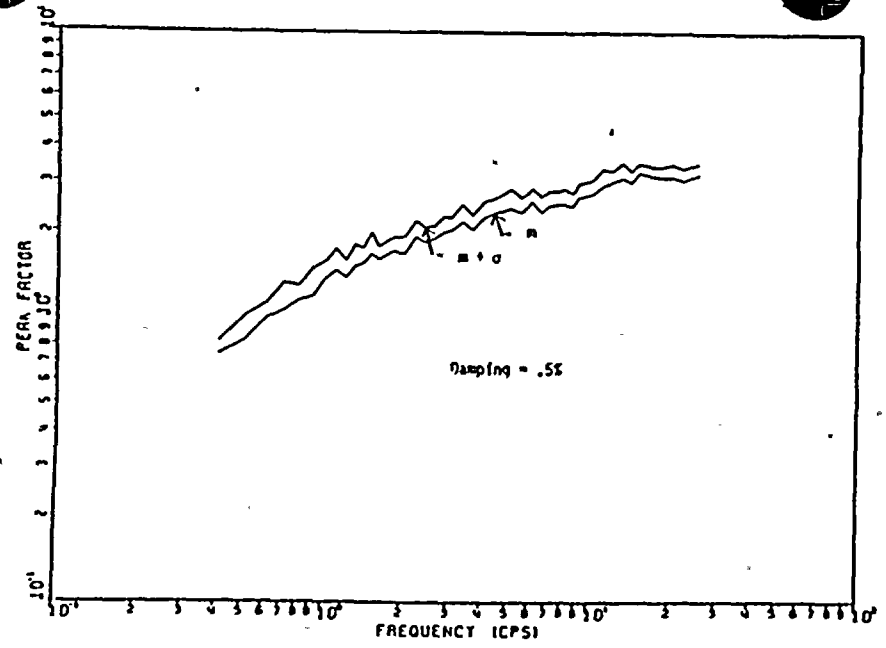

Fig. 4.10 Simulated Peak Factors for Responses to Stationary Ground Motions

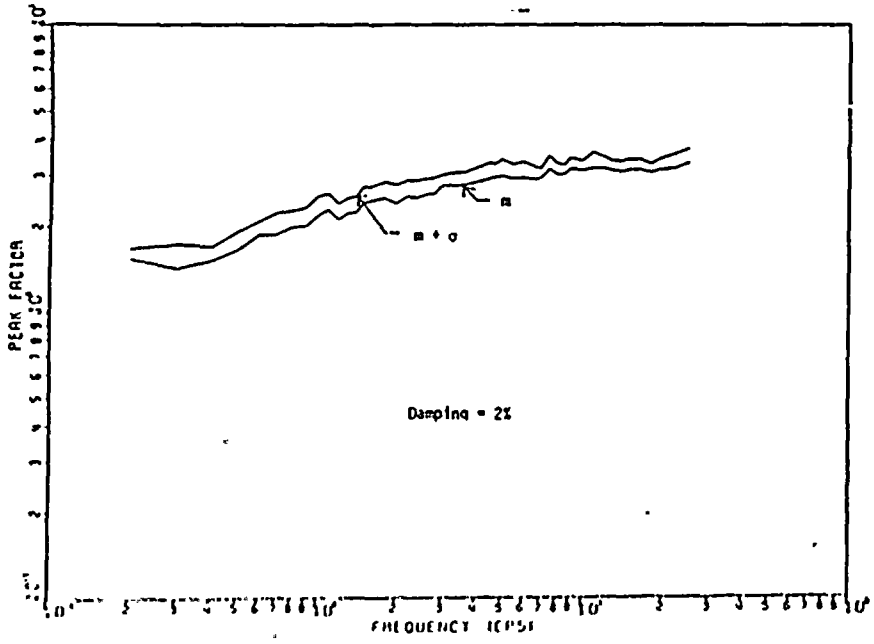

Fig. 4.11 Simulated Peak Factors for Responses to Stationary Ground Motions

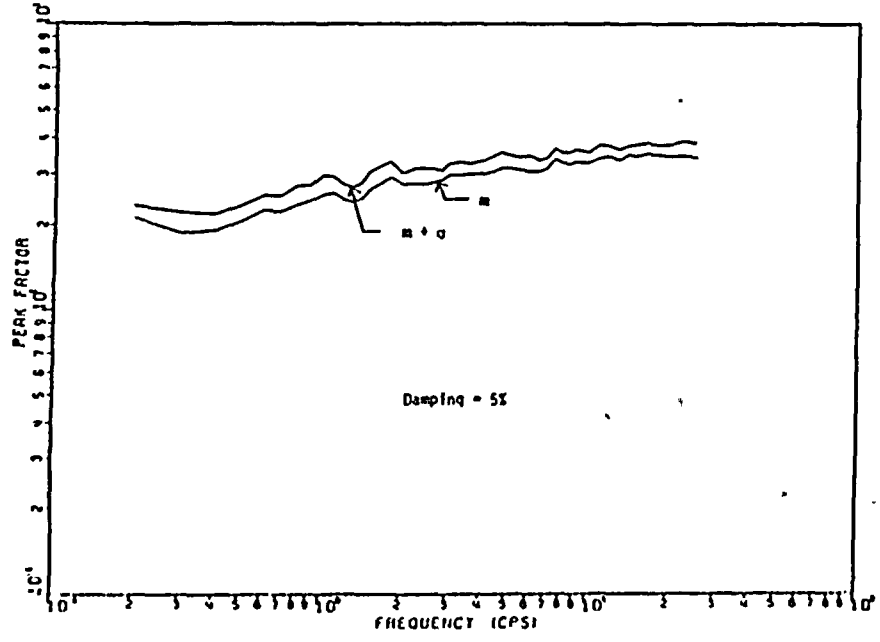

Fig. 4.12 Simulated Peak Factors for Responses, to Stationary Ground Motions

Type	t_1(sec.)	t_2(sec.)	t_3(sec.)	α
B	4	15	30	.099
C	2	4	12	.268

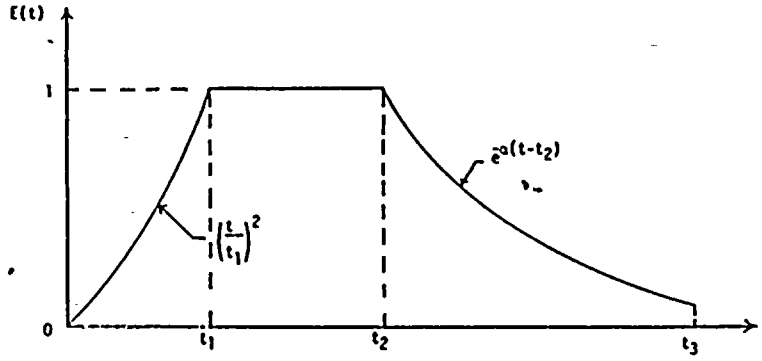

Fig. 4.13 Envelopes for Types B and C Ground Motions

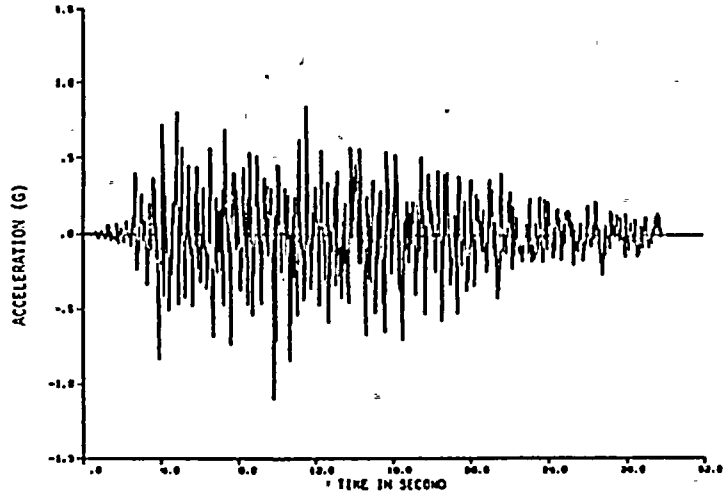

Fig. 4.14 A Typical Type B Ground Motion

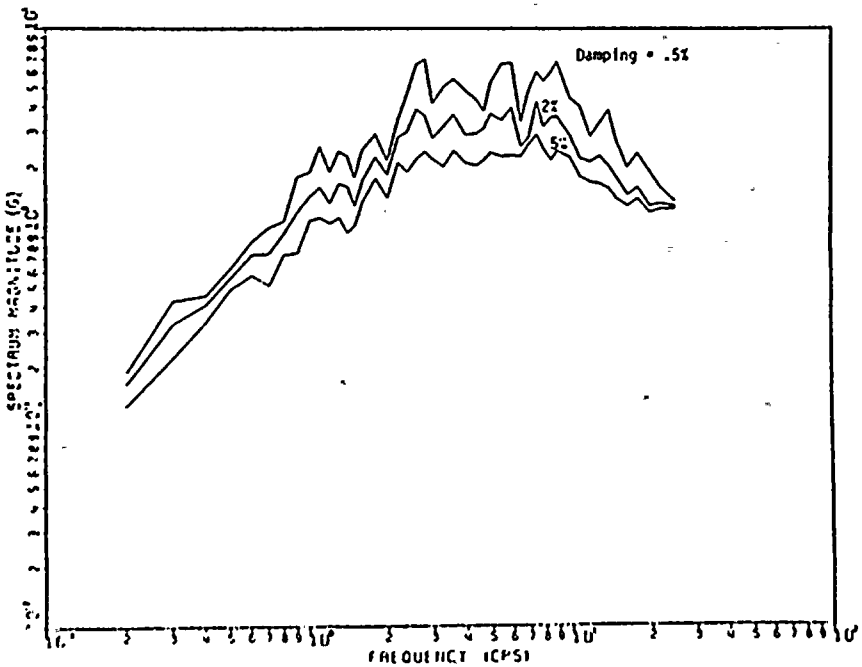

Fig. 4.15 Response Spectra of the Type B Ground Motion in Fig. 4.14

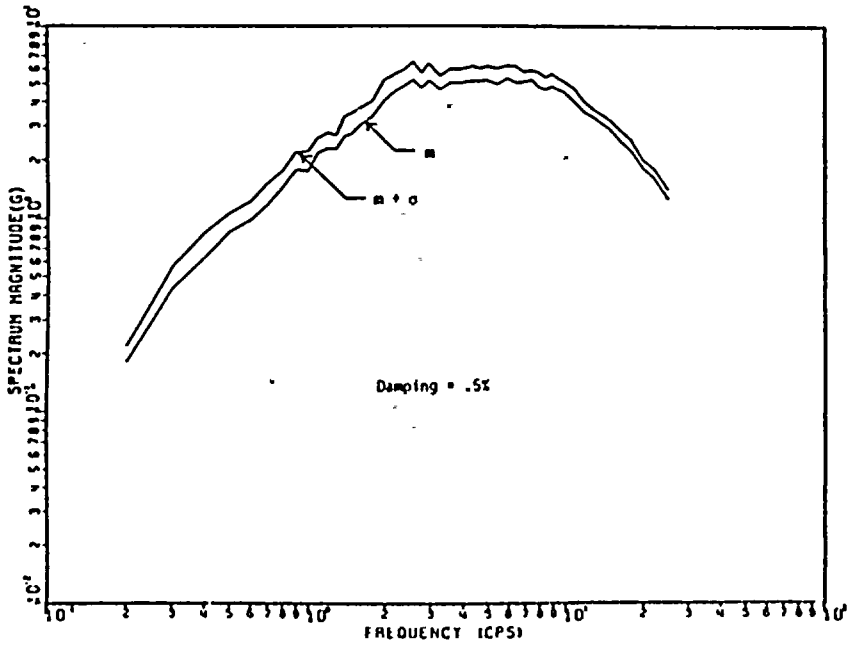

Fig. 4.16 Simulated Response Spectra of Type B Ground Motions

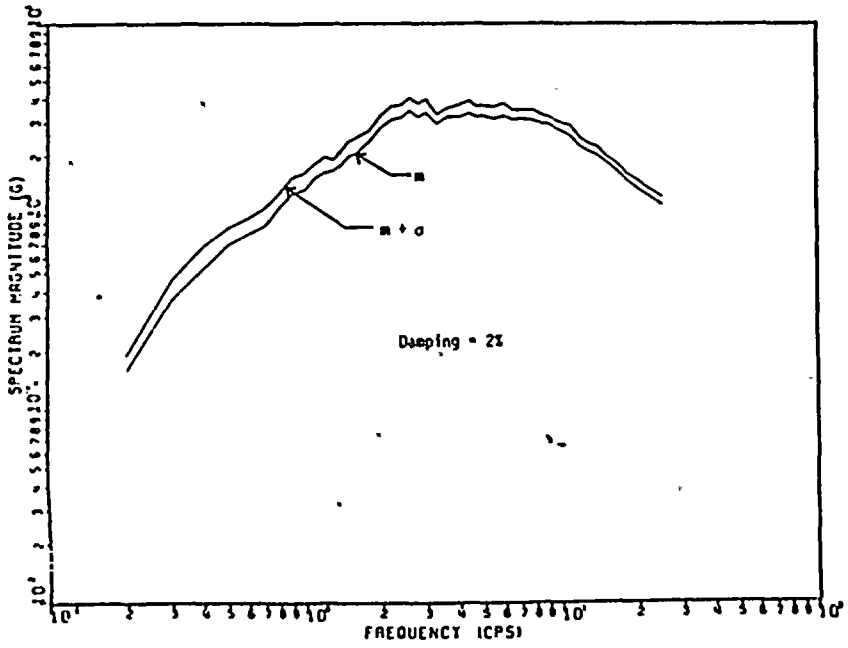

Fig. 4.17 Simulated Response Spectra of Type B Ground Motions

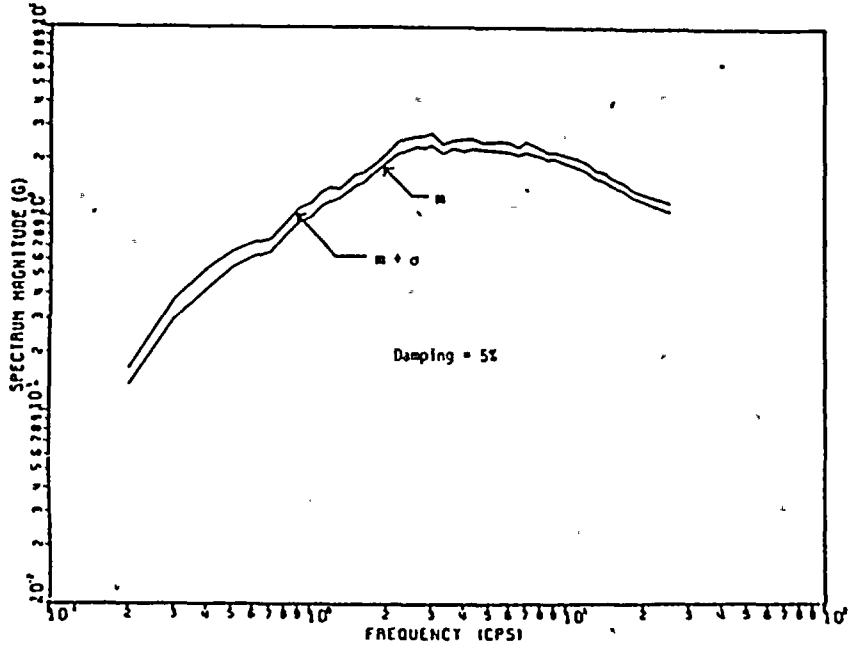

Fig. 4.18 Simulated Response Spectra of Type B Ground Motions

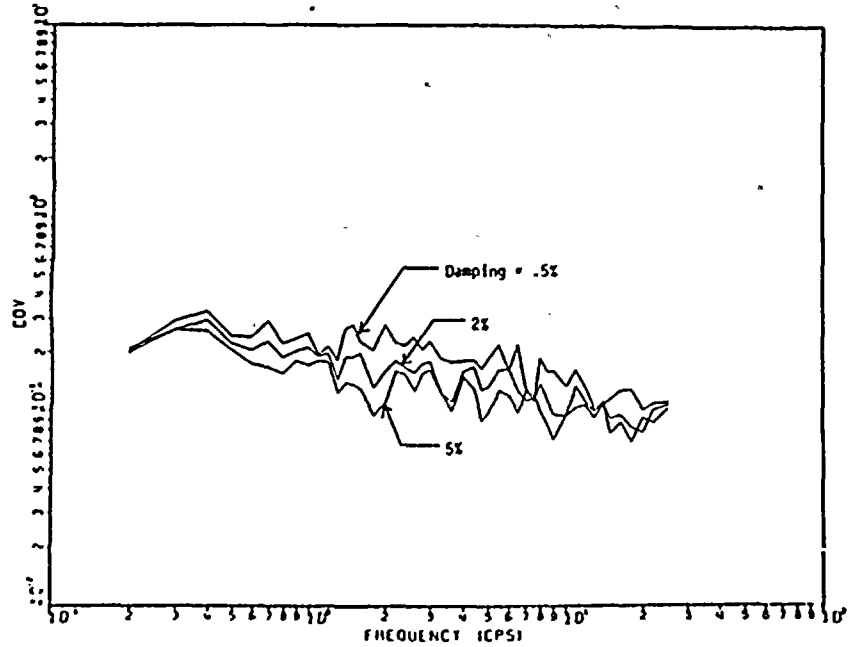

Fig. 4.19 COV of Simulated Response Spectra of Type B Ground Motions

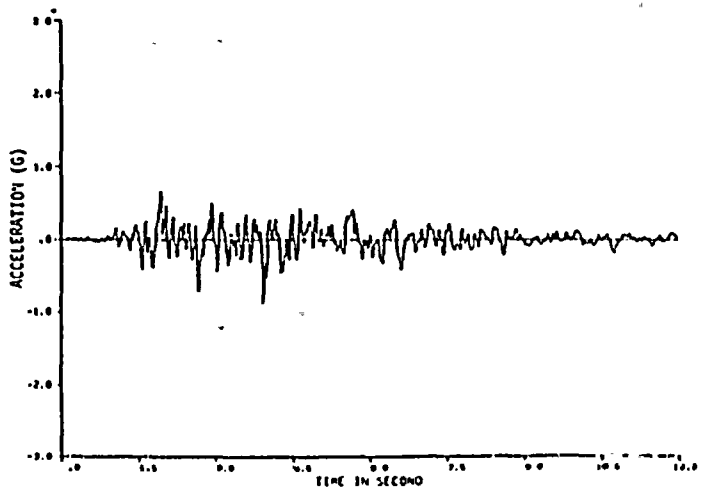

Fig. 4.20 A Typical Type C Ground Motion

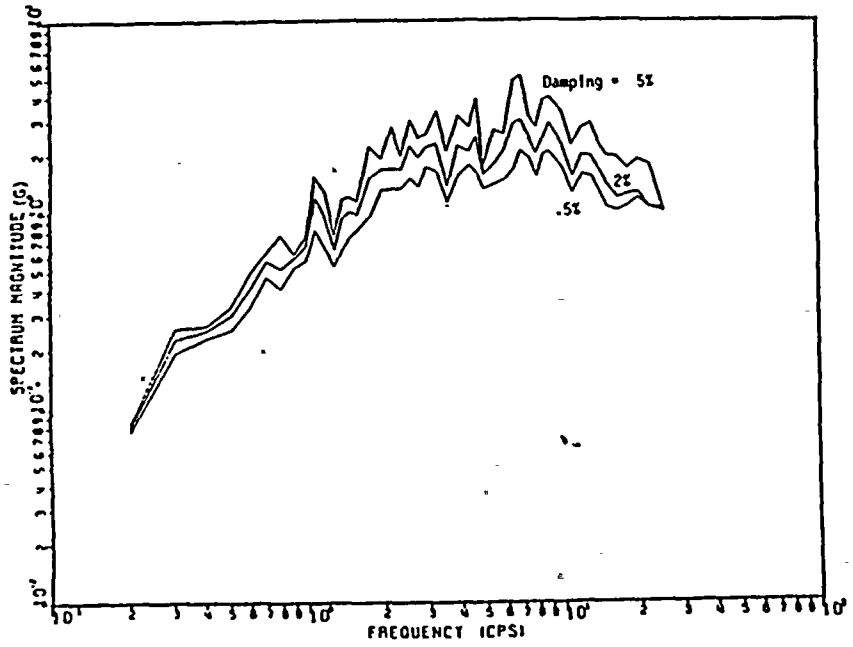

Fig. 4.21 Response Spectra of the Type C Ground Motion in Fig. 4.20

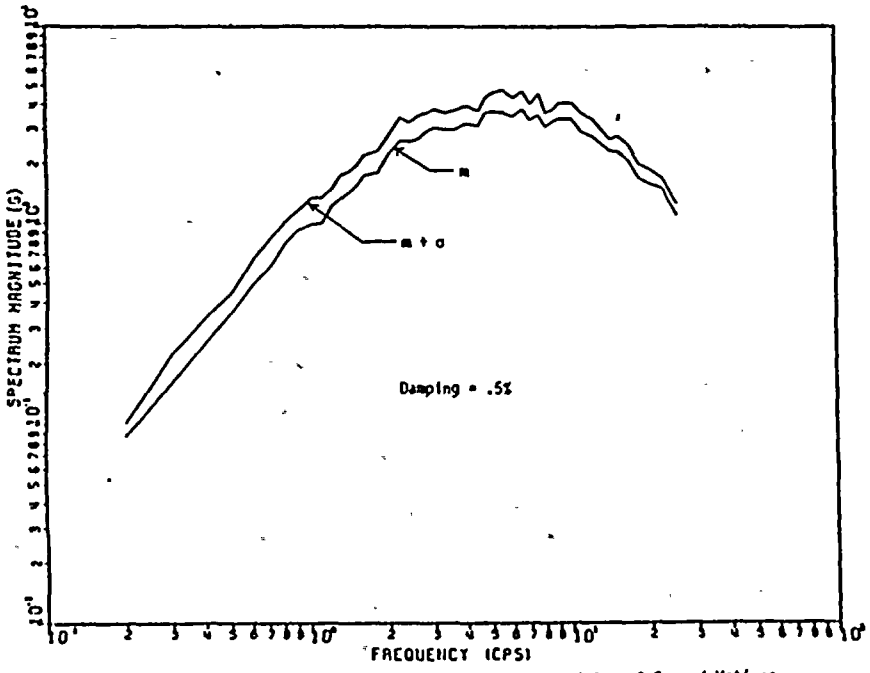

Fig. 4.22 Simulated Response Spectra of Type C Ground Motions

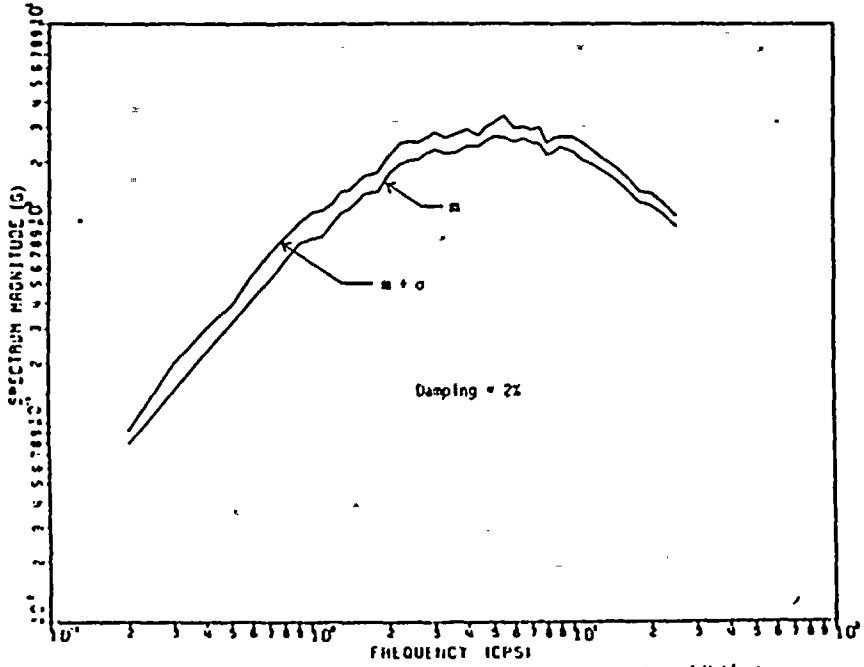

Fig. 4.23 Simulated Response Spectra of Type C Ground Motions

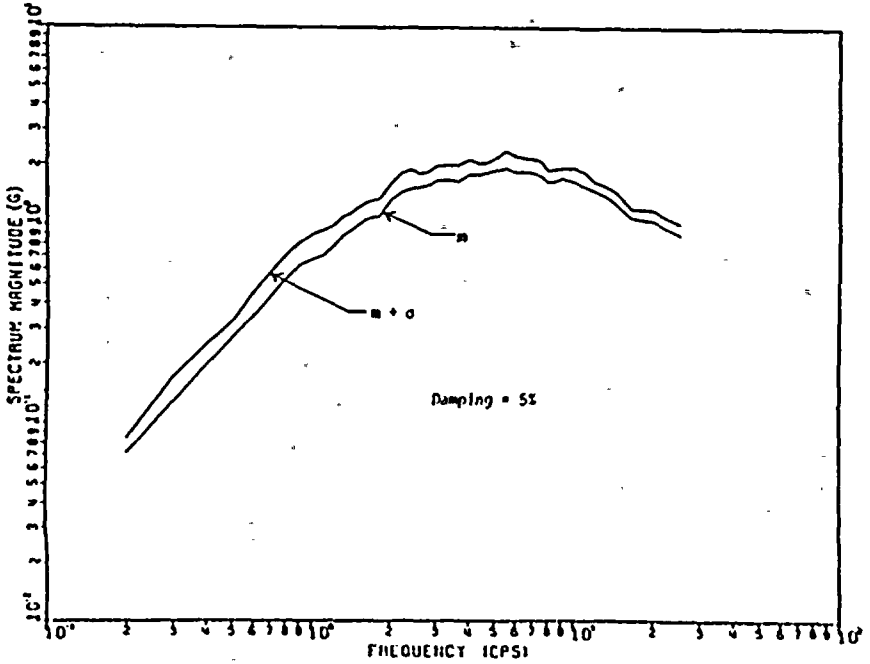

Fig. 4.24 Simulated Response Spectra of Type C Ground Motions

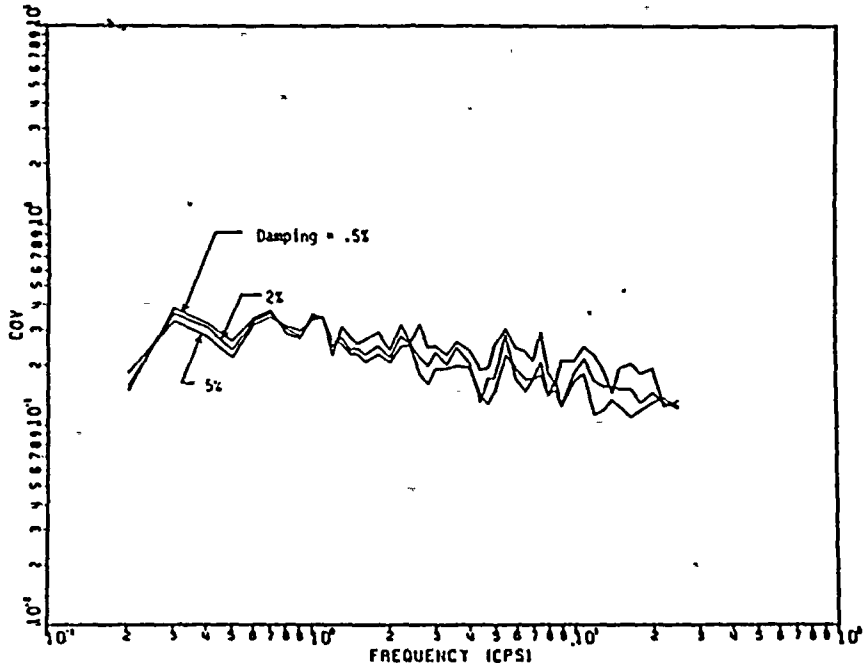

Fig. 4.25 COV of Simulated Response Spectra of Type C Ground Motions

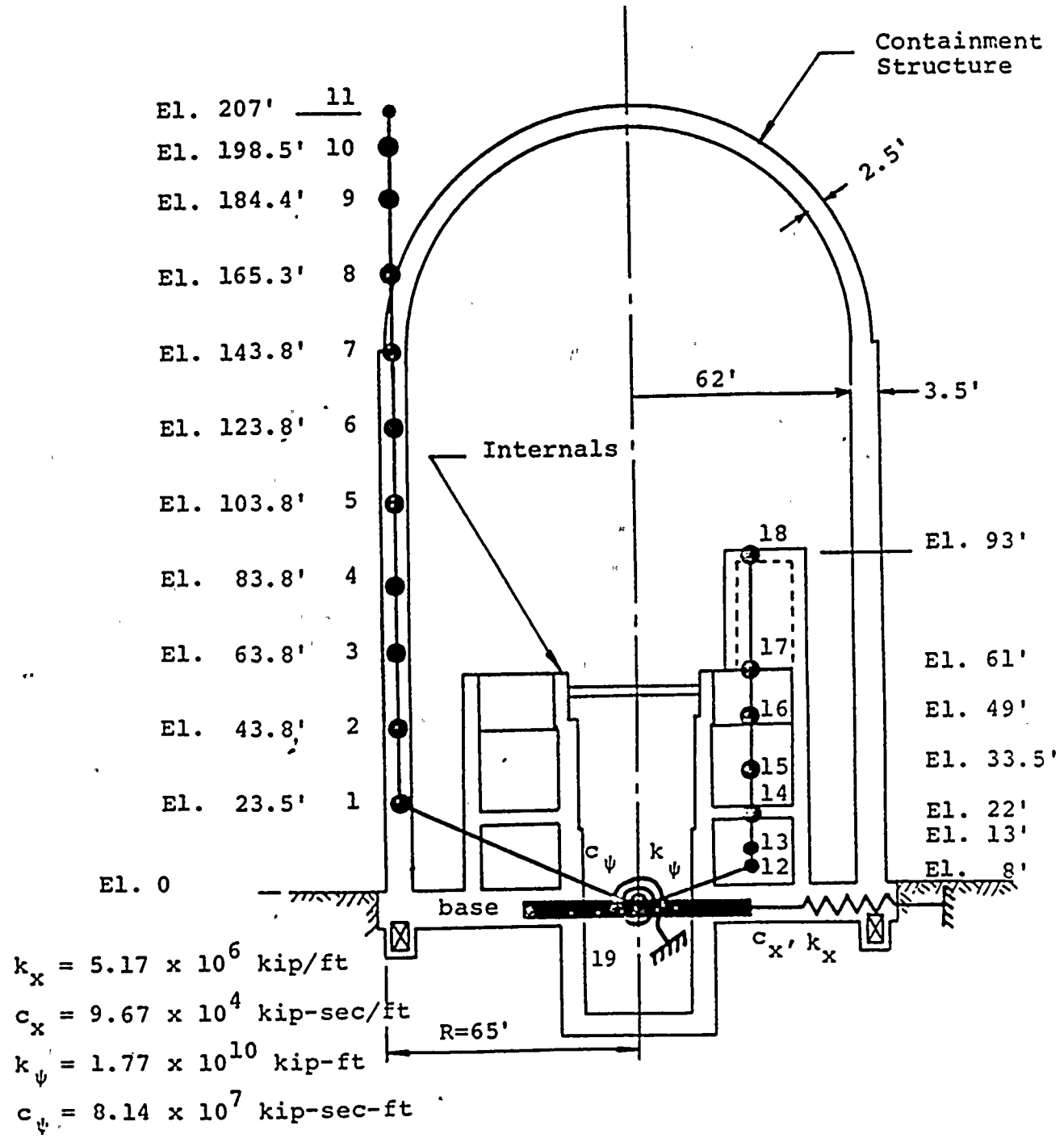

Fig. 5.1 Soil-Structure System of the PWR Containment and Its Internal System

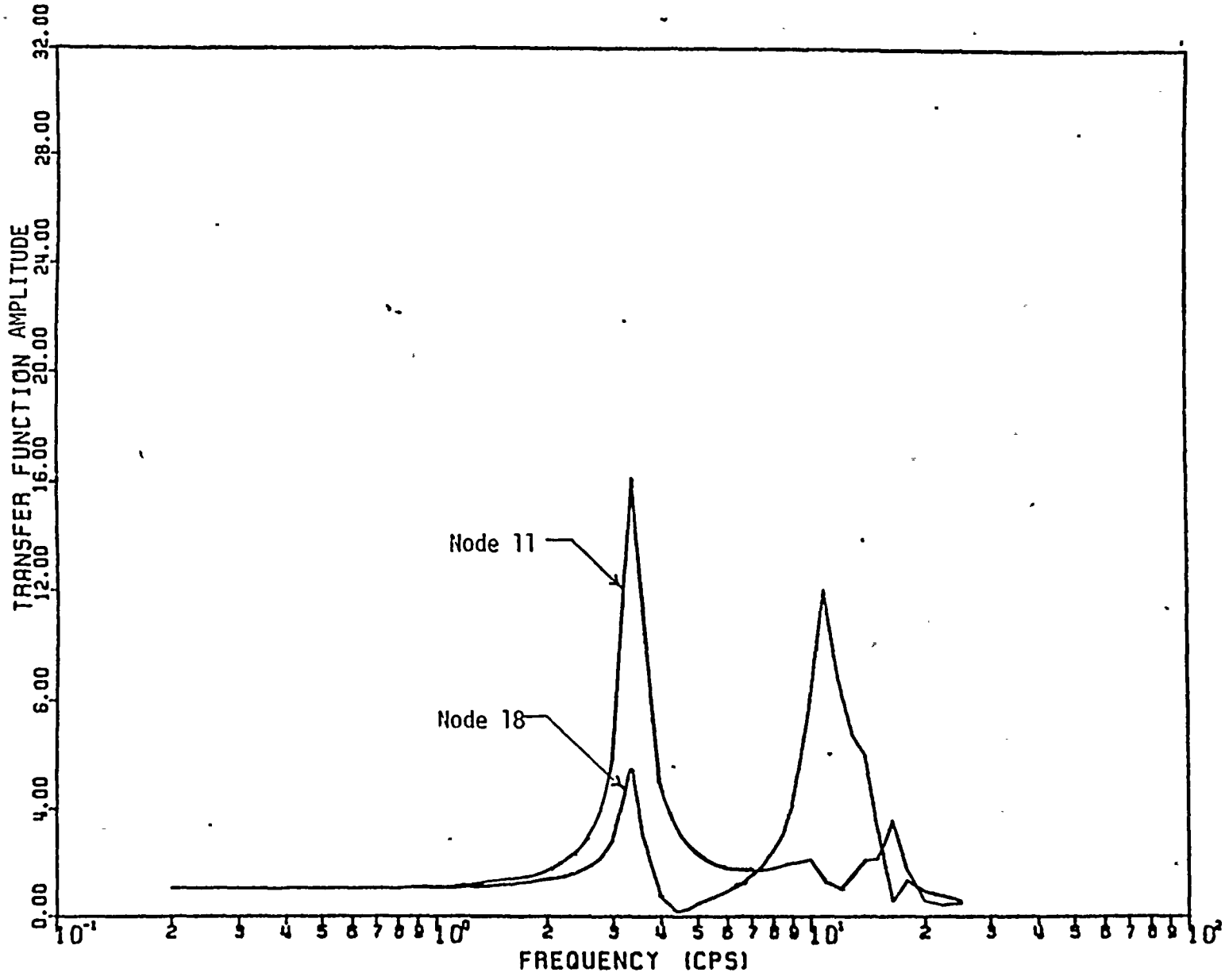

Fig. 5.2 Structural Response Transfer Functions

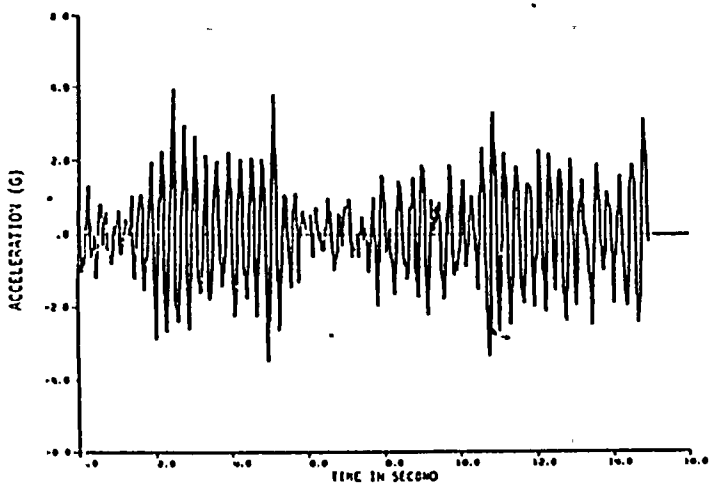

Fig. 6.1 A Typical Response Motion at Node 11 to the Stationary Ground Motion

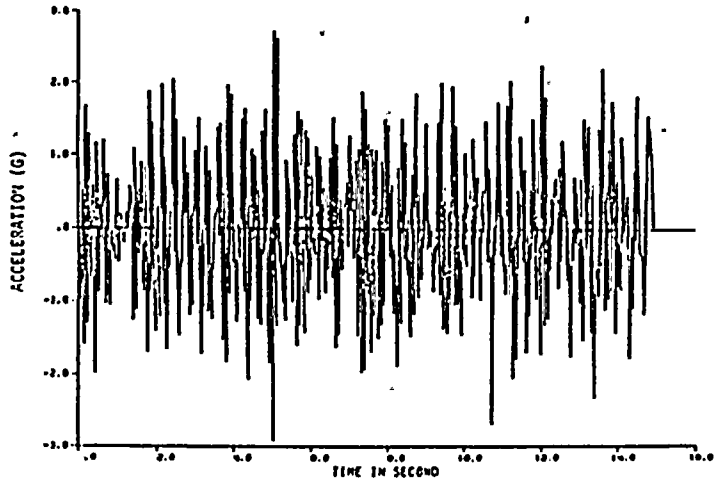

Fig. 6.2 A Typical Response Motion at Node 18 to the Stationary Ground Motion

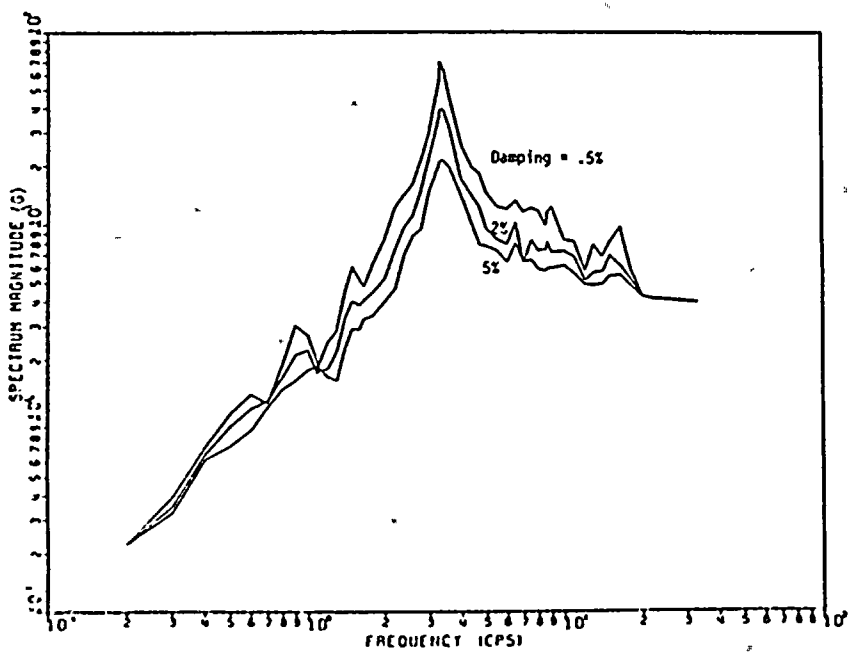

Fig. 6.3 Floor Response Spectra of the Response Motion at Node 11 in Fig. 6.1

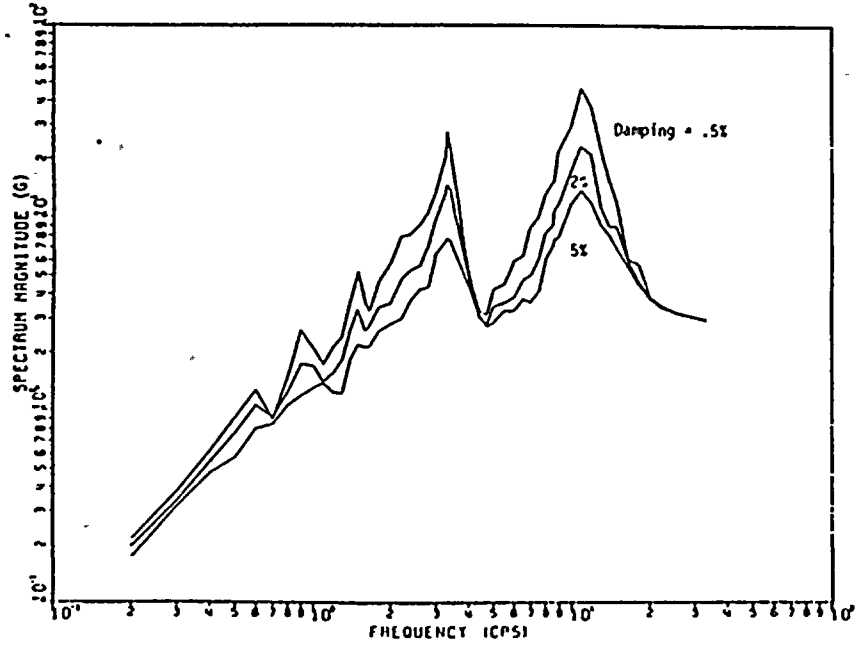

Fig. 6.4 Floor Response Spectra of the Response Motion at Node 18 in Fig. 6.2

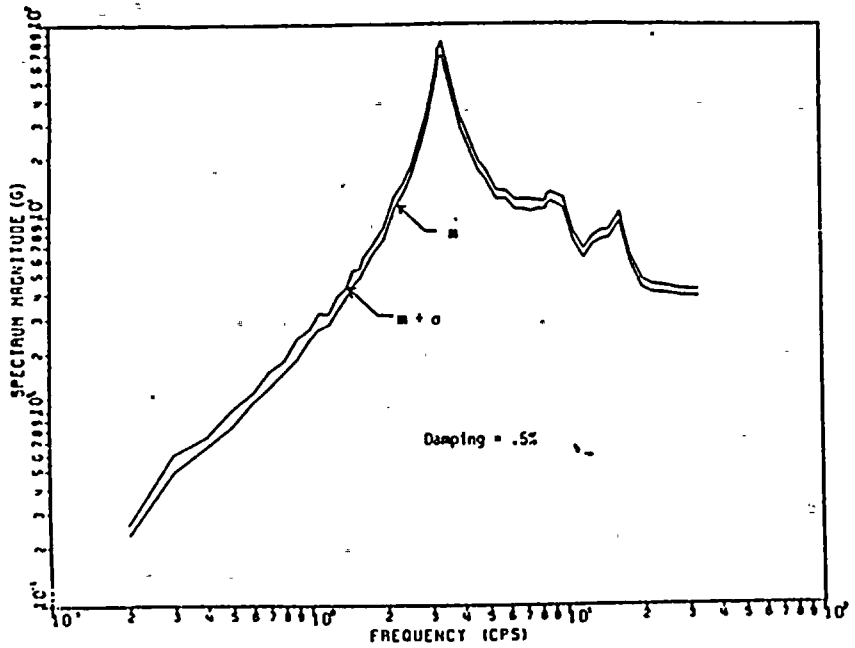

Fig. 6.5 Simulated Floor Response Spectra of Response Motions at Node 11 to Stationary Ground Motions

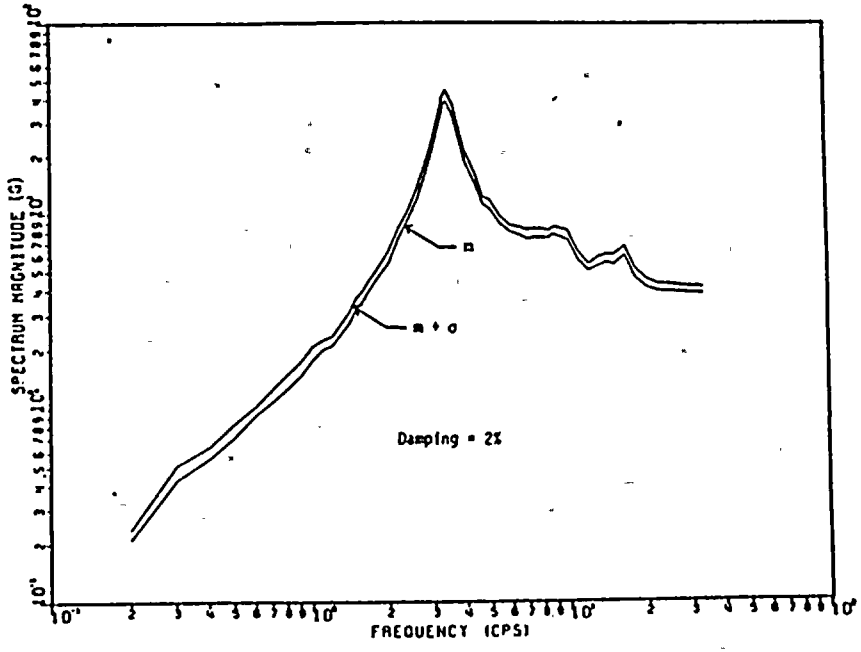

Fig. 6.6 Simulated Floor Response Spectra of Response Motions at Node 11 to Stationary Ground Motions

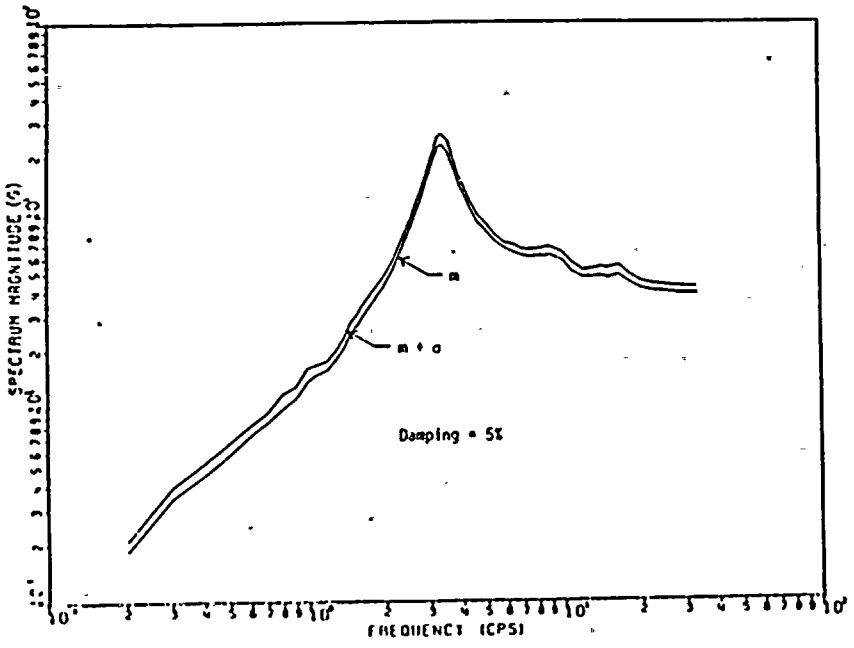

Fig. 6.7 Simulated Floor Response Spectra of Response Motions at Node 11 to Stationary Ground Motions

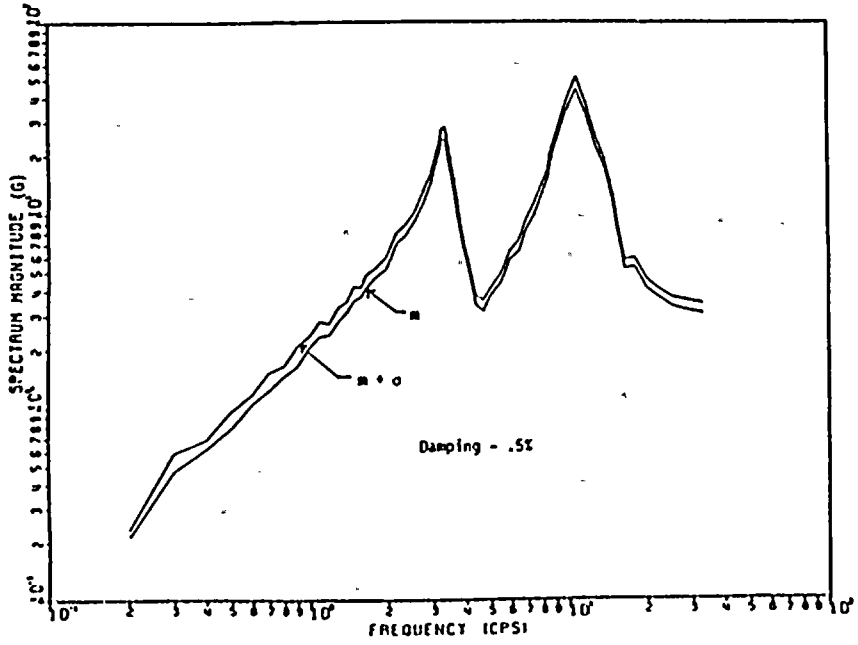

Fig. 6.8 Simulated Floor Response Spectra of Response Motions at Node 18 to Stationary Ground Motions

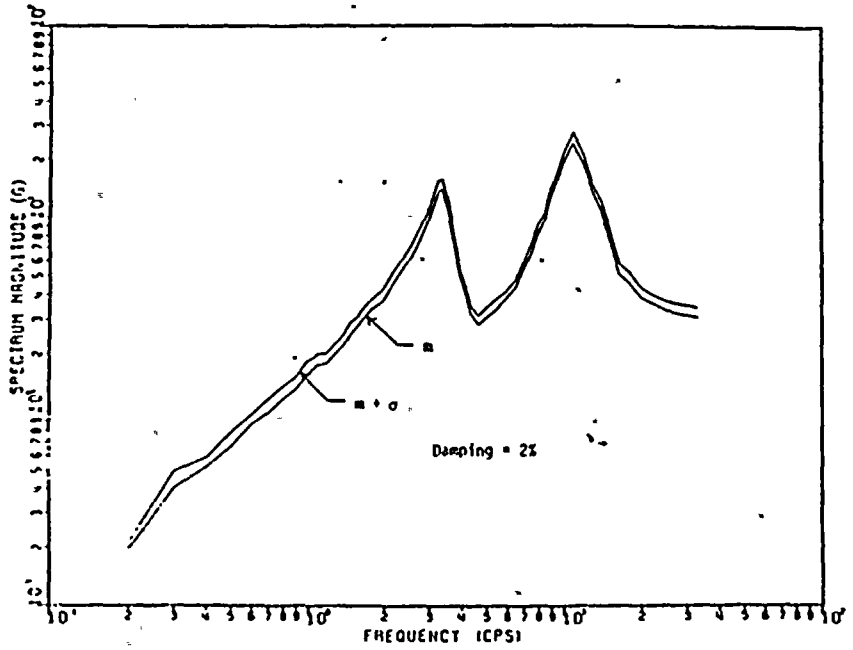

Fig. 6.9 Simulated Floor Response Spectra of Response Motions at Node 18 to Stationary Ground Motions

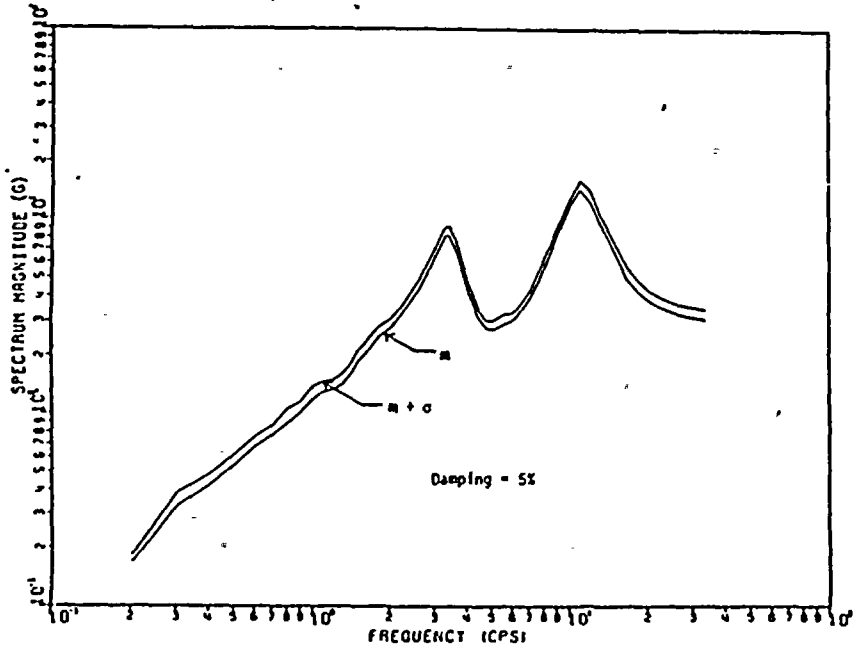

Fig. 6.10 Simulated Floor Response Spectra of Response Motions at Node 18 to Stationary Ground Motions

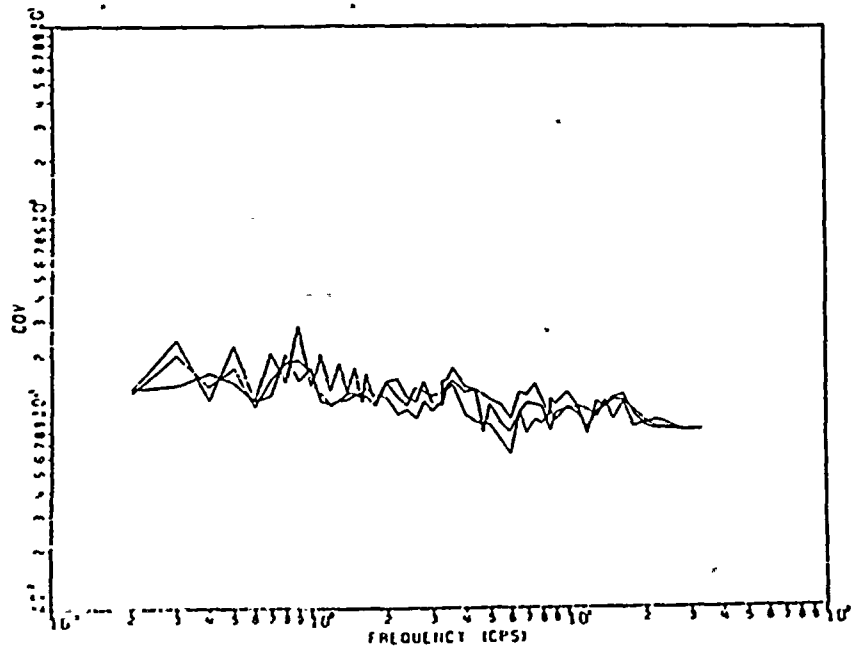

Fig. 6.11 COV of Simulated Floor Response Spectra at Node 11 for Stationary Ground Motions

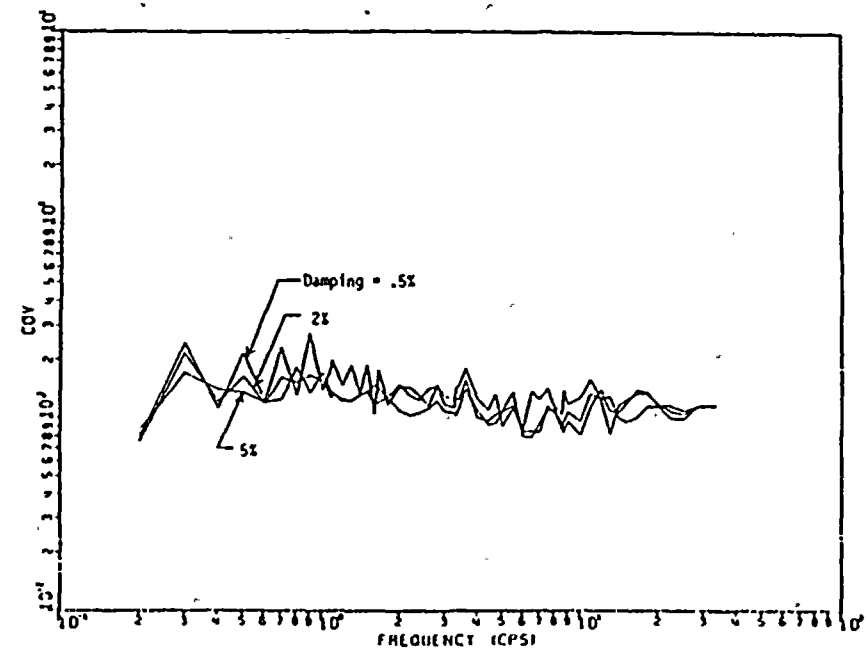

Fig. 6.12 COV of Simulated Floor Response Spectra at Node 18 for Stationary Ground Motions

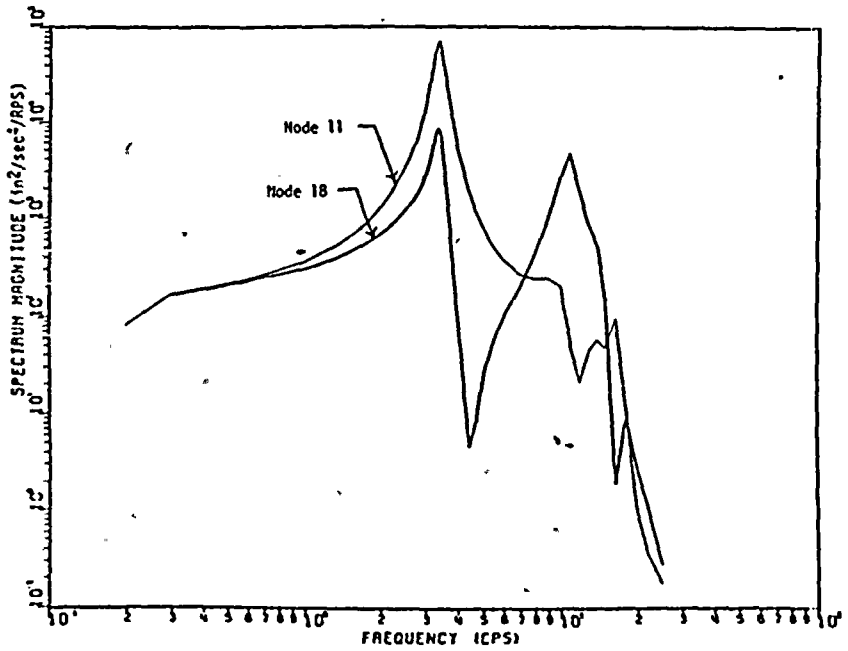

Fig. 6.13 PSDF of Response Motions to Stationary Ground Motions

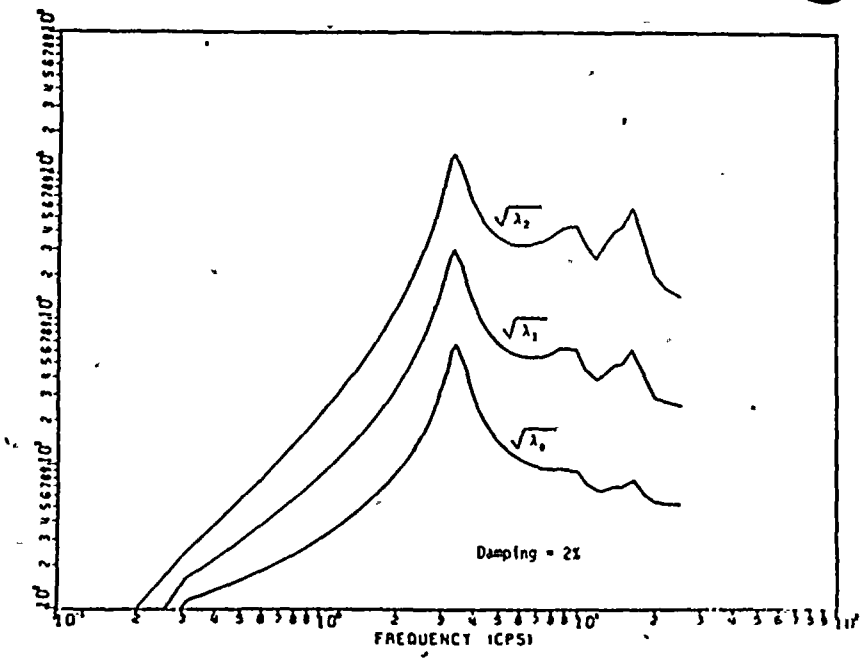

Fig. 6.14 Spectral Moments of Response Motions at Node 11 to Stationary Ground Motions

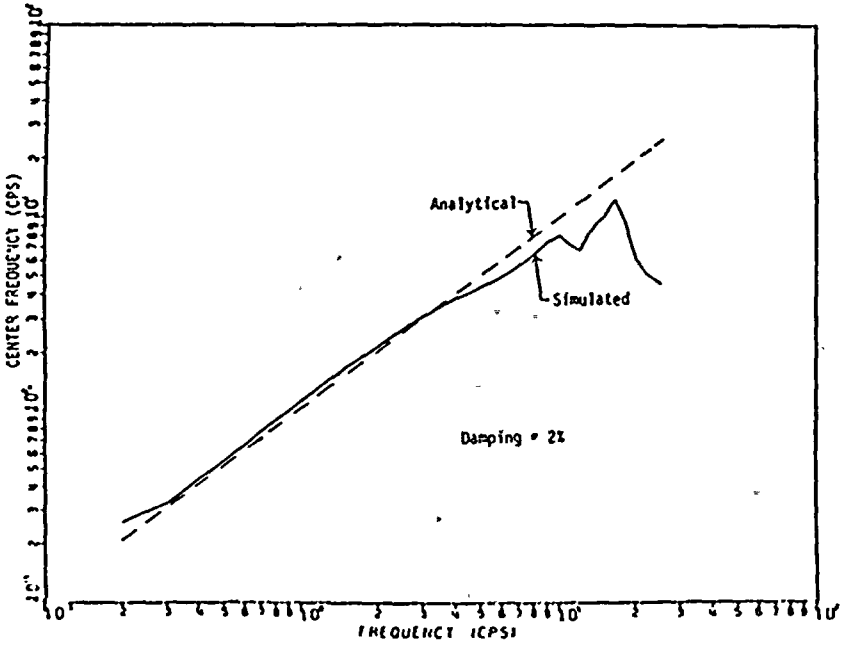

Fig. 6.15 Spectral Center Frequencies of Response Motions at Node 11 to Stationary Ground Motions

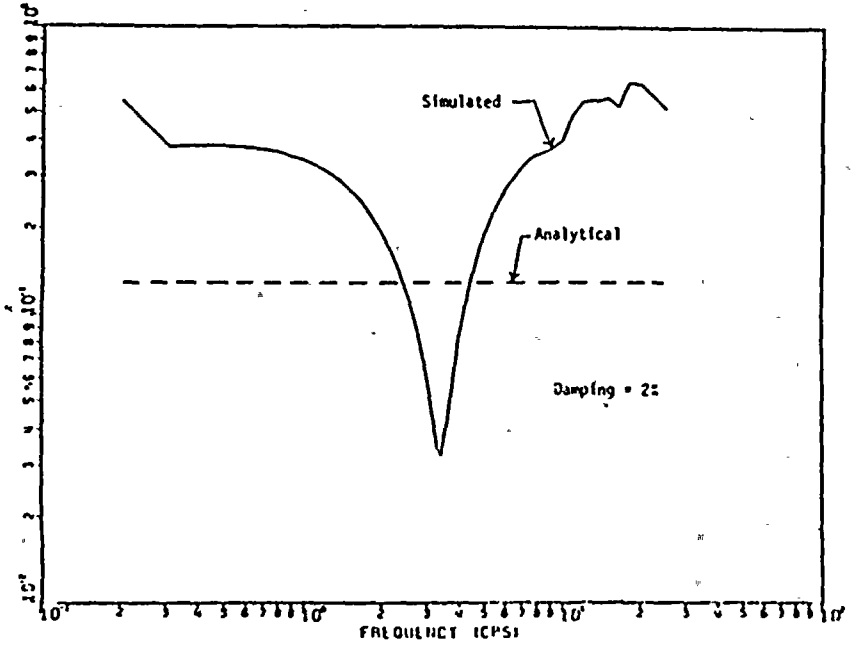

Fig. 6.16 Spectral Dispersion Parameter ϵ_2 of Response Motions at Node 11 to Stationary Ground Motions

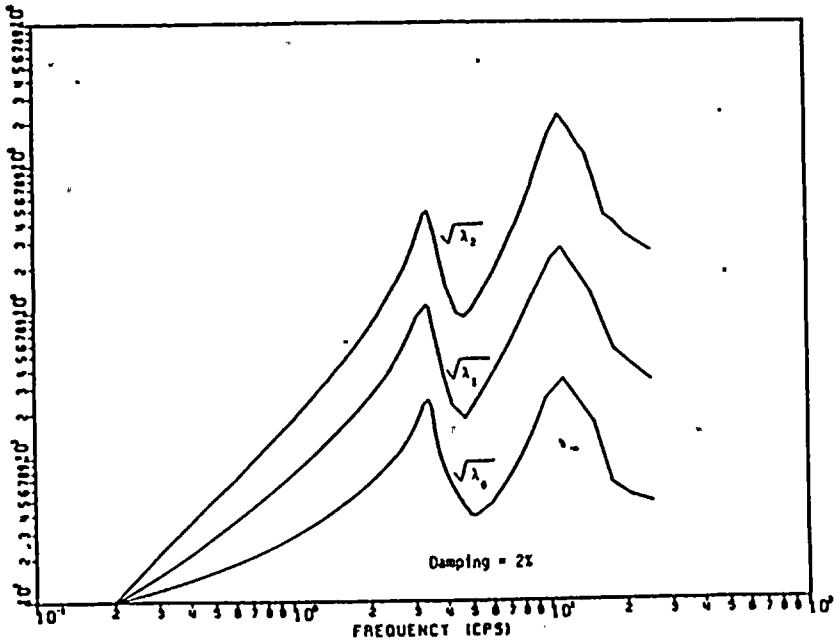

Fig. 6.17 Spectral Moments of Response Motions at Node 18 to Stationary Ground Motions

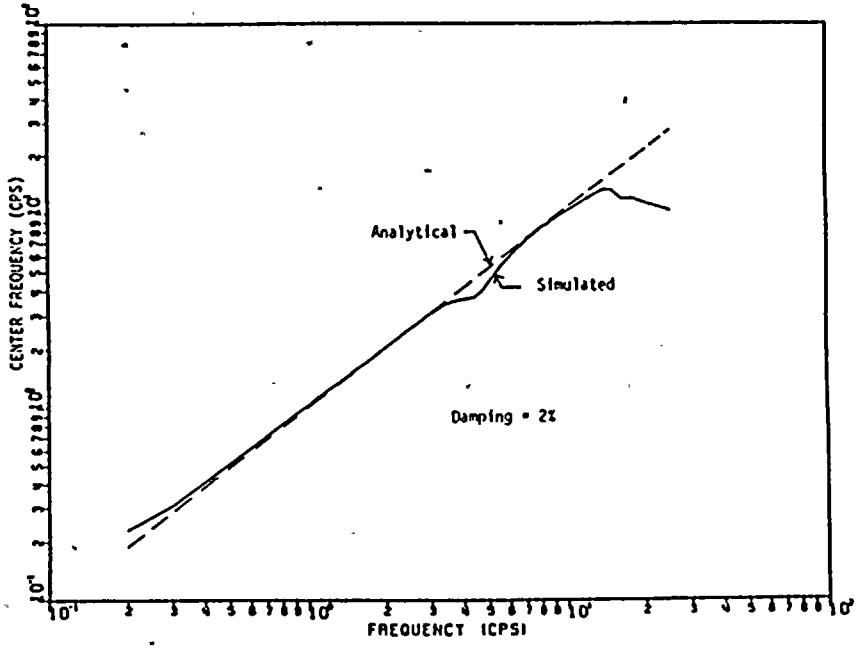

Fig. 6.18 Spectral Center Frequencies of Response Motions at Node 18 to Stationary Ground Motions

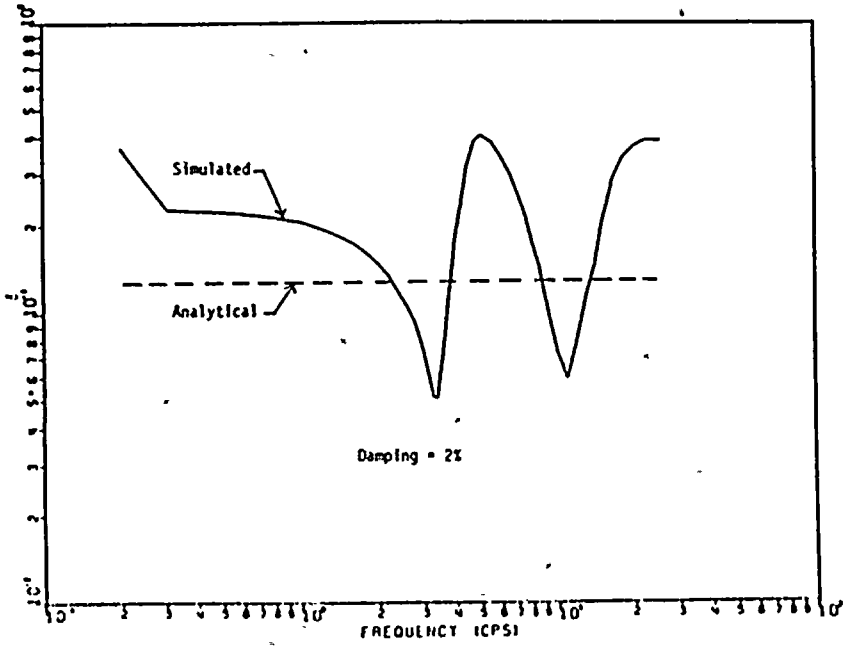

Fig. 6.19 Spectral Dispersion Parameter δ of Response Motions at Node 18 to Stationary Ground Motions

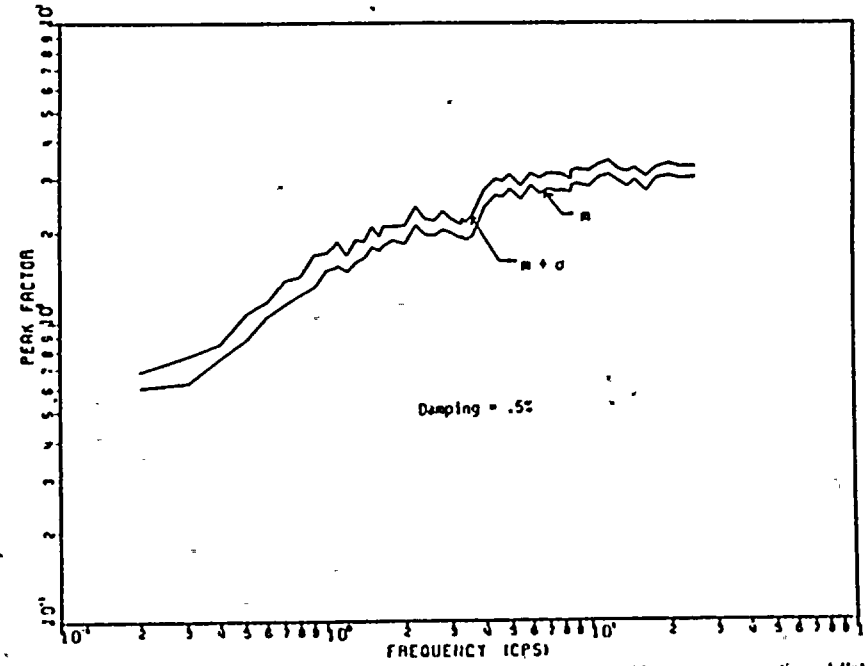

Fig. 6.20 Simulated Peak Factors for Floor Response at Node 11 to Stationary Ground Motions

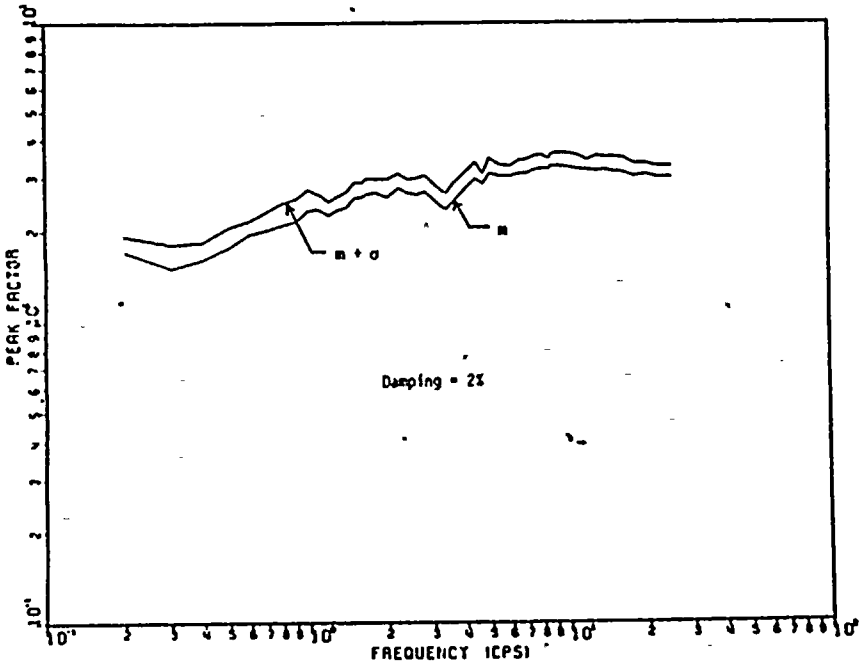

Fig. 6.21 Simulated Peak Factors for Floor Responses at Node 11 to Stationary Ground Motions

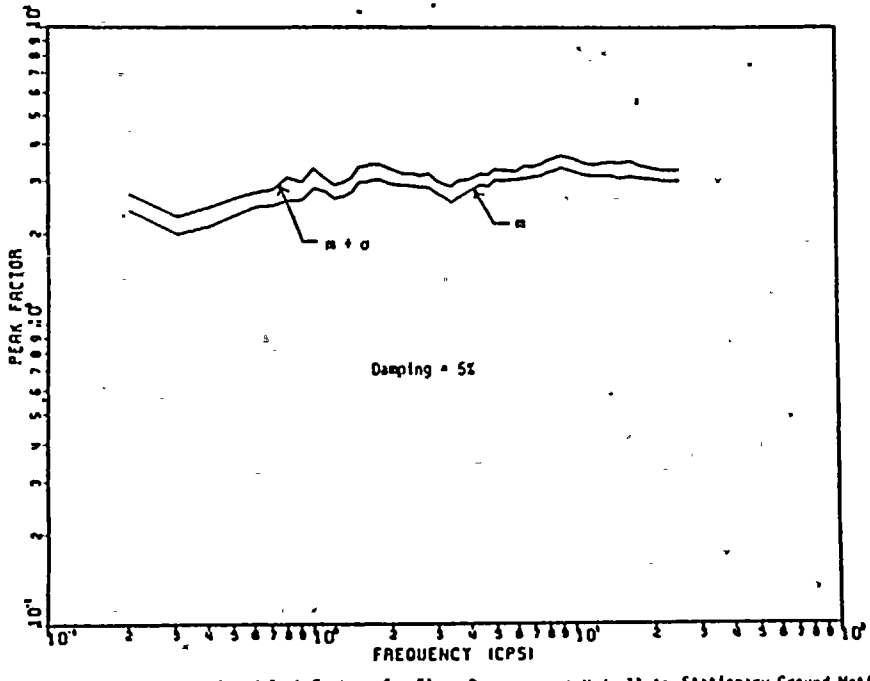

Fig. 6.22 Simulated Peak Factors for Floor Responses at Node 11 to Stationary Ground Motions

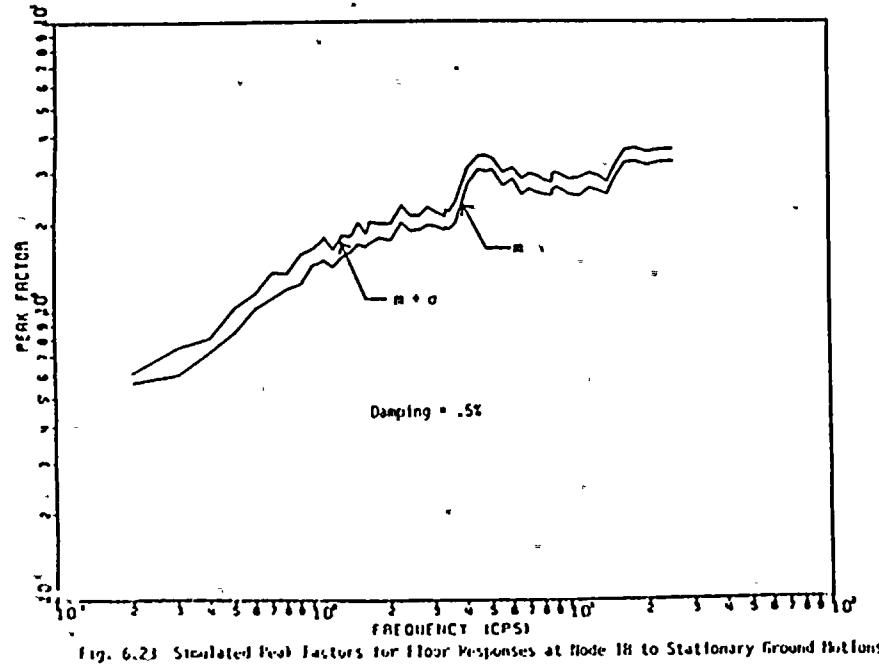

Fig. 6.23 Simulated Peak Factors for Floor Responses at Node 18 to Stationary Ground Motions

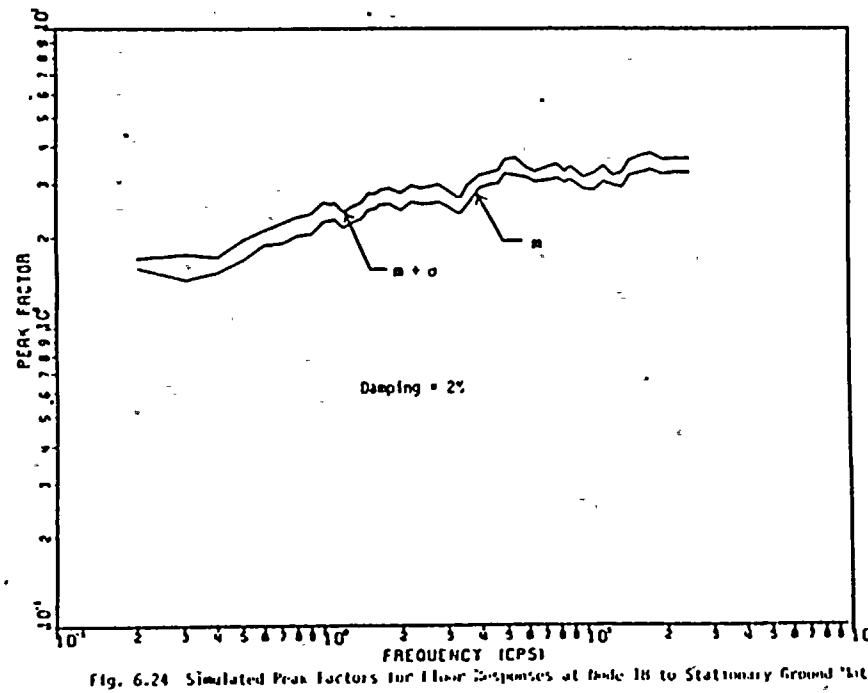

Fig. 6.24 Simulated Peak Factors for Floor Responses at Node 18 to Stationary Ground Motions

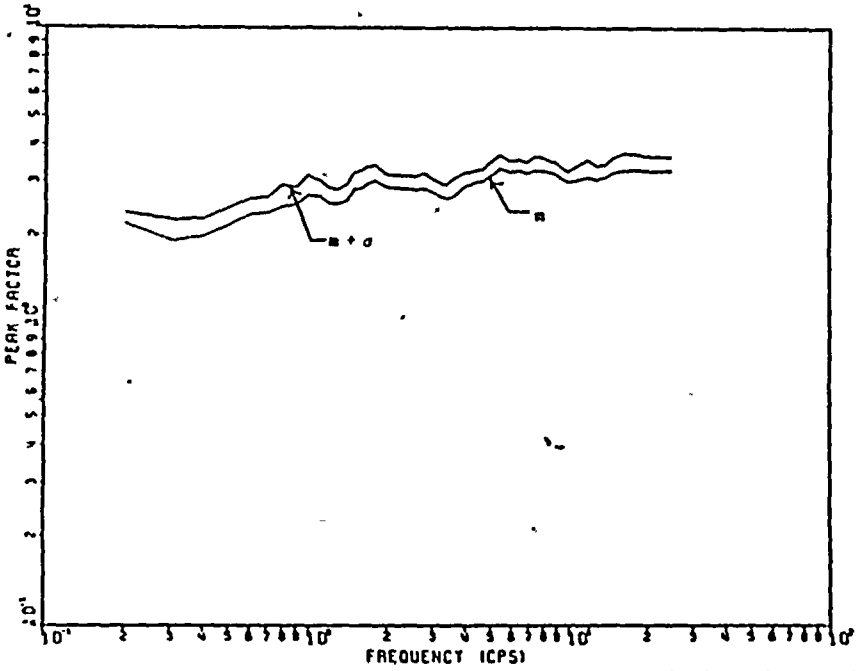

Fig. 6.25 Simulated Peak Factors for Floor Responses at Node 18 to Stationary Ground Motions

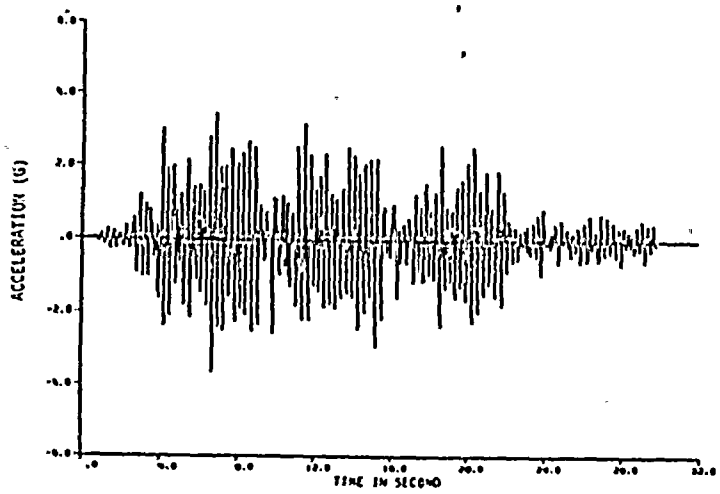

Fig. 6.26 A Typical Response Motion at Node 11 to the Type B Ground Motion

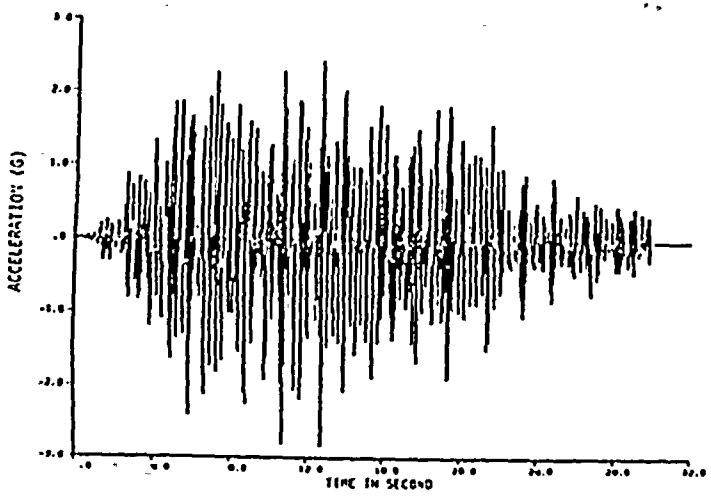

Fig. 6.27 A Typical Response Motion at Node 18 to the Stationary Ground Motion

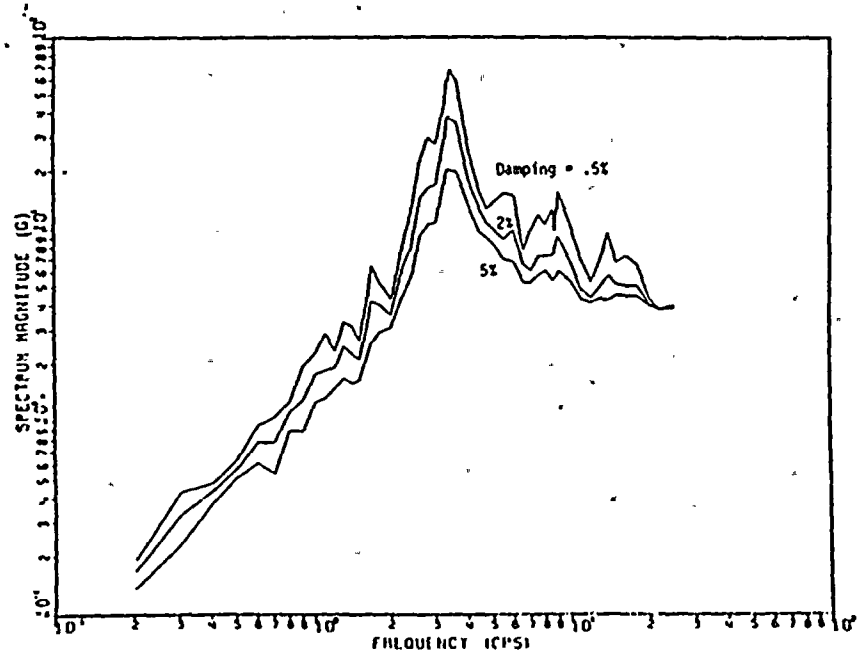

Fig. 6.28 Floor Response Spectra of the Response Motion at Node 11 in Fig. 6.26

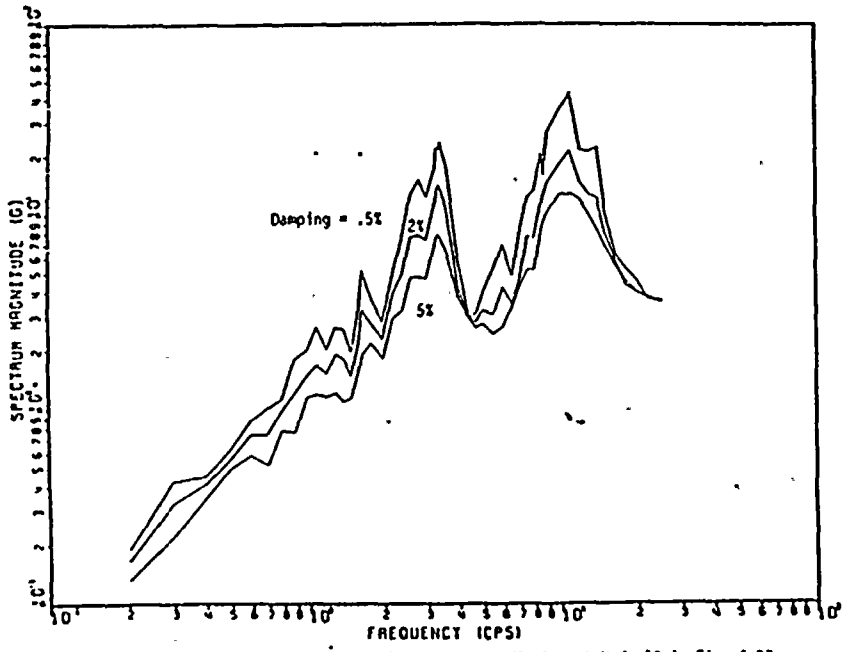

Fig. 6.29 Floor Response Spectra of the Response Motion at Node 18 in Fig. 6.27

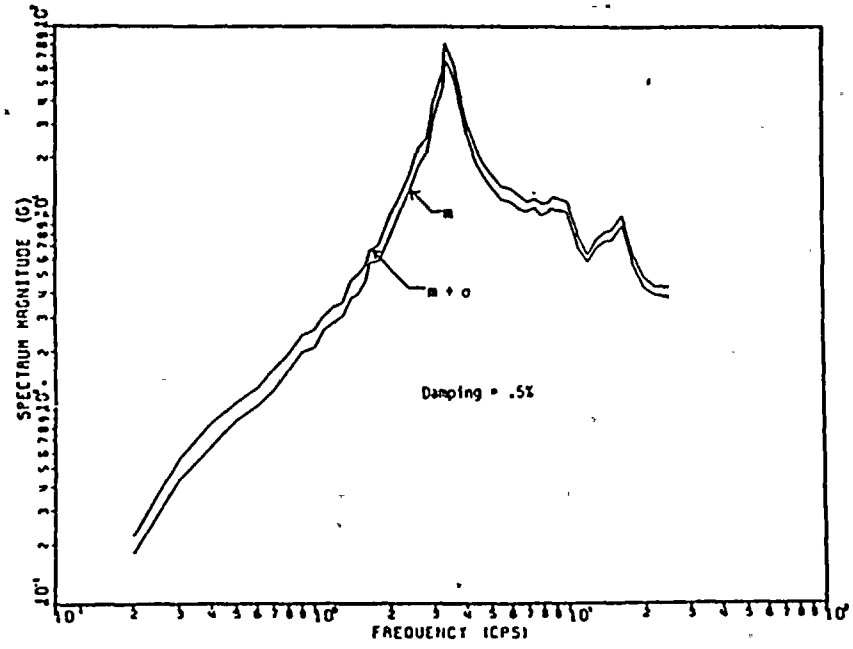

Fig. 6.30 Simulated Floor Response Spectra of Response Motions at Node 11 to Type B Ground Motions

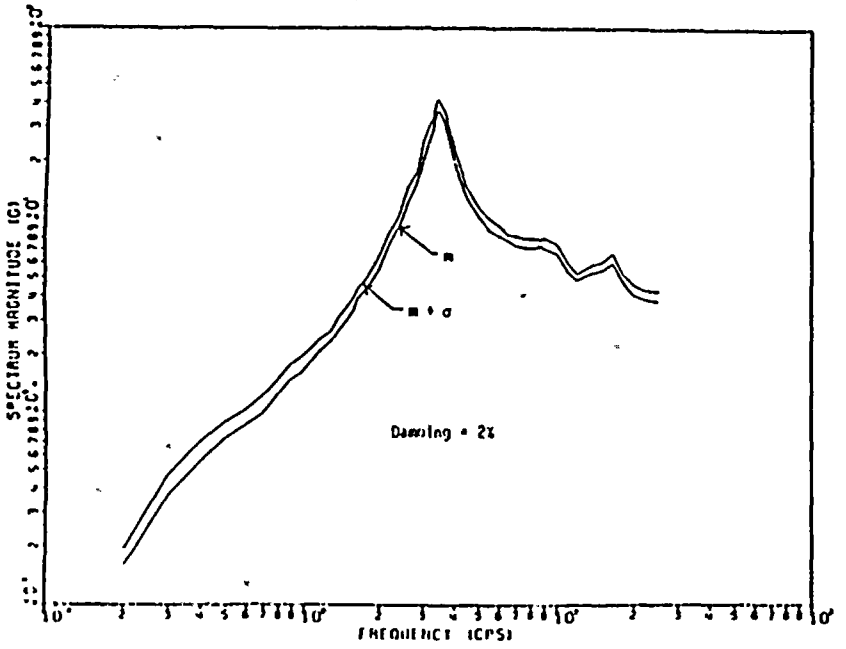

Fig. 6.31 Simulated Floor Response Spectra of Response Motions at Node 11 to Type B Ground Motions

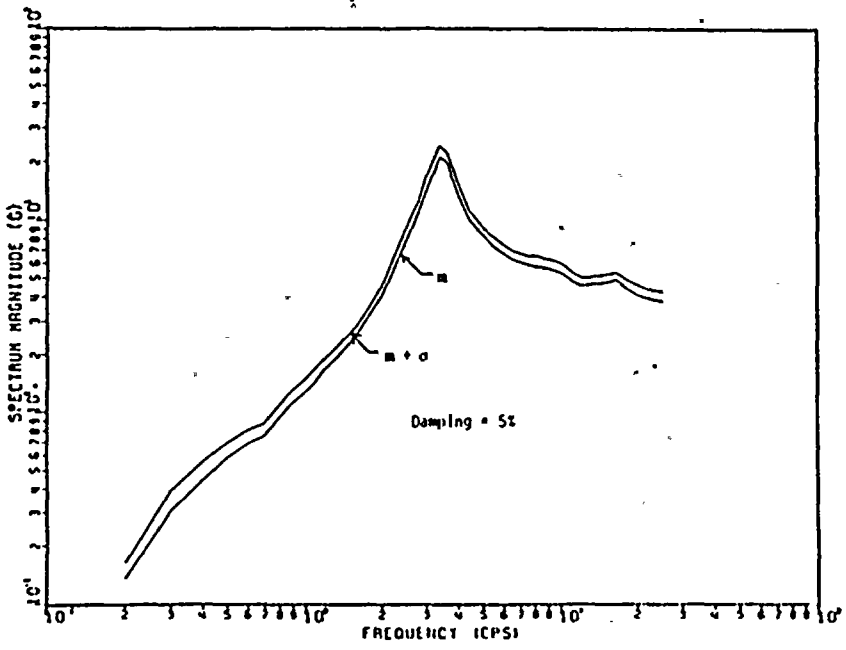

Fig. 6.32 Simulated Floor Response Spectra of Response Motions at Node 11 to Type B Ground Motions

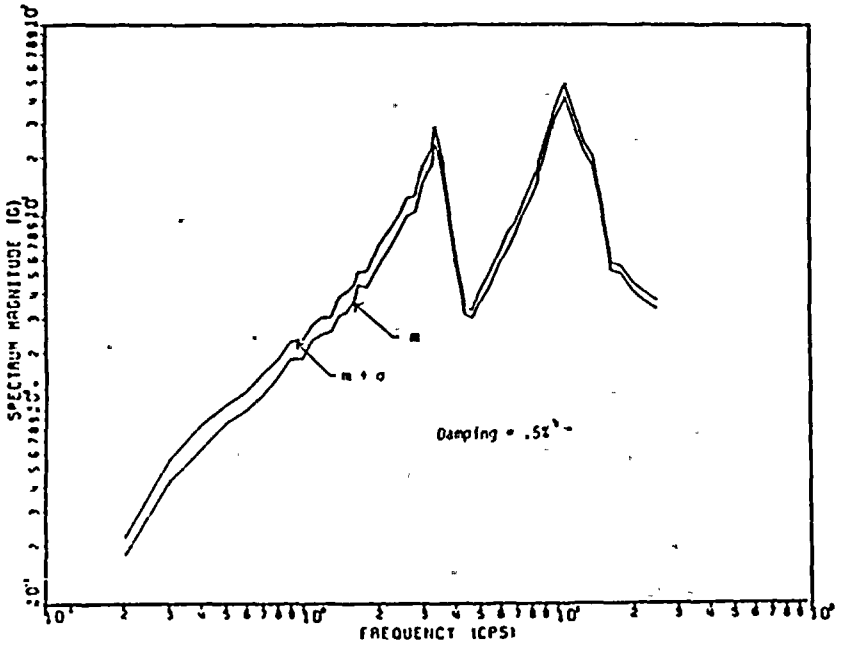

Fig. 6.33 Simulated Floor Response Spectra of Response Motions at Node 18 to Type B Ground Motions

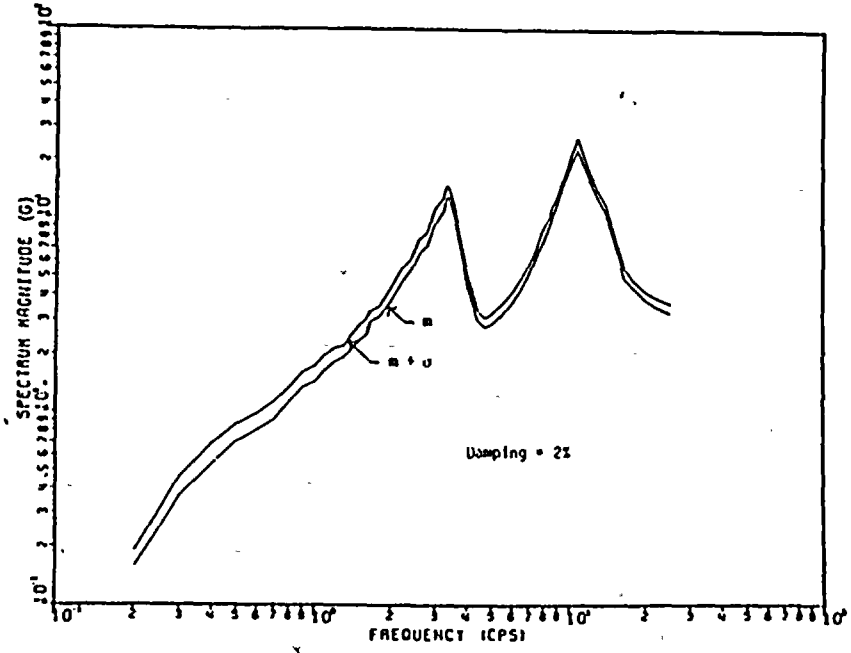

Fig. 6.34 Simulated Floor Response Spectra of Response Motions at Node 18 to Type B Ground Motions

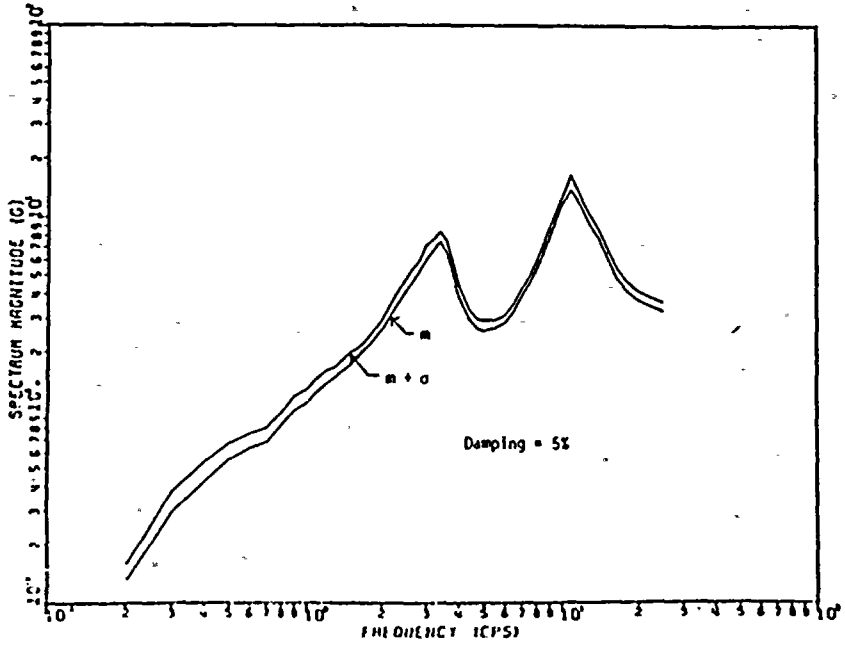

Fig. 6.35 Simulated Floor Response Spectra of Response Motions at Node 18 to Type B Ground Motions

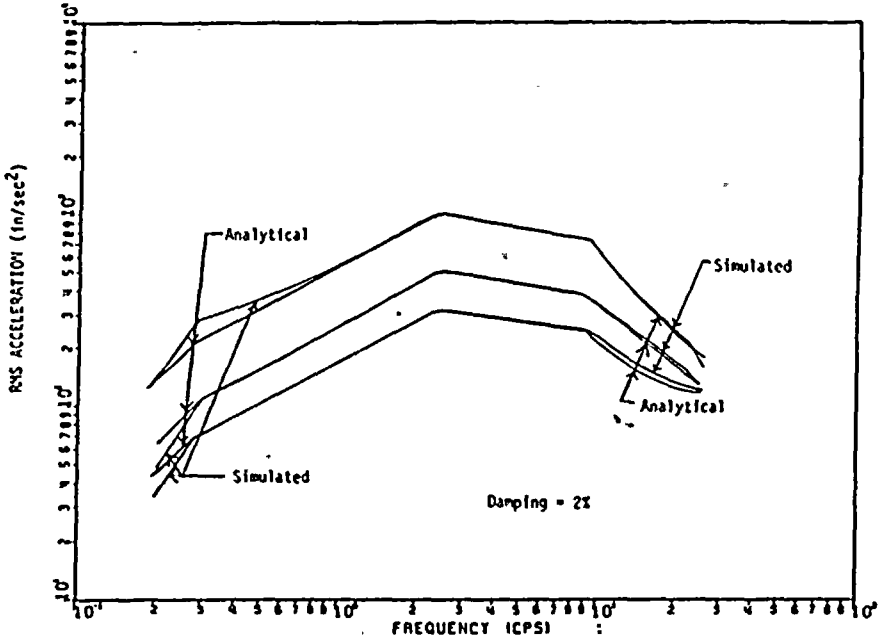

Fig. 7.1 Comparison of the Analytical with the Simulated RMS Spectral Responses to Stationary Ground Motions

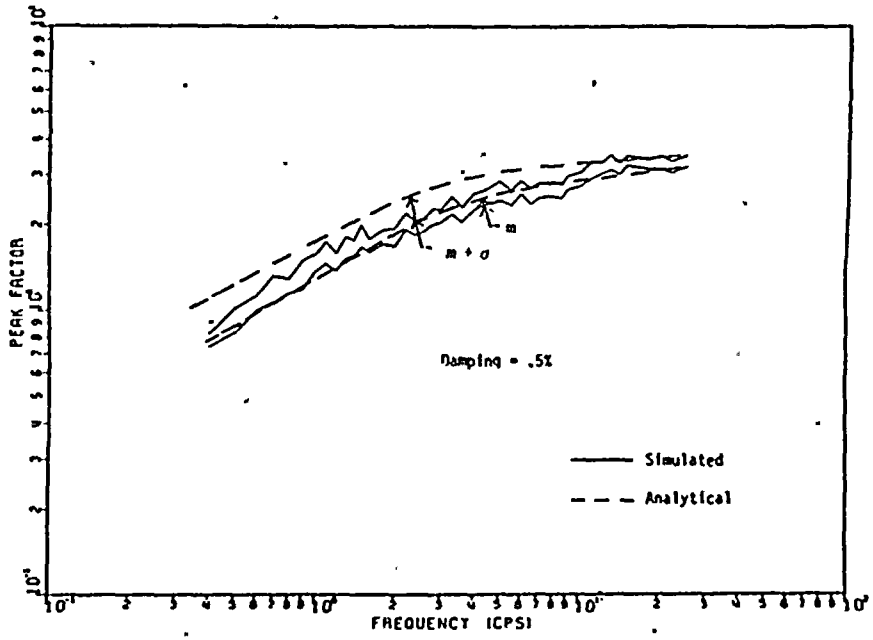

Fig. 7.2 Comparison of the Analytical with the Simulated Peak Factors for Stationary Ground Motions

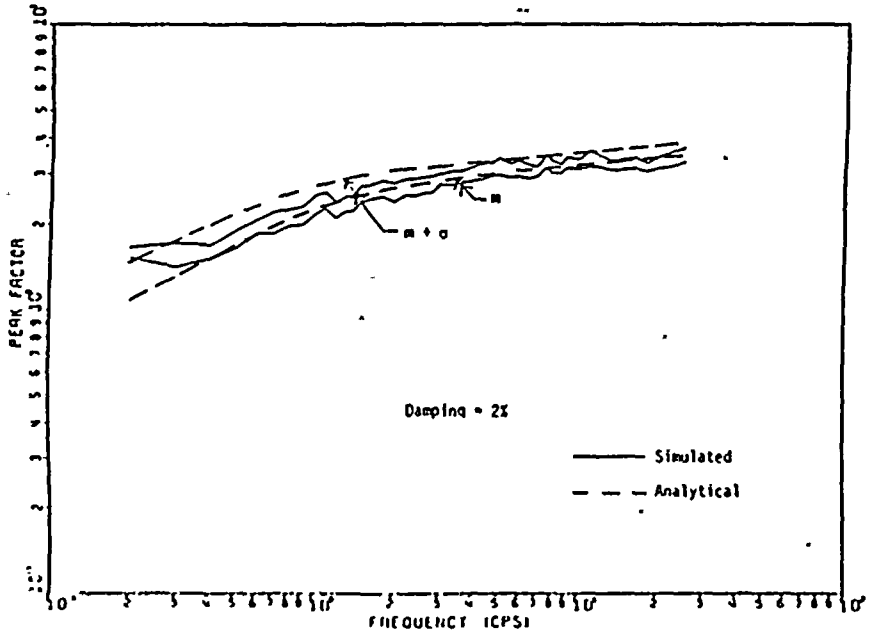

Fig. 7.3 Comparison of the Analytical with the Simulated Peak Factors for Stationary Ground Motions

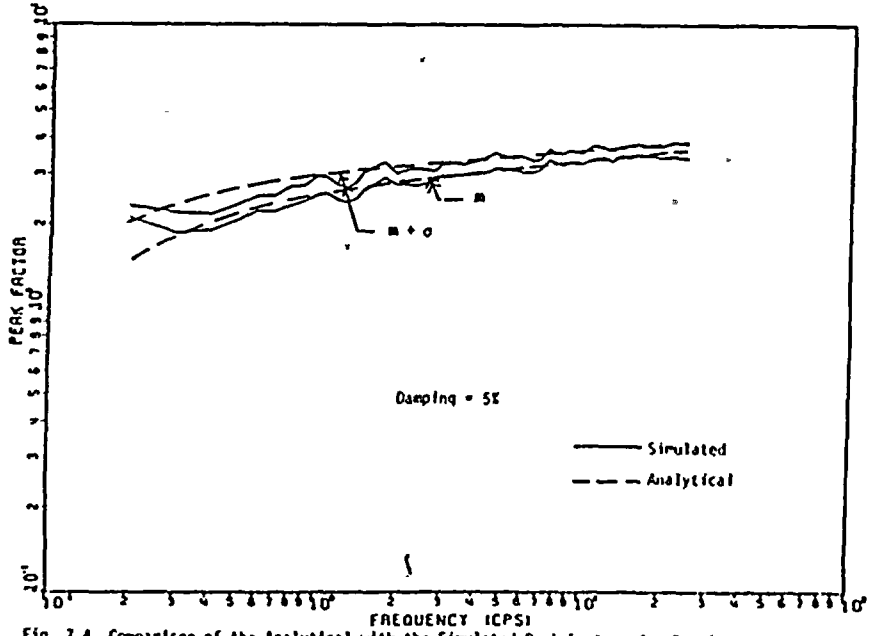

Fig. 7.4 Comparison of the Analytical with the Simulated Peak Factors for Stationary Ground Motions

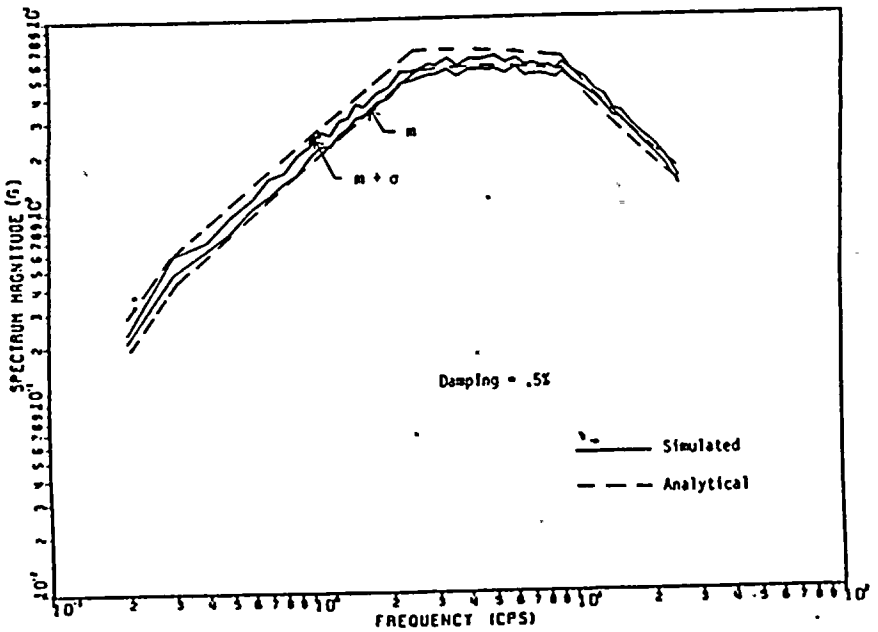

Fig. 7.5 Comparison of the Analytical with the Simulated Response Spectra of Stationary Ground Motions

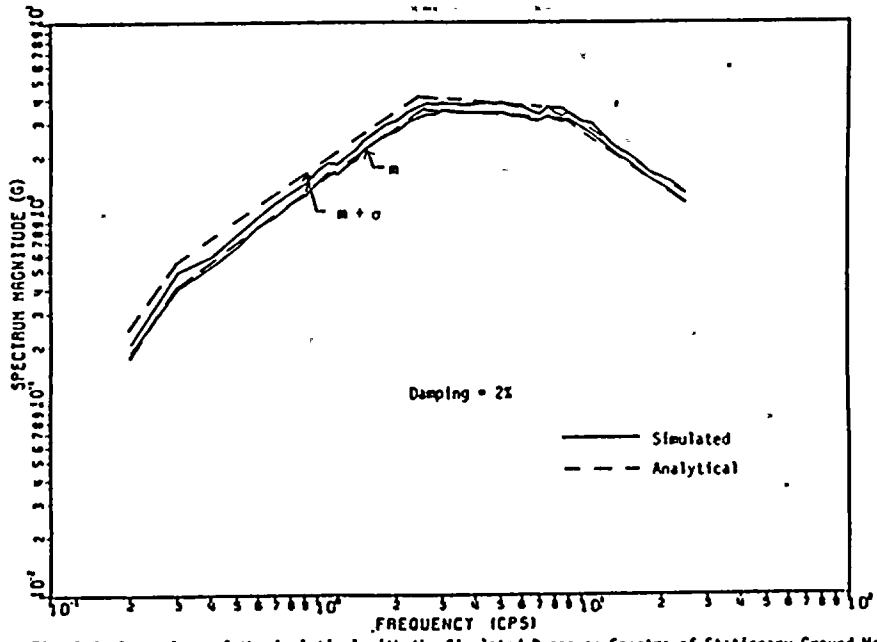

Fig. 7.6 Comparison of the Analytical with the Simulated Response Spectra of Stationary Ground Motions

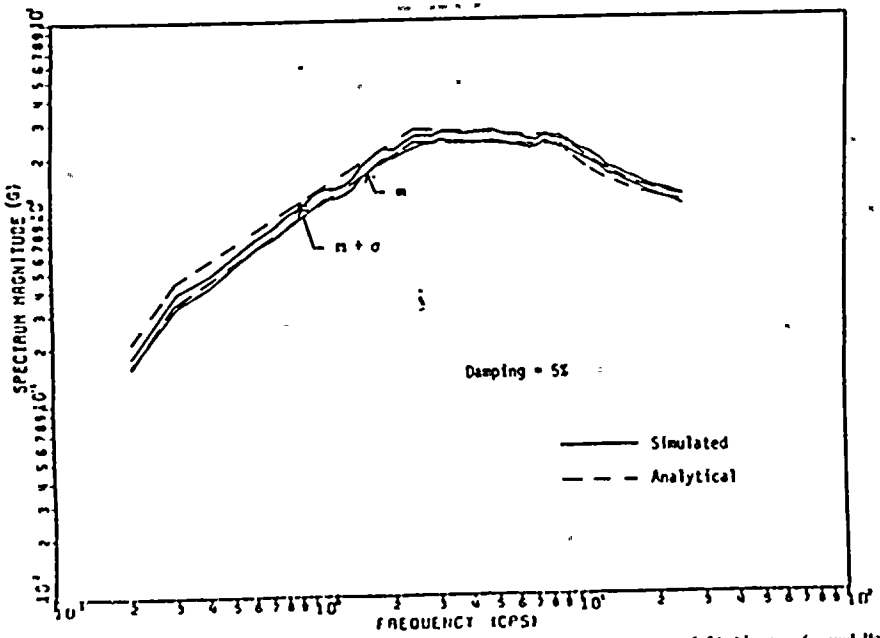

Fig. 7.7 Comparison of the Analytical with the Simulated Response Spectra of Stationary Ground Motions

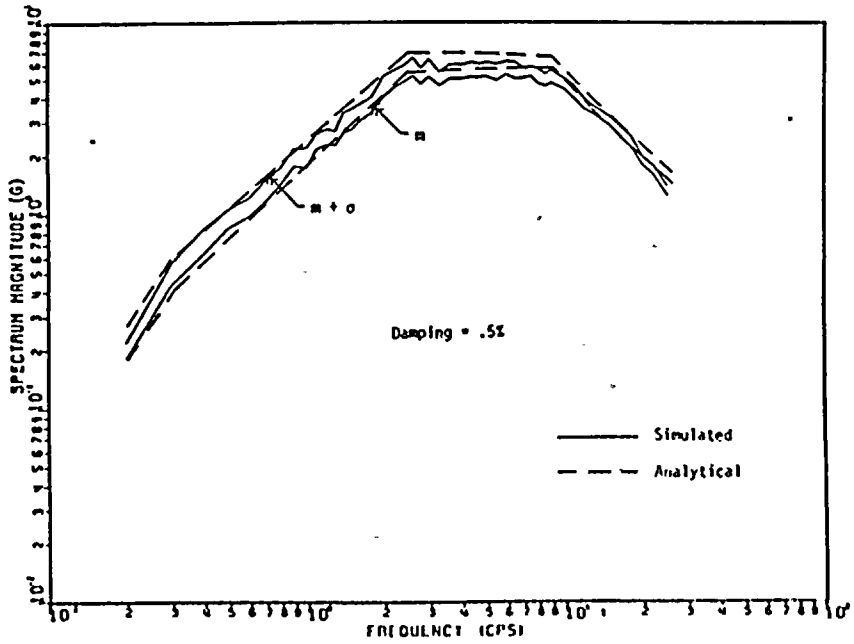

Fig. 7.8 Comparison of the Analytical with the Simulated Response Spectra of Type B Ground Motions

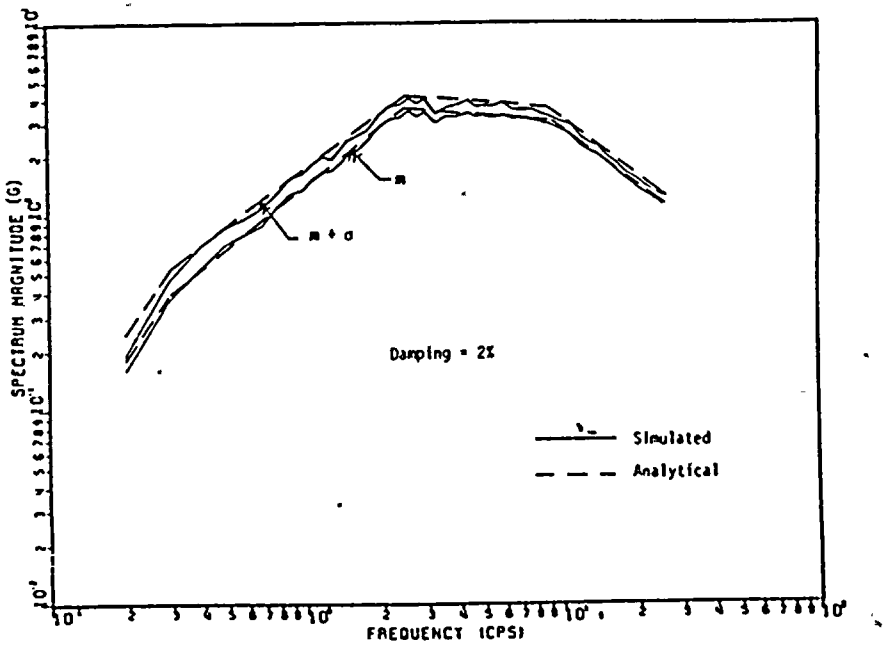

Fig. 7.9 Comparison of the Analytical with the Simulated Response Spectra of Type B Ground Motions

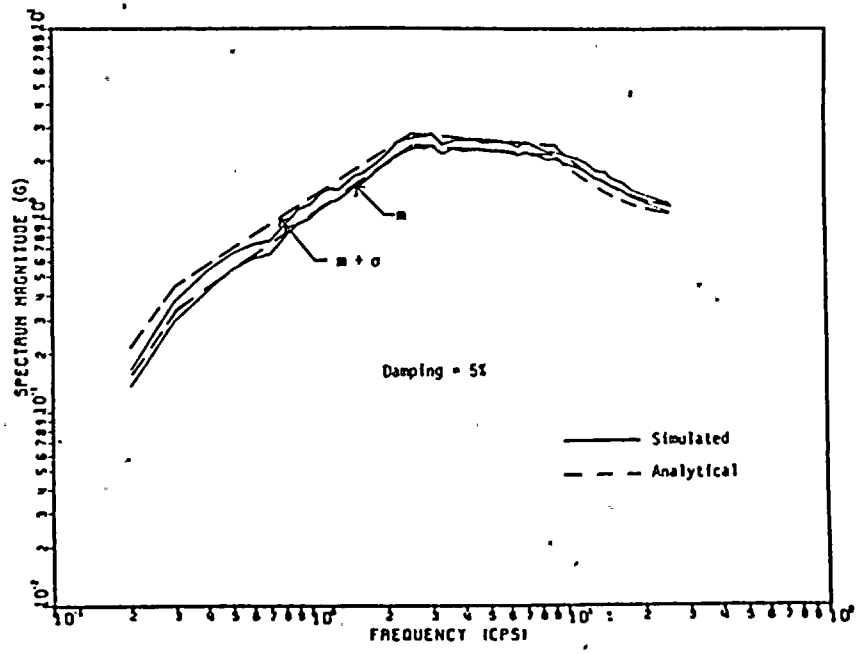

Fig. 7.10 Comparison of the Analytical with the Simulated Response Spectra Type B Ground Motions

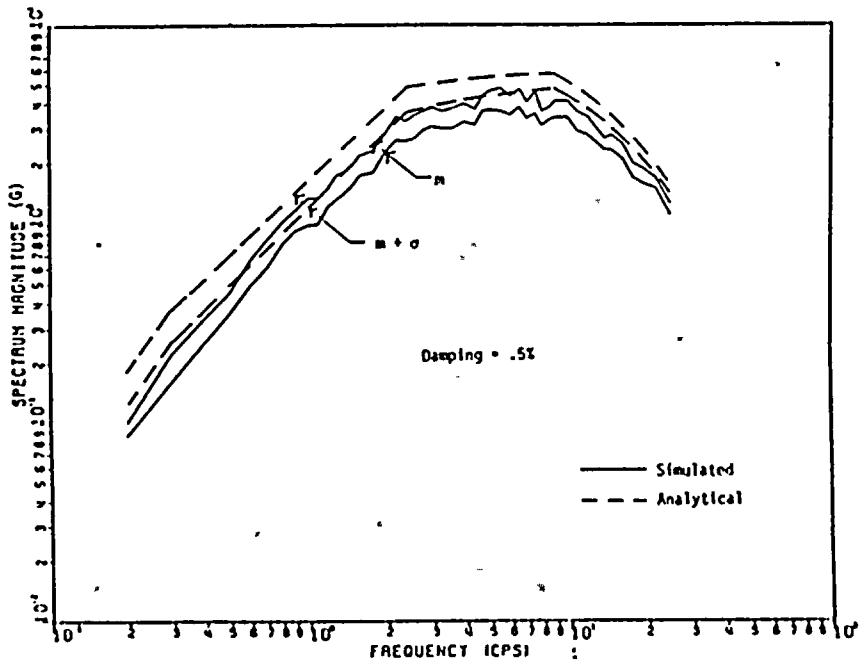

Fig. 7.11 Comparison of the Simulated with the Analytical Response Spectra of Type C Ground Motions

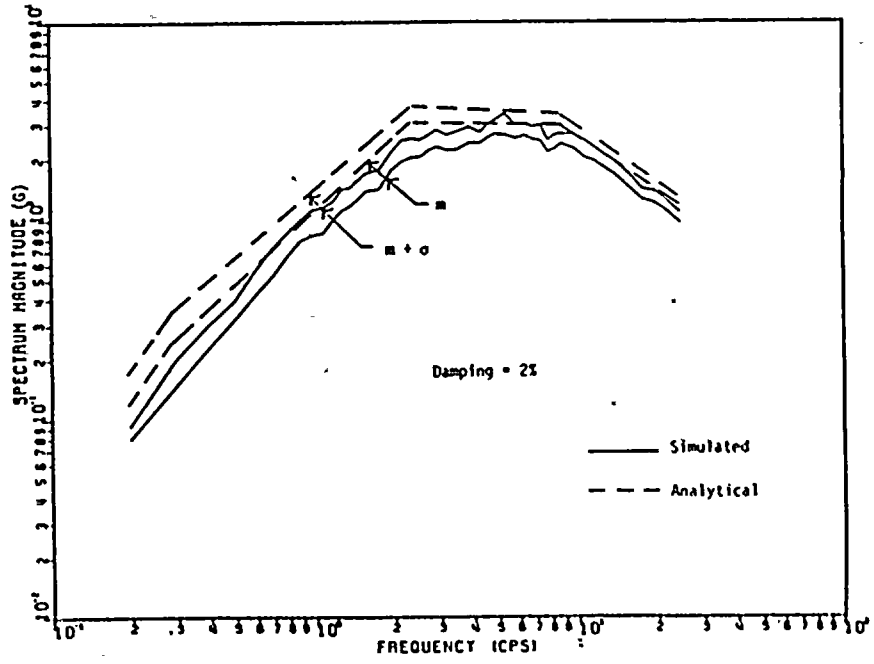

Fig. 7.12 Comparison of the Analytical with the Simulated Response Spectra of Type C Ground Motions

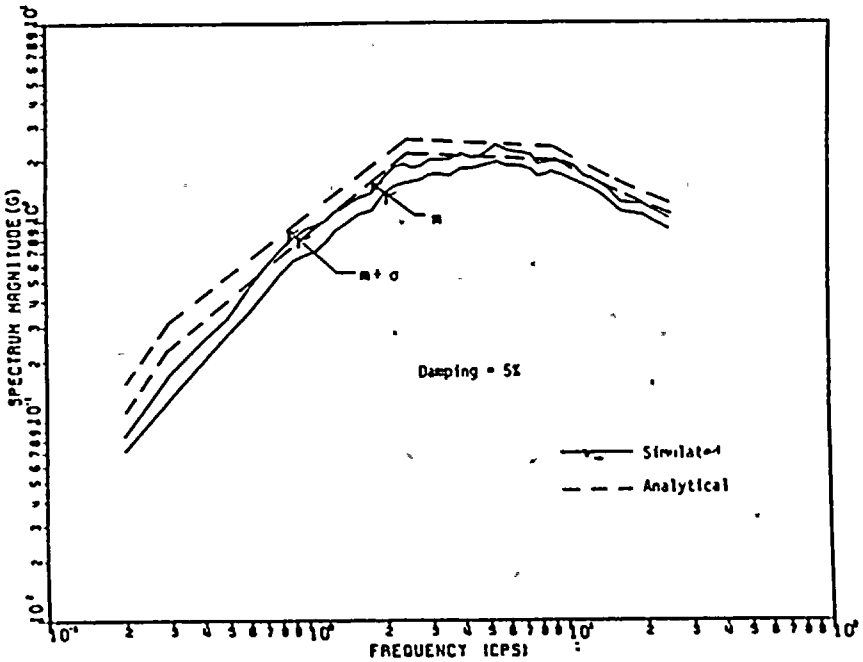

Fig. 7.13 Comparison of the Analytical with the Simulated Response Spectra of Type C Ground Motions

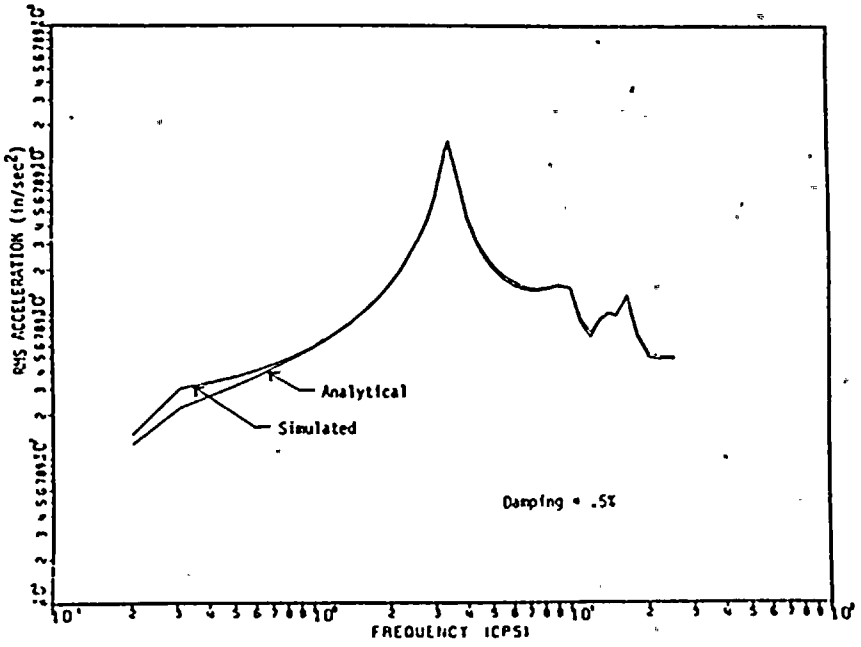

Fig. 7.14-a Comparison of the Analytical with the Simulated RMS Floor Spectral Response at Node 11 to Stationary Ground Motions

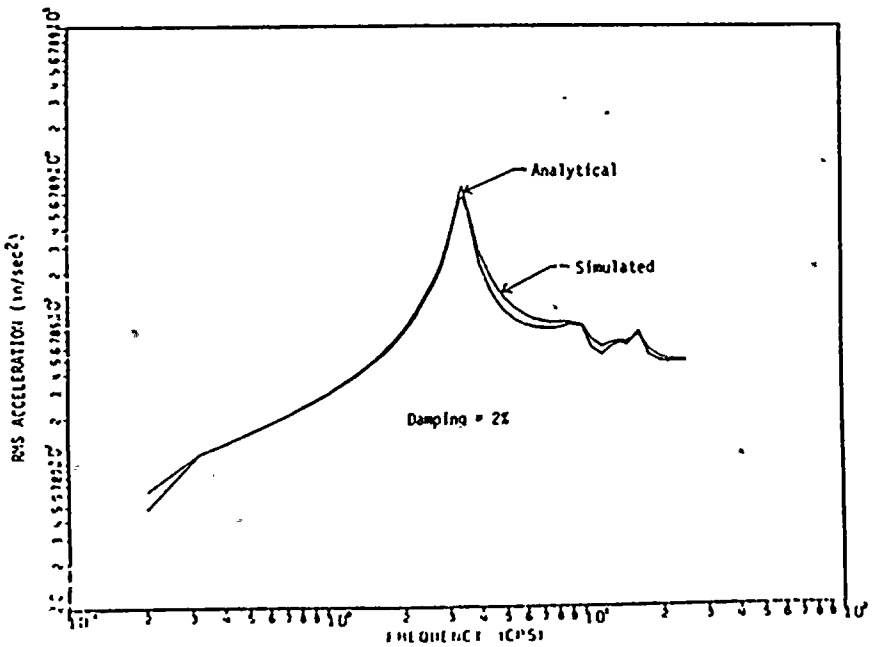

Fig. 7.14-b Comparison of the Analytical with the Simulated RMS Floor Spectral Response at Node 11 to Stationary Ground Motions

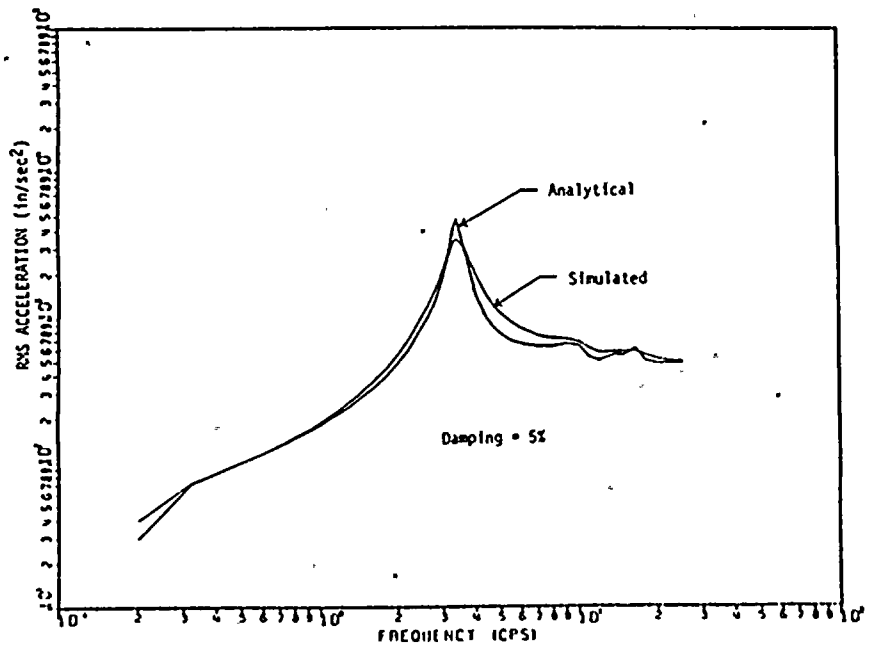

Fig. 7.14-c Comparison of the Analytical with the Simulated RMS Floor Spectral Response at Node 11 to Stationary Ground Motions

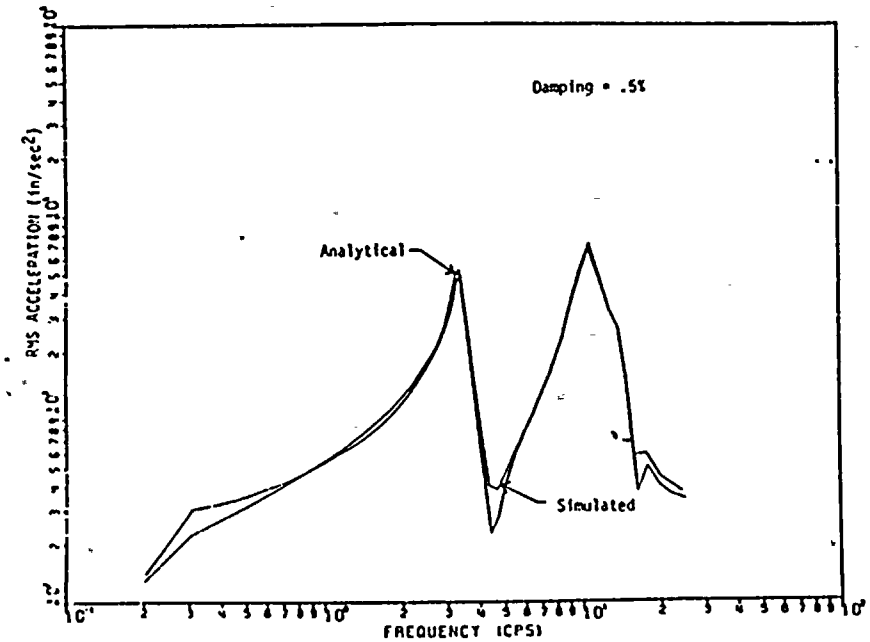

Fig. 7.15-a A Comparison of the Analytical with the Simulated RMS Floor Spectral Response at Node 18 to Stationary Ground Motions

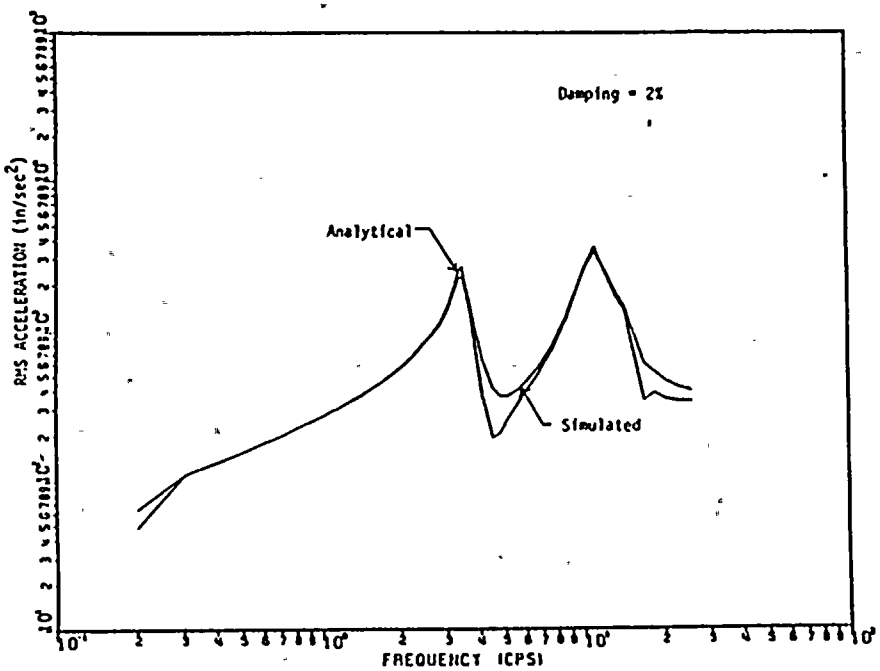

Fig. 7.15-b Comparison of the Analytical with the Simulated RMS Floor Spectral Response at Node 18 to Stationary Ground Motions

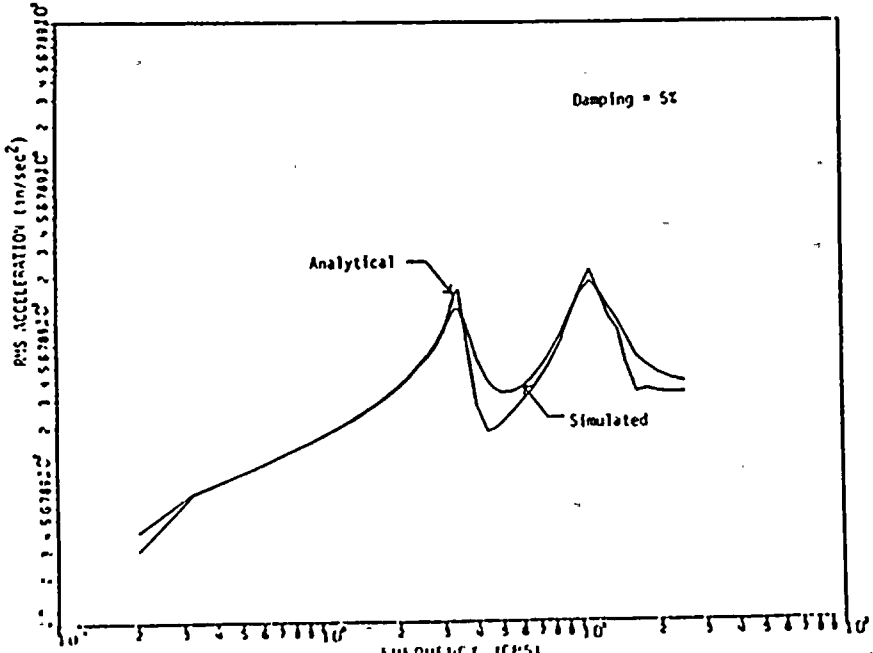

Fig. 7.15-c Comparison of the Analytical with the Simulated RMS Floor Spectral Response at Node 18 to Stationary Ground Motions

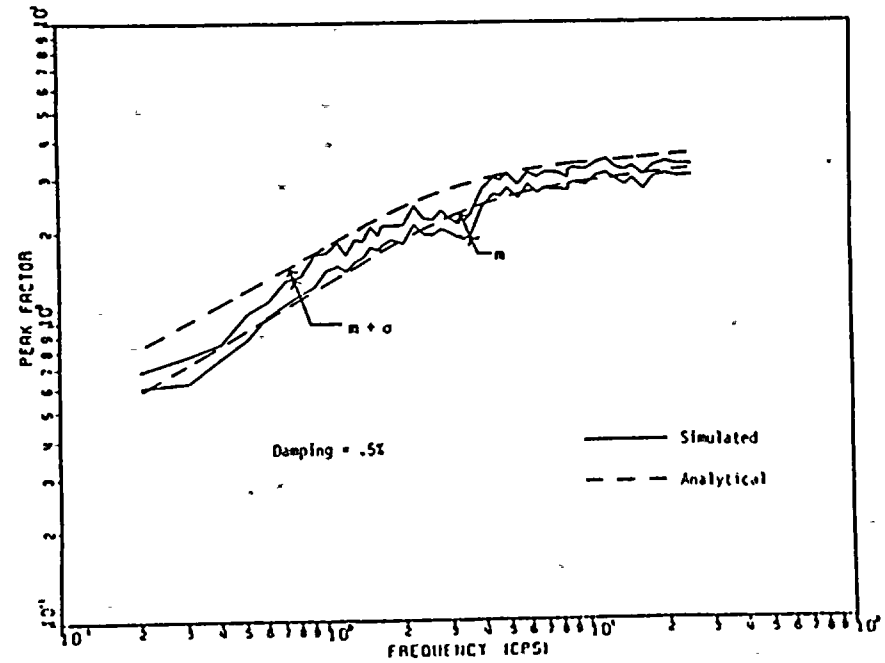

Fig. 7.16 Comparison of the Analytical with the Simulated Peak Factors for Floor Response Motions of Node 11 to Stationary Ground Motions

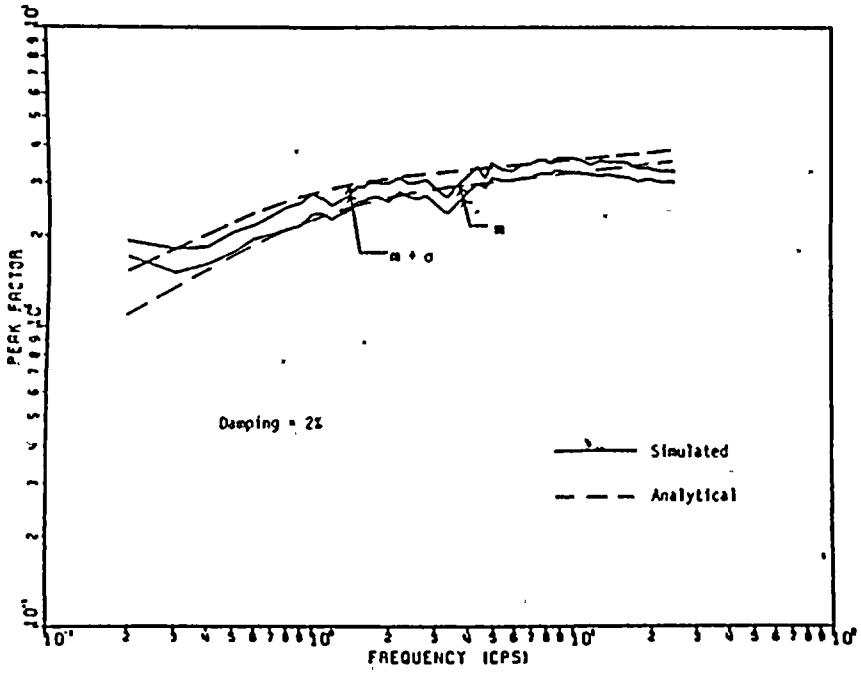

Fig. 7.17 Comparison of the Analytical with the Simulated Peak Factors for Floor Response Motions at Node 11 to Stationary Ground Motions

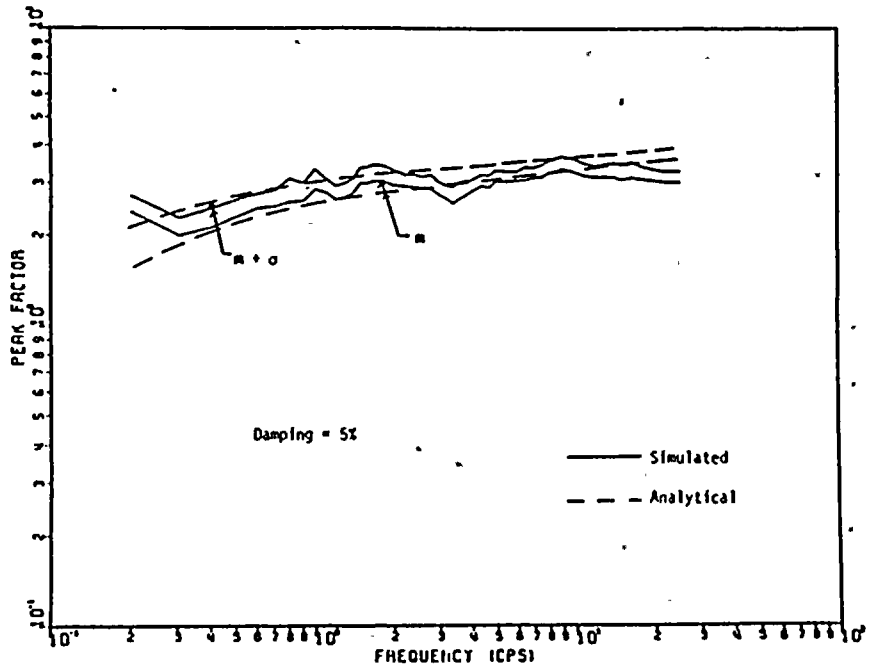

Fig. 7.18 Comparison of the Analytical with the Simulated Peak Factors for Floor Response Motions at Node 11 to Stationary Ground Motions

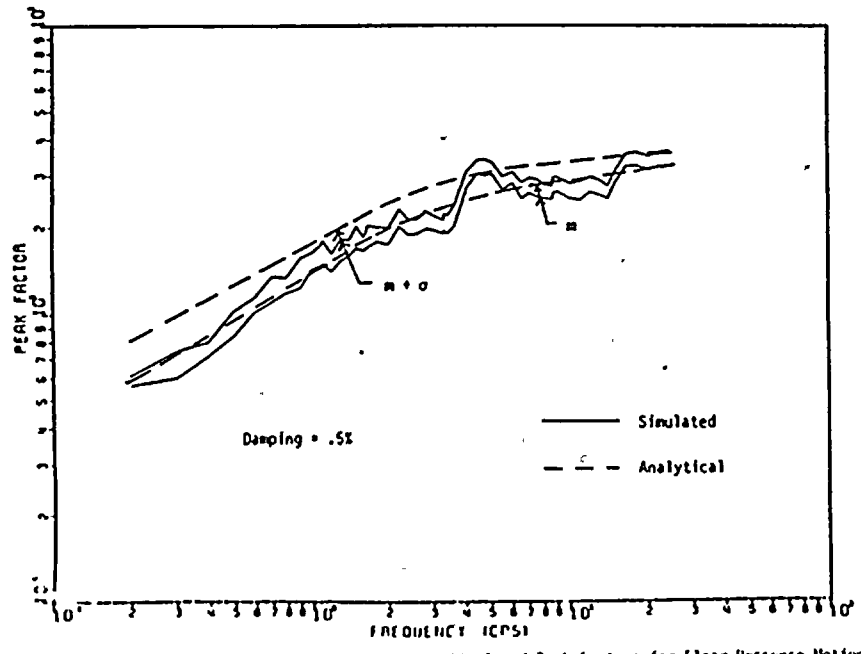

Fig. 7.19 Comparison of the Analytical with the Simulated Peak Factors for Floor Response Motions at Node 18 to Stationary Ground Motions

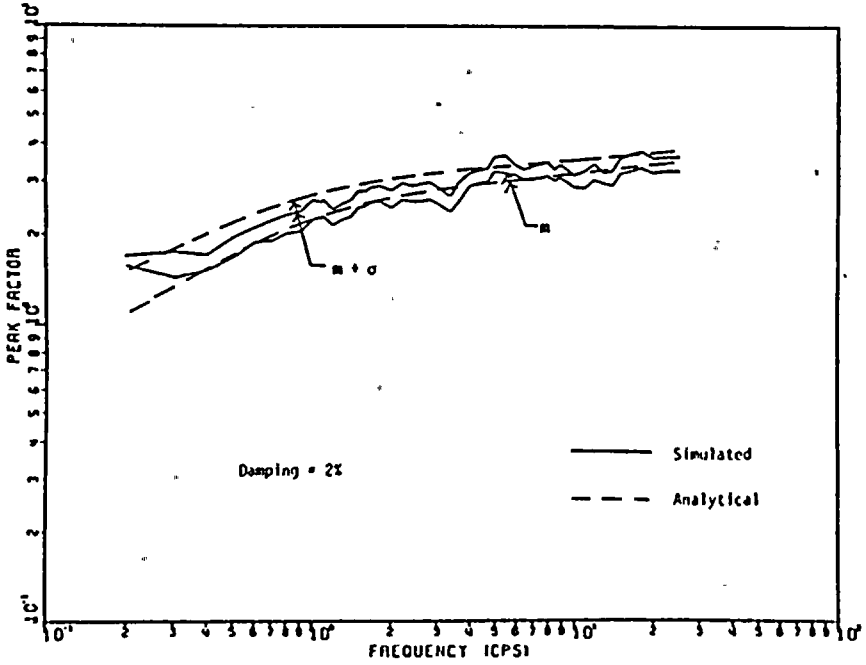

Fig. 7.20 Comparison of the Analytical with the Simulated Peak Factors for Floor Response Motions at Node 18 to Stationary Ground Motions

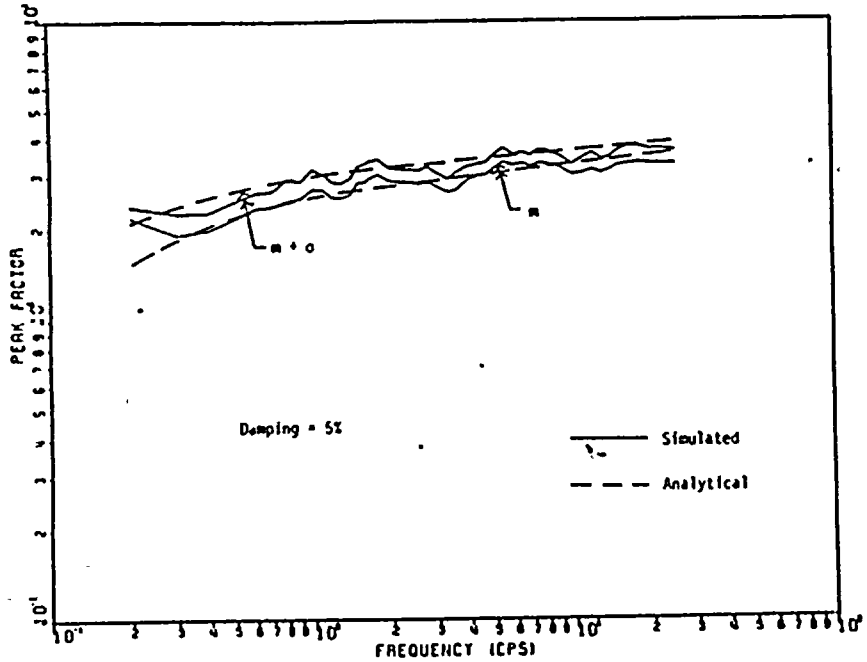

Fig. 7.21 Comparison of the Analytical with the Simulated Peak Factors for Floor Response Motions at Node 18 to Stationary Ground Motions

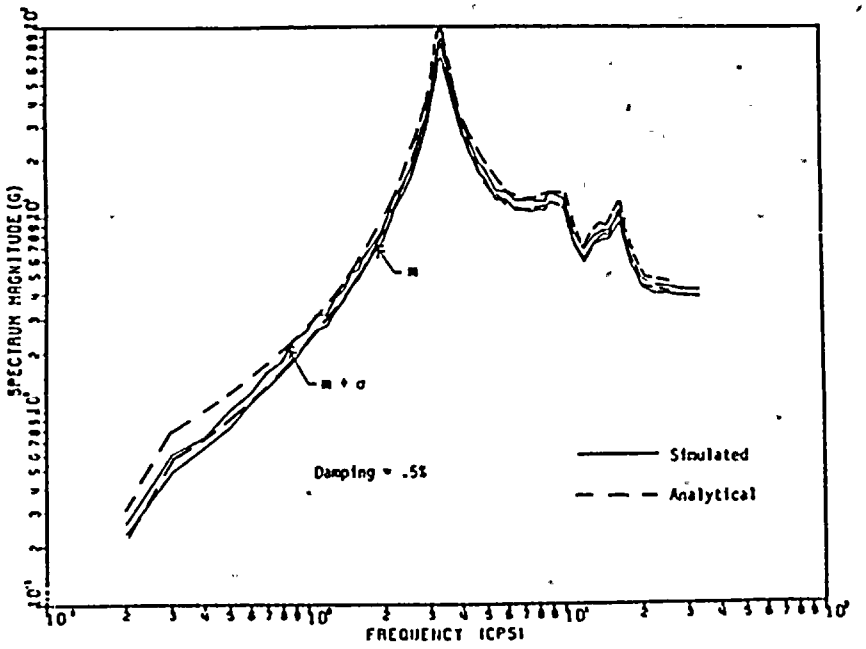

Fig. 7.22 Comparison of the Analytical with the Simulated Floor Response Spectra of Response Motions at Node 11 to Stationary Ground Motions

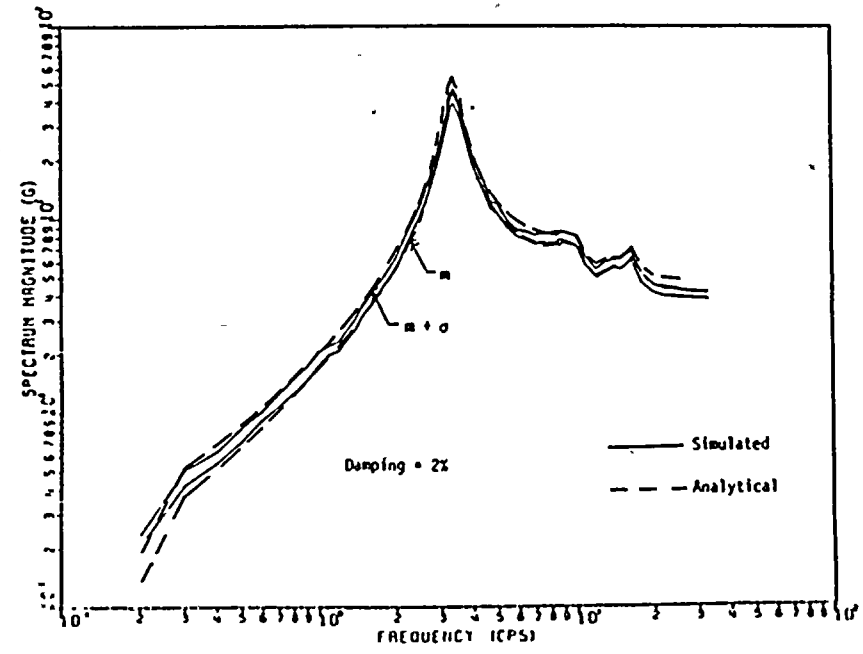

Fig. 7.23 Comparison of the Analytical with the Simulated Floor Response Spectra of Response Motions at Node 11 to Stationary Ground Motions

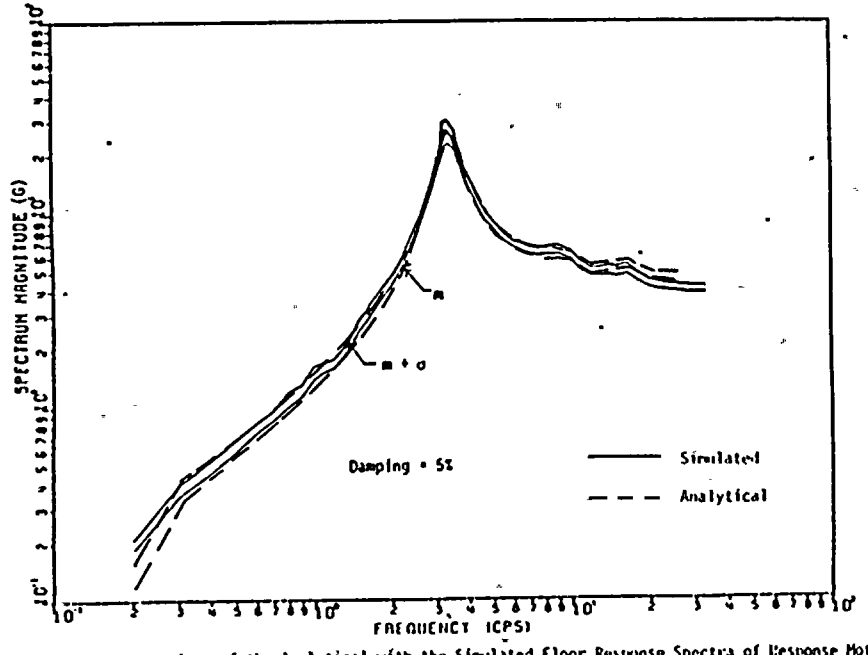

Fig. 7.24 Comparison of the Analytical with the Simulated Floor Response Spectra of Response Motions at Node 11 to Stationary Ground Motions

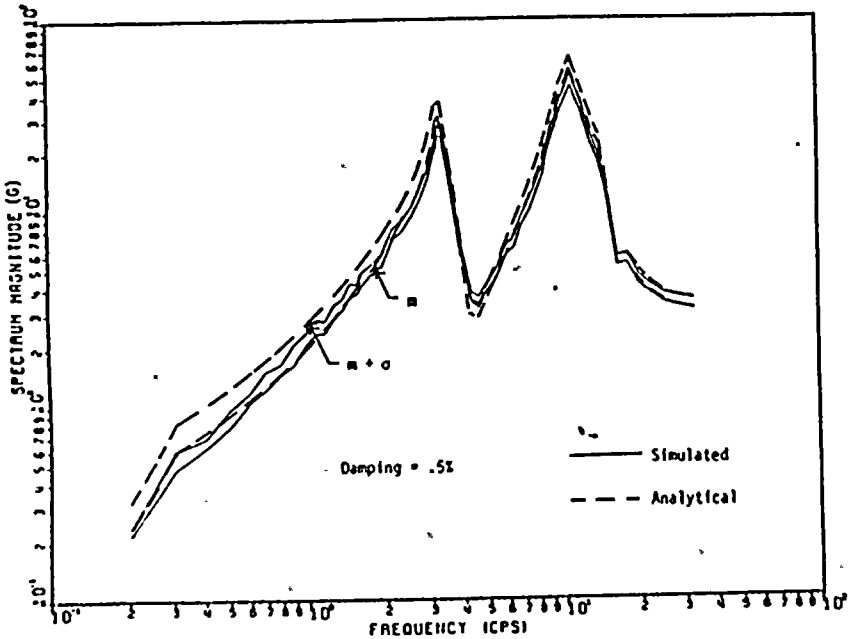

Fig. 7.25 Comparison of the Analytical with the Simulated Floor Response Spectra of Response Motions at Node 13 to Stationary Ground Motions

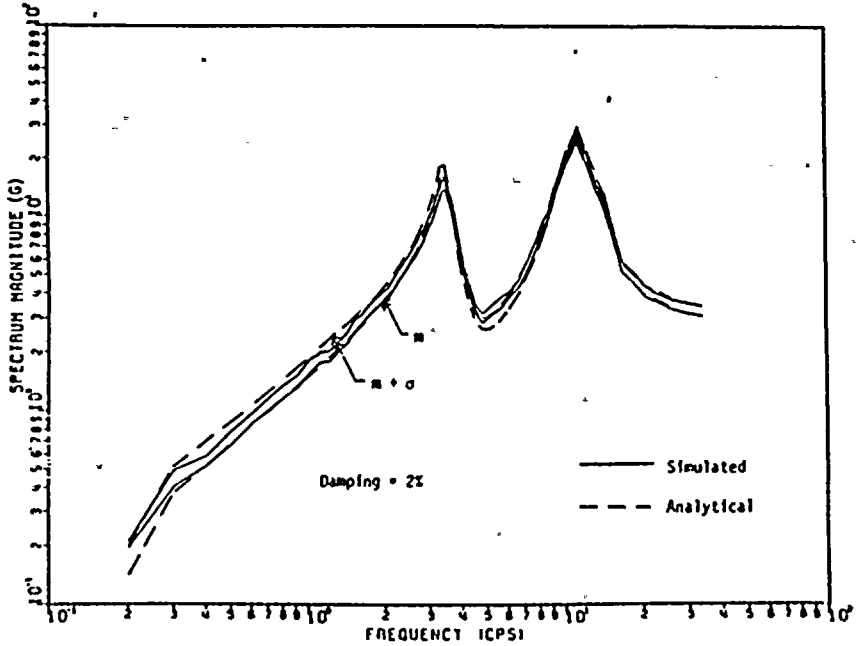

Fig. 7.26 Comparison of the Analytical with the Simulated Floor Response Spectra of Response Motions at Node 18 to Stationary Ground Motions

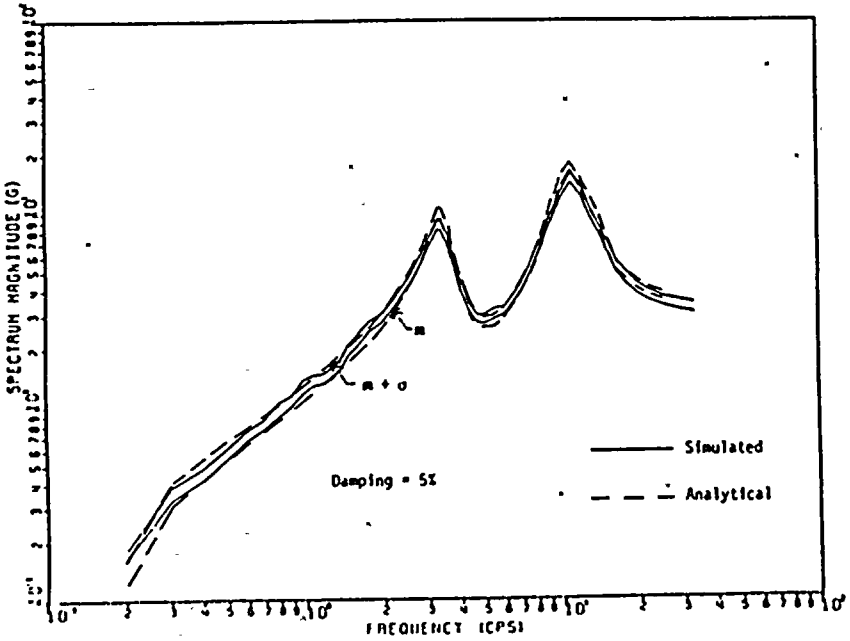

Fig. 7.27 Comparison of the Analytical with the Simulated Floor Response Spectra of Response Motions at Node 18 to Stationary Ground Motions

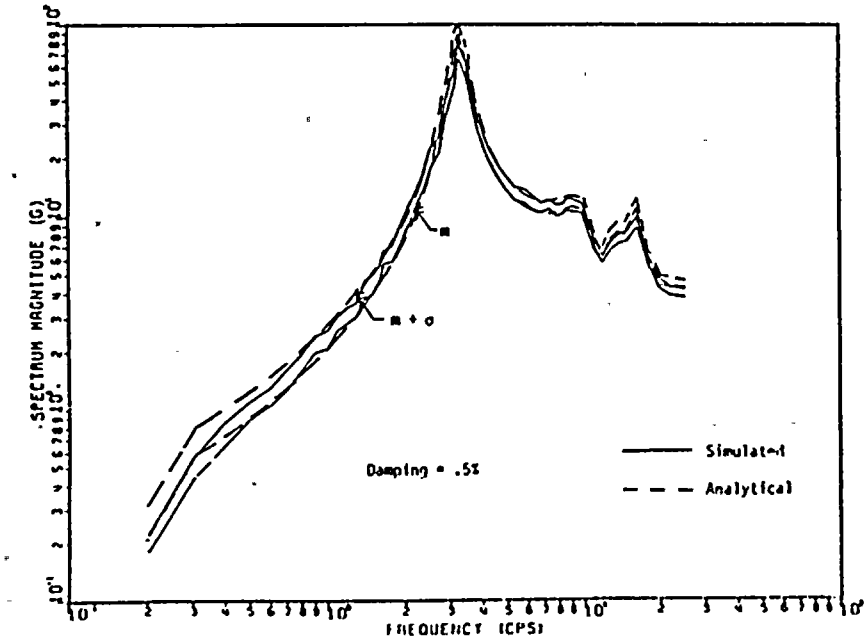

Fig. 7.28 Comparison of the Analytical with the Simulated Floor Response Spectra of Response Motions at Node 11 to Type B Ground Motions

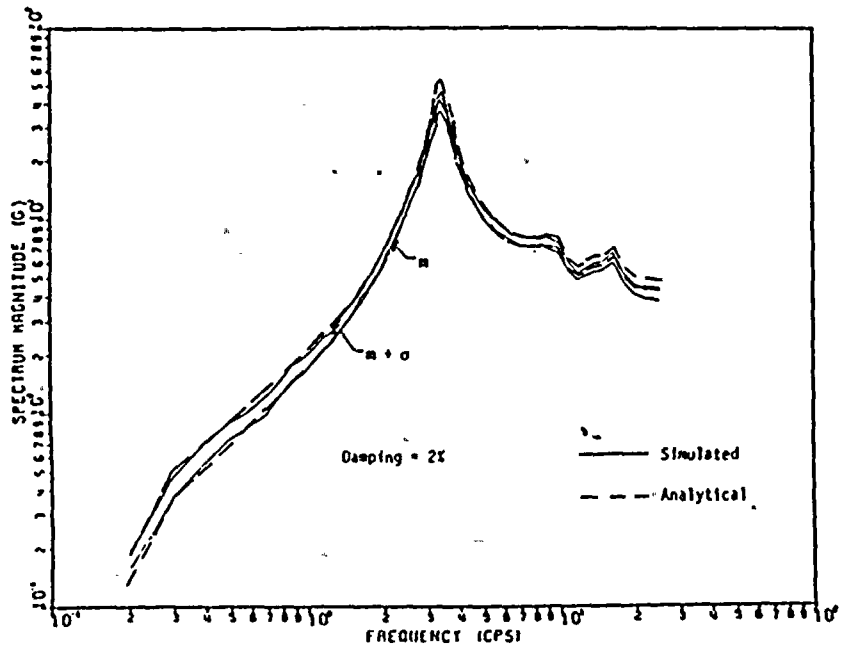

Fig. 7.29 Comparison of the Analytical with the Simulated Floor Response Spectra of Response Motions at Node 11 to Type B Ground Motions

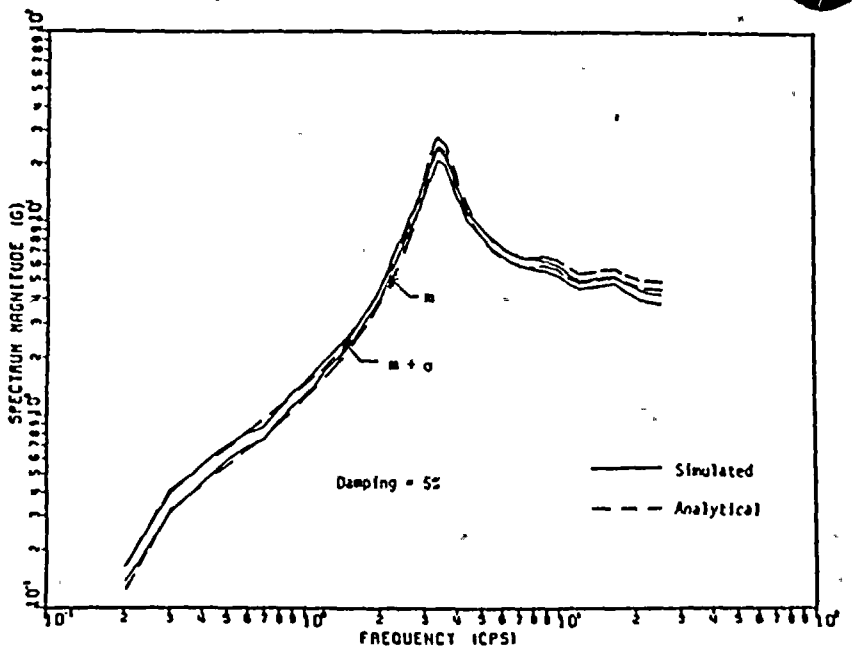

Fig. 7.30 Comparison of the Analytical with the Simulated Floor Response Spectra of Response Motions at Node 11 to Type B Ground Motions

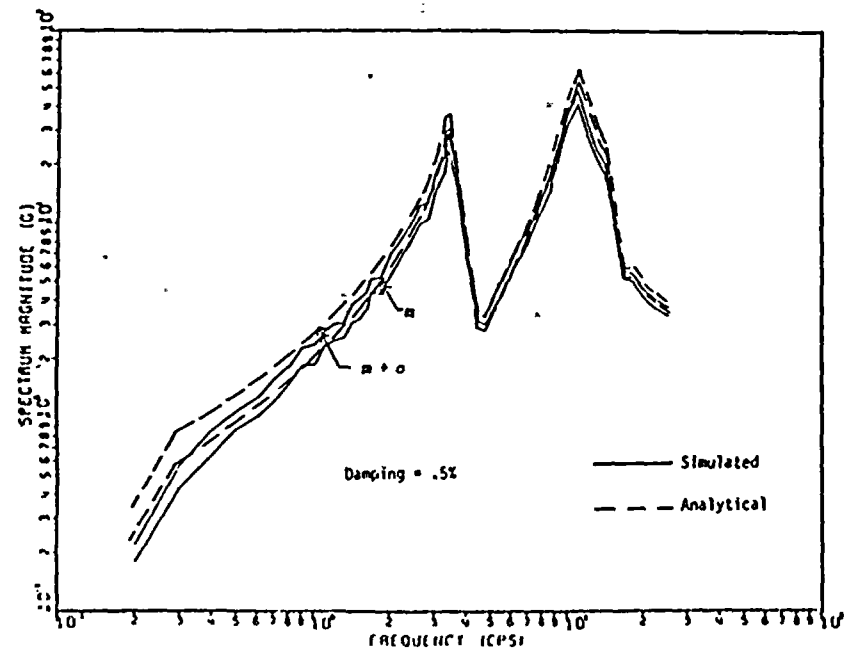

Fig. 7.31 Comparison of the Analytical with the Simulated Floor Response Spectra of Response Motions at Node 18 to Type B Ground Motions

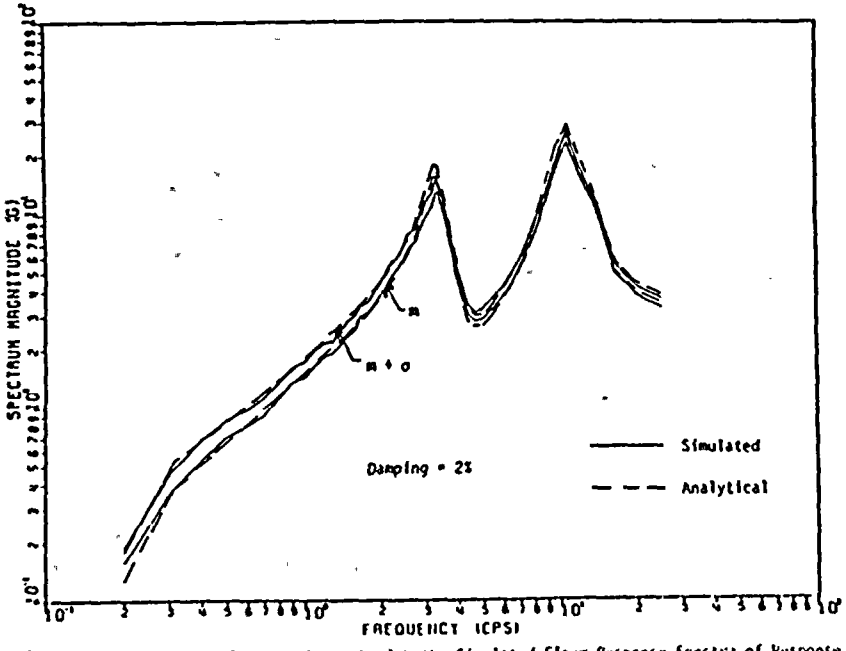

Fig. 7.32 Comparison of the Analytical with the Simulated Floor Response Spectra of Response Motions at Node 18 to Type B Ground Motions

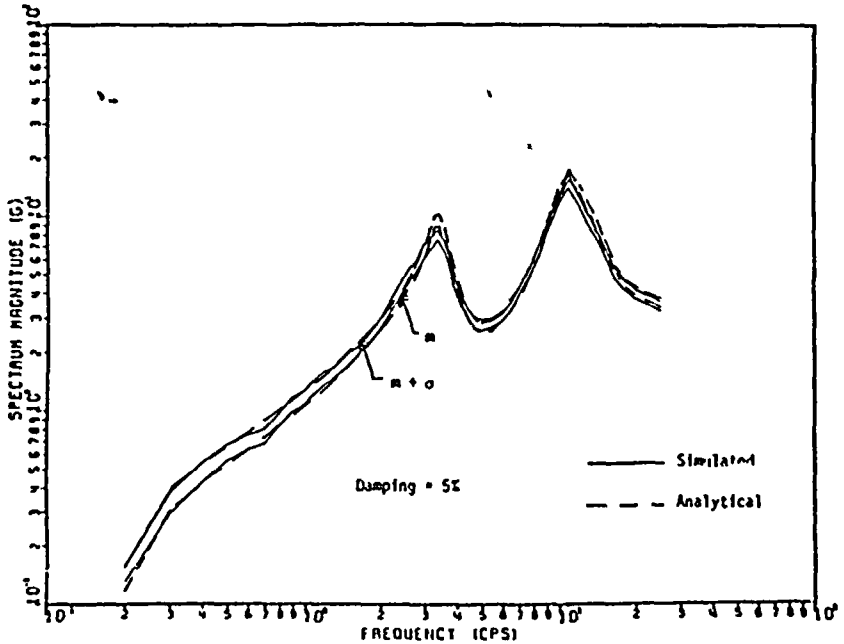

Fig. 7.33 Comparison of the Analytical with the Simulated Response Spectra of Response Motions at Node 16 to Type B Ground Motions

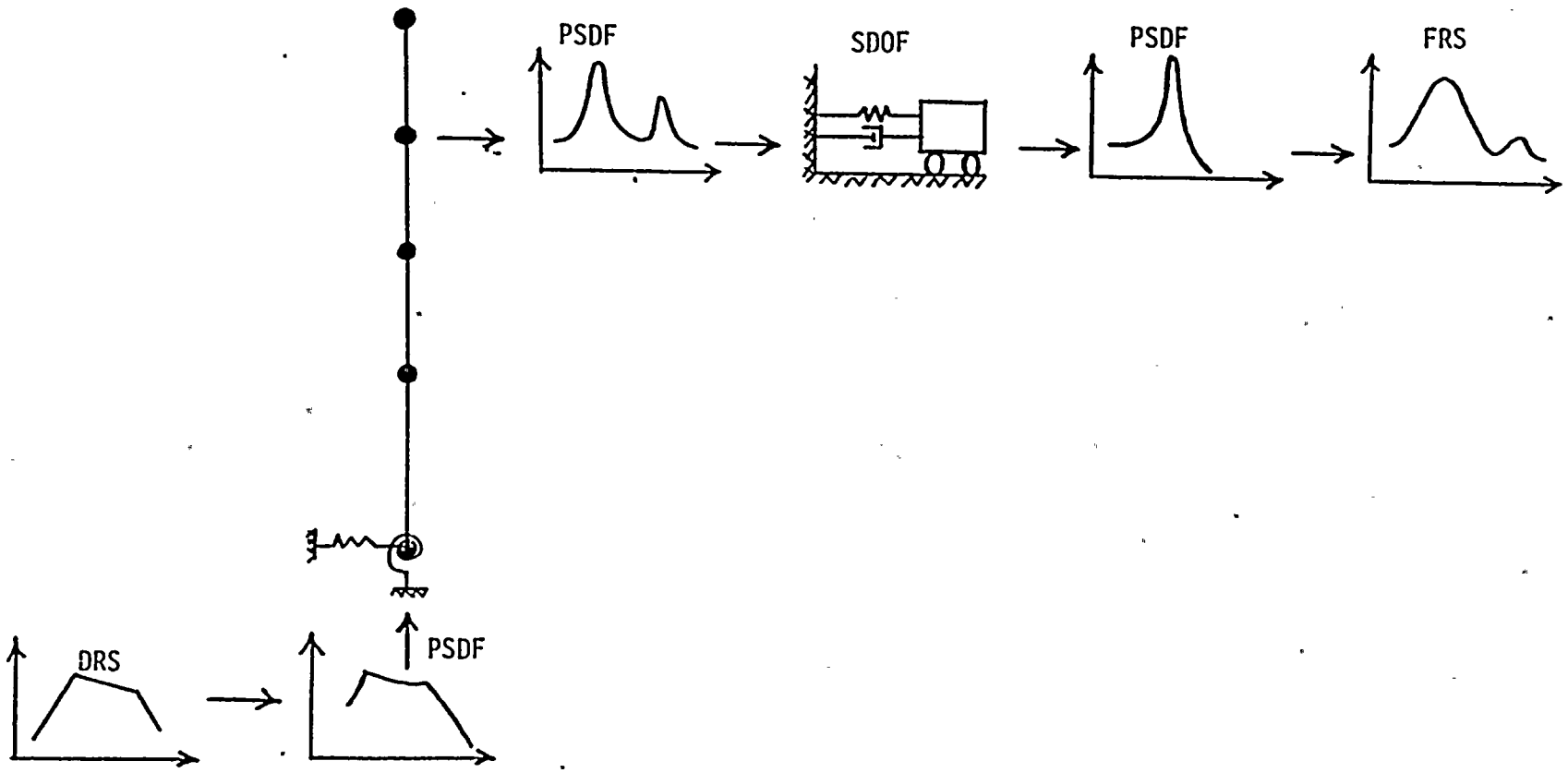

Fig. 8.1 Schematic Diagram of the Approach Adopted in the Computer Program PROSPEC

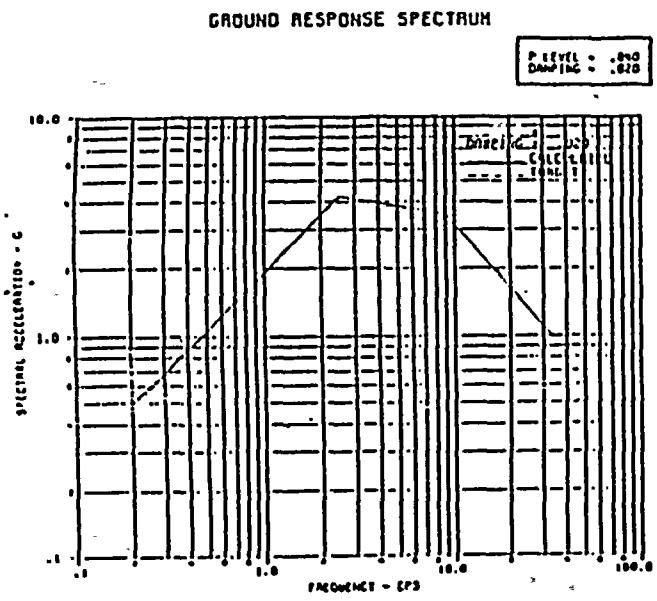

Fig. 9.1 Comparison of the Calculated Spectrum of the Synthetic Time History in Fig. 9.2 with the Design Spectrum from the USNRC R.G. 1.60.

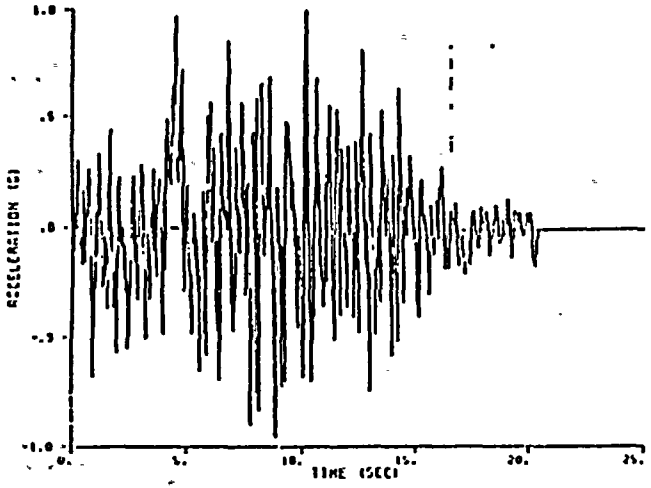

Fig. 9.2 Synthetic Acceleration Time History

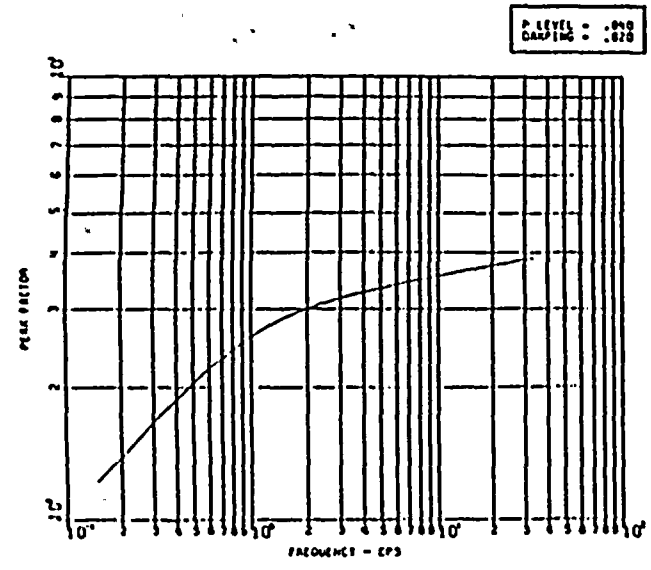

Fig. 9.3 The Modified-Vanmarcke Peak Factor for Ground Motion with the Use of the Approximate Values of δ and ν_0

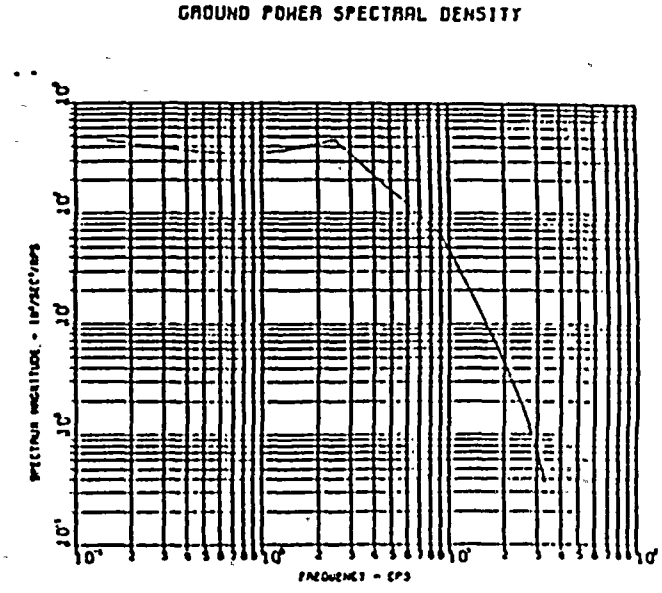

Fig. 9.4 PSDF of the Ground Motion

TRANSFER FUNCTION AT MASS POINT 11

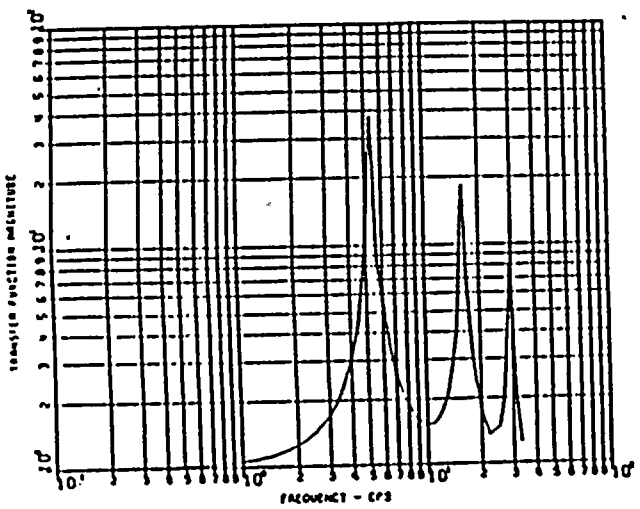

Fig. 9.5 Structural Transfer Function at Node 11

TRANSFER FUNCTION AT MASS POINT 18

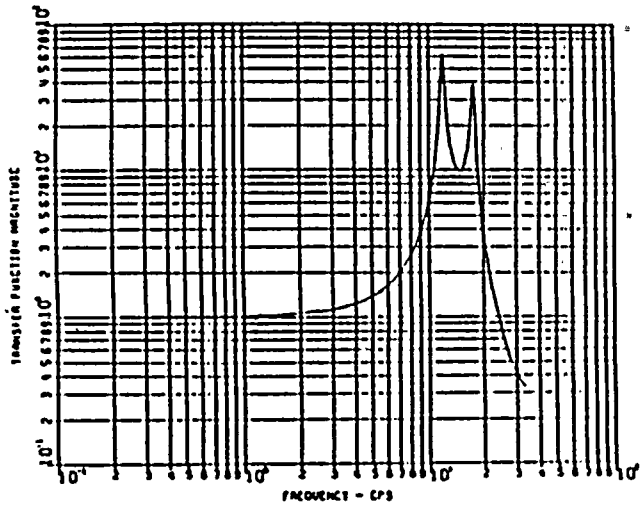

Fig. 9.6 Structural Transfer Function at Node 18

FLOOR POWER SPECTRAL DENSITY AT MASS POINT 11

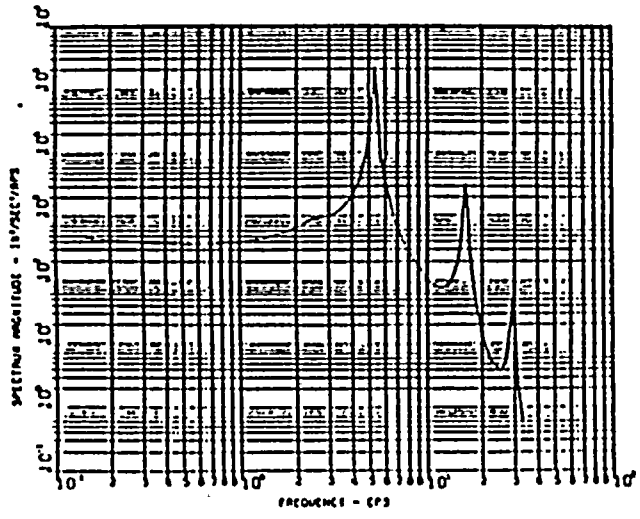

Fig. 9.7 PSDF of Floor Response Motion at Node 11

FLOOR POWER SPECTRAL DENSITY AT MASS POINT 18

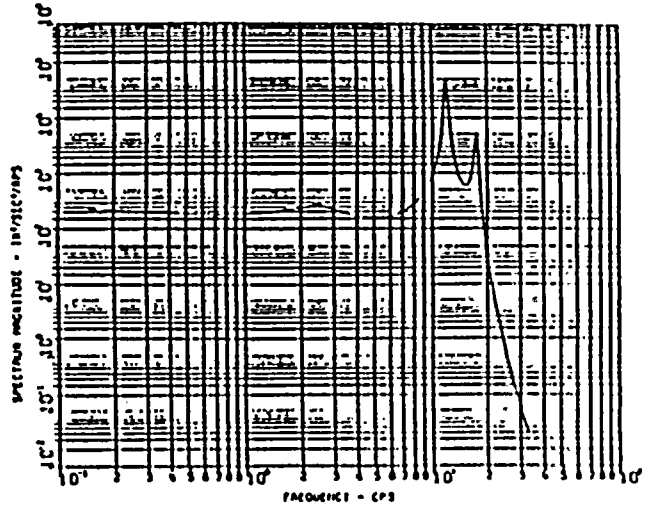

Fig. 9.8 PSDF of Floor Response Motion at Node 18

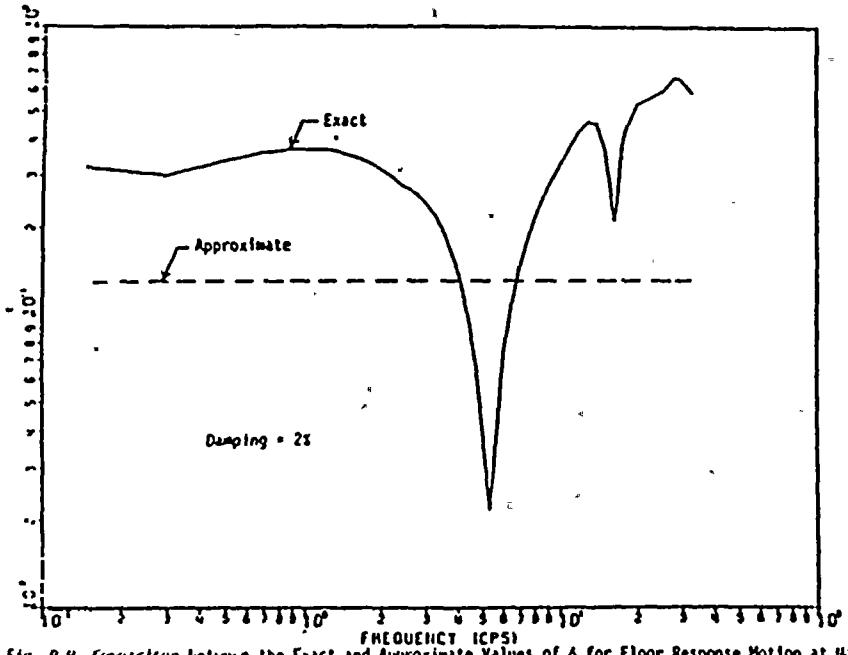

Fig. 9.9 Comparison between the Exact and Approximate Values of δ for Floor Response Motion at Node 11

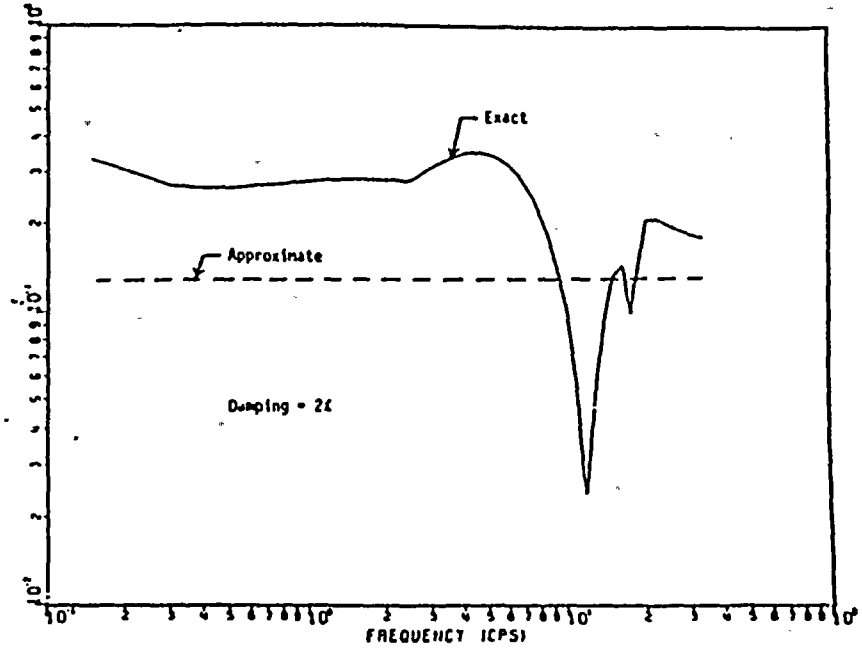

Fig. 9.10 Comparison Between the Exact and Approximate Values of δ for Floor Response Motion at Node 18

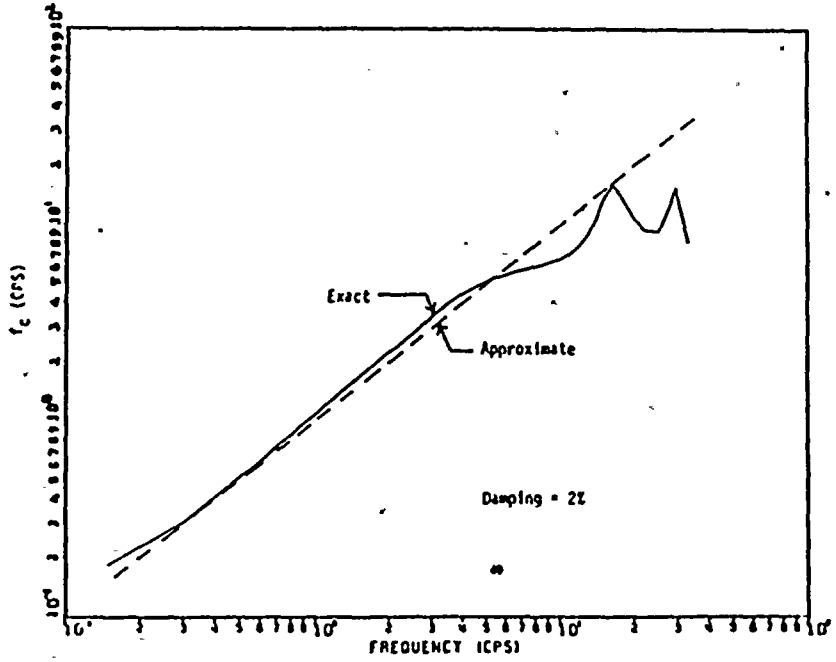

Fig. 9.11 Comparison Between the Exact and Approximate Values of f_c for Floor Response Motion at Node 11

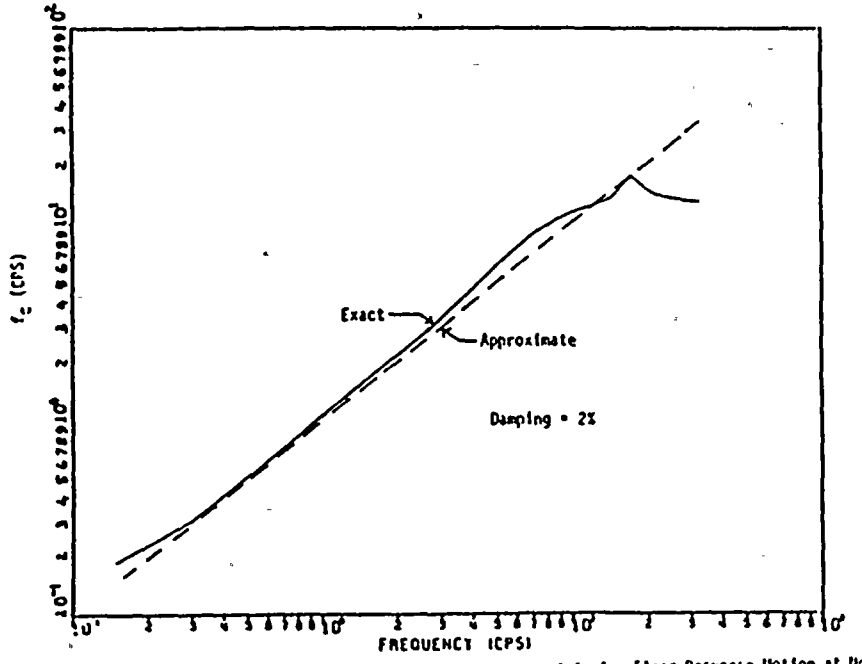

Fig. 9.12 Comparison Between the Exact and Approximate Values of f_c for Floor Response Motion at Node 18

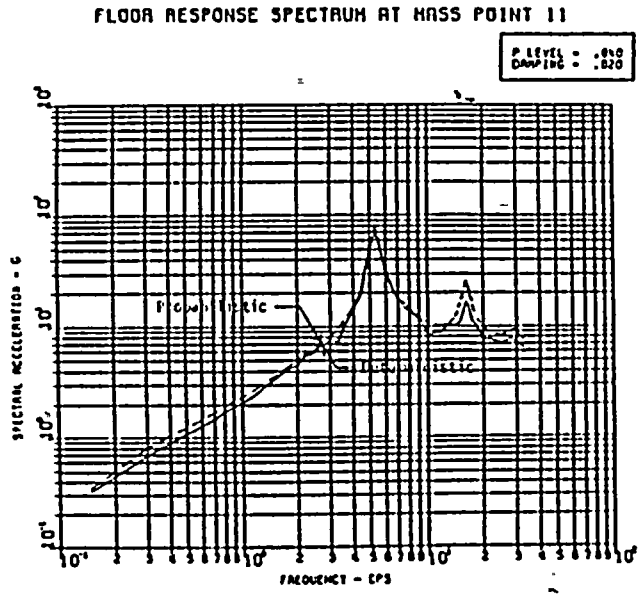

Fig. 9.17 Comparison Between the Deterministic FRS and the Probabilistic FRS Generated from Using the Exact Value of the Modified-Vanmarcke Peak Factor for Node 11

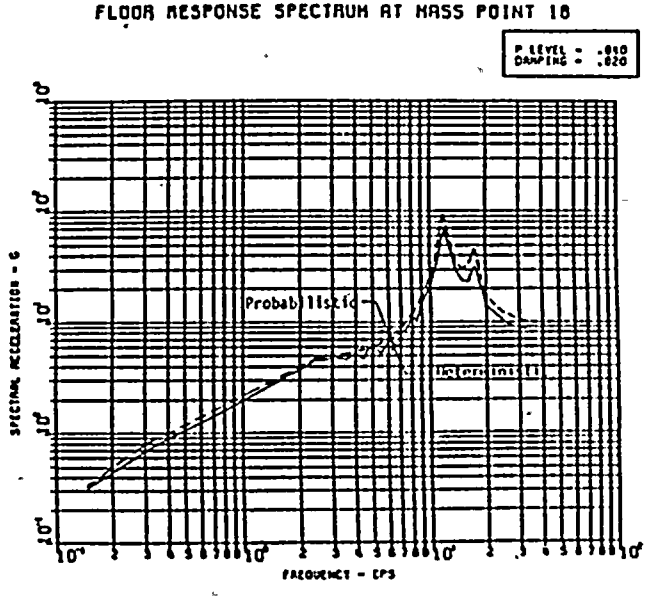

Fig. 9.18 Comparison Between the Deterministic FRS and the Probabilistic FRS Generated from Using the Exact Value of the Modified-Vanmarcke Peak Factor for Node 18

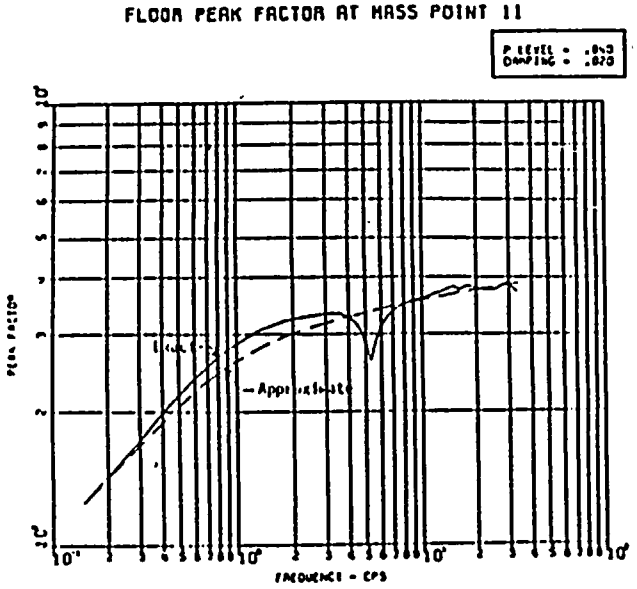

Fig. 9.13 Comparison Between the Approximate and Exact Values of the Modified-Vanmarcke Peak Factors for Floor Response at Node 11

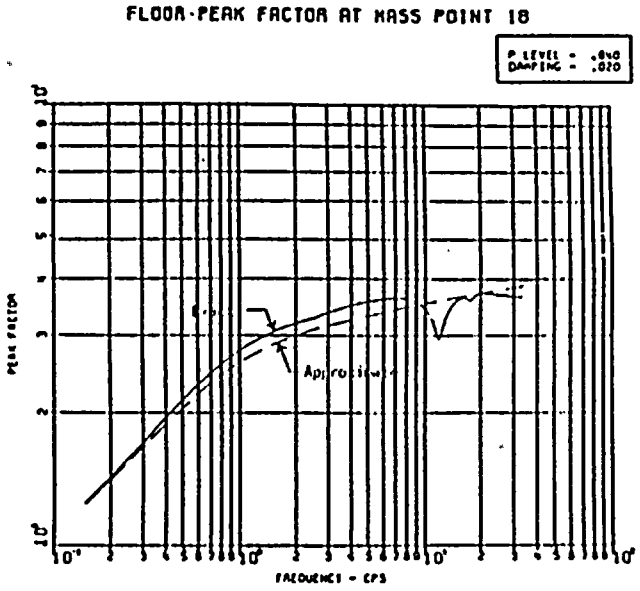

Fig. 9.14 Comparison Between the Approximate and Exact Values of the Modified-Vanmarcke Peak Factors for Floor Response at Node 18

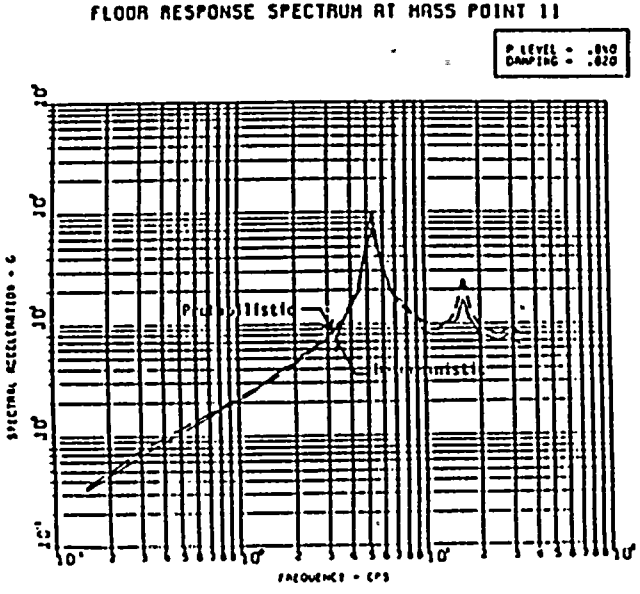

Fig. 9.15 Comparison Between the Deterministic FRS and the Probabilistic FRS Generated from Using the Approximate Value of the Modified-Vanmarcke Peak Factor for Node 11

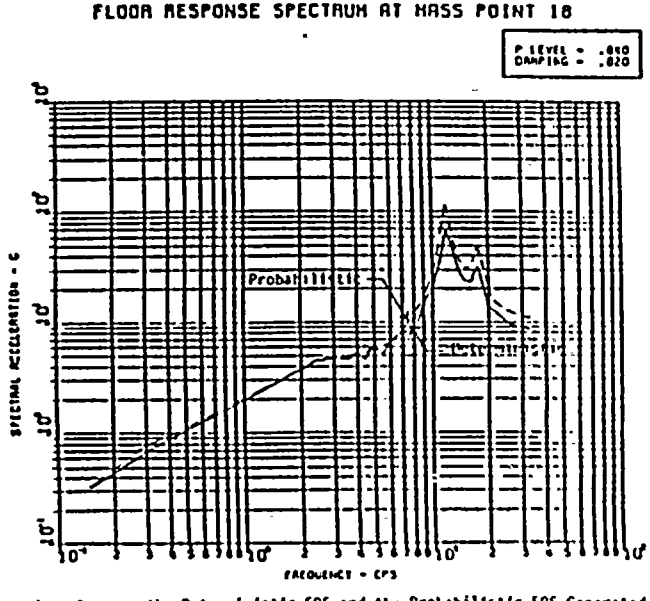

Fig. 9.16 Comparison Between the Deterministic FRS and the Probabilistic FRS Generated from Using the Approximate Value of the Modified-Vanmarcke Peak Factor for Node 18